MAGNETO-OPTICAL PROPERTIES OF NARROW-GAP SEMICONDUCTOR
HETEROSTRUCTURES

By

XINGYUAN PAN

A DISSERTATION PRESENTED TO THE GRADUATE SCHOOL
OF THE UNIVERSITY OF FLORIDA IN PARTIAL FULFILLMENT
OF THE REQUIREMENTS FOR THE DEGREE OF
DOCTOR OF PHILOSOPHY

UNIVERSITY OF FLORIDA

2010

I dedicate this to my wife, Shuyang Gu, and my parents.

ACKNOWLEDGMENTS

I would like to thank my thesis advisor, Dr. Christopher Stanton for his consistent supporting and advising during my graduate study. His insight in condensed matter physics always help me a lot whenever I was in trouble during my research. I also learned a lot on how to be a scientist from his professional attitude towards scientific research. I cannot forget those numerous hours we spent together in his office, discussing all kinds of physics problem in general, and my graduate research on semiconductor physics in particular.

I also like to thank my Ph.D. supervisory committee members, Dr. David Reitze, Dr. Pradeep Kumar, Dr. Hai-Ping Cheng and Dr. Cammy Abernathy, for spending their valuable time on reviewing my Ph.D. proposal for my qualifying exam, and on reviewing my manuscript for this dissertation.

There are also several colleagues I want to thank. Dr. Gary Sanders helped me a lot during my graduate research, especially when I met some difficulties in the coding using Fortran programming language. He always tried his best to help me locate the bug. I also like to thank David Hansen and Brent Nelson for their support in computer related problems. I would like to thank our collaborators Dr. Sophia Hayes in St. Louis, and Dr. Mike Santos and Dr. Ryan Doezema in Oklahoma, for providing the experimental data. I want to thank Ms. Kristin Nichola for her help during my stay here, and I also like to thank all my friends in Gainesville. Last I want to thank my wife, Shuyang Gu, and my parents. Their love are always the best support to me.

LIST OF TABLES

LIST OF FIGURES

Abstract of Dissertation Presented to the Graduate School
of the University of Florida in Partial Fulfillment of the
Requirements for the Degree of Doctor of Philosophy

MAGNETO-OPTICAL PROPERTIES OF NARROW-GAP SEMICONDUCTOR
HETEROSTRUCTURES

By

Xingyuan Pan

December 2010

Chair: Christopher Stanton
Major: Physics

Next generation of semiconductor device will not only based on the charge transport

properties of the carrier, but also their spin degree of freedom. In order to understand

or predict how those devices work one need to understand the spin-dependent

electronic structures of both bulk and low-dimensional semiconductors. We have

theoretically studied the spin-dependent Landau levels for electrons or holes in

bulk GaAs system and AlInSb/InSb multiple quantum wells system. We use the

envelope function approximation for the electronic and magneto-optical properties

of AlInSb/InSb superlattices. Our model includes the conduction electrons, heavy

holes, light holes and the split-off holes for a total of 8 bands when spin is taken into

account. It is a generalization of the Pidgeon-Brown model to include the wave vector

dependence of the electronic states, as well as quantization of wave vector due to

multiple quantum well superlattice effects. In addition, we take strain effects into account

by assuming pseudomorphic growth conditions. For bulk GaAs system, we calculated

the spin-dependent absorption coefficients which can be directly compared with the

optically pumped NMR experiment. We show that the optically pumped NMR is a

complimentary tool to traditional magneto optical absorption measurement, in the sense

that optically pumped NMR is more sensitive to the light hole transitions which are very

hard to resolve in the traditional magneto absorption measurement. For the AlInSb/InSb

multiple quantum well system, we calculated both the magneto absorption spectra and

the cyclotron resonance spectra. We compare both spectra to experimental results and achieve a good agreement. This agreement assures us that our understanding of the valence band structure of the narrow gap InSb materials are correct.

CHAPTER 1
INTRODUCTION

Understanding the electronic, transport and optical properties of real materials enable us to utilize the unique properties of each material to make devices applications. Many of these properties are closely related to the electronic structures. Nowadays certain experimental tools can be used to probe the electronic structures, for example, the de Haas-van Alphen effect is a very useful tool to probe the Fermi surface for metals. Another example is using the magneto-optical absorption to probe the Landau levels for semiconductors, or using cyclotron resonance measurement to probe the effective mass tensor. From all these available experimental tools we found that magnetic field is very important in studying the electronic structures. Theoretically we also want to model the electronic structures of materials in the magnetic field. Because the materials we are interested in are direct-gap semiconductors, and we are only interested in a very small range of the Brillouin zone around the zone center, the $\boldsymbol{k} \cdot \boldsymbol{p}$ method is most suitable here for our purpose.

The fact that the solid can be categorized into metals, insulators and semiconductors is based on its electronic structure. Metals do not have a band gap, insulators have a large band gap and semiconductors usually have a band gap less than 4 electron volts. Many types of electronic devices are designed based on the semiconductors materials and it is fair to say semiconductor materials are the basis of the modern electronic industry. At this time the most important and most famous semiconductor is silicon, not only because of its properties but also because its manufacture is so mature that the cost is low compared with other materials. However, III-V semiconductors also found themselves important device applications. Wide bandgap semiconductors such as GaN find their applications in light-emitting diodes (LEDs), lasers and detectors in the visible and ultraviolet range. At the other end, narrow bandgap III-V semiconductors have some unique properties that can be used in a number of electronic devices[1–3].

InSb is the III-V binary semiconductor with the smallest band gap[4], smallest electron effective mass and largest g-factor. Table 1-1 shows the electron effective mass m^* and g-factor for three important III-V materials. It has potential applications such as a optoelectronic device in the infrared range due to the narrow gap[5], and fast transistors due to the small effective mass[6]. It also has potential applications in the area of spin electronics, since its large g factor can be used to control its spin degree of freedom through its orbital environment.

Table 1-1. Electron effective mass and g-factor of GaAs, InAs and InSb

	Electron m^*	Electron g-factor
GaAs	$0.067m_0$	-0.5
InAs	$0.023m_0$	-15
InSb	$0.014m_0$	-51

Theoretically it is hard to calculate the band structure of InSb compared with other III-V semiconductors[7], because of the strong mixing between conduction bands and valence bands that comes from the narrow band gap. Before we attack this complicated problem, we begin with a simpler problem of calculating the electronic structures of bulk GaAs in the magnetic field. The theoretical model is based on reference [8]. It is simpler than the InSb problem because it is not a quantum confined system, and also there is no need to consider strain effect. However we will still keep the eight band model to fully account for the coupling between conduction bands and valence bands. This model can be extended later to deal with the InSb quantum well system. Because of the very large g factor InSb has, magneto-absorption can be used to determine the spin splittings in the conduction band[9, 10]. In order to get a deeper understanding of the valence band structure, especially the dependence of the valance bands on strain and confinement, we performed theoretical studies of magneto-optical transitions across the bandgap in strained InSb quantum wells with AlInSb barriers, and compared to experimental studies by Santos group at the University of Oklahoma.

CHAPTER 2
THEORY

2.1 $k \cdot p$ **Method**

The electron energy and wave function in a periodic potential is the starting point of the theoretical model. This is given by the well-know Schrödinger equation for a Bloch electron

$$H\psi_{\boldsymbol{k}}(\boldsymbol{r}) = E\psi_{\boldsymbol{k}}(\boldsymbol{r}) \qquad (2\text{–}1)$$

where $\boldsymbol{k}$ is the wave vector and the Hamiltonian H is given by

$$H = \frac{\boldsymbol{p}^2}{2m_0} + V_0(\boldsymbol{r}), \qquad (2\text{–}2)$$

here $\boldsymbol{p}$ is the momentum operator, m_0 is the electron mass and $V_0(\boldsymbol{r})$ is the periodic potential. Right now the Hamiltonian is the simple form of a single Bloch electron, and I will add more terms to this simple Hamiltonian as I go to more complicated situations such as spin-orbit interaction, confinement potential and magnetic field etc.

Many different methods exist to solve equation (2–1) which can be found in standard textbook such as [11]. I am interested in the magneto-optical properties of the III-V semiconductors and for this kind of system, the properties are determined by the lowest lying excited states near the band edge. The $\boldsymbol{k} \cdot \boldsymbol{p}$ method is the most suitable method here to solving for electron energy and wave functions. This method is a perturbative method, assuming the solution to equation (2–1) for a certain $\boldsymbol{k} = \boldsymbol{k_0}$ value are already known and expand the solutions of other $\boldsymbol{k}$ in terms of the linear combination of those $\boldsymbol{k} = \boldsymbol{k_0}$ solutions. When choosing $\boldsymbol{k_0} = \boldsymbol{0}$, i.e., the center of the Brillouin zone, the solutions are of high symmetry and serve as a natural basis.

From Bloch theorem the wave function $\psi_{\boldsymbol{k}}(\boldsymbol{r})$ in equation (2–1) can be chosen to have the form

$$\psi_{\boldsymbol{k}}(\boldsymbol{r}) = e^{i\boldsymbol{k}\cdot\boldsymbol{r}}u_{\boldsymbol{k}}(\boldsymbol{r}), \qquad (2\text{–}3)$$

where $u_{\boldsymbol{k}}(\boldsymbol{r})$ has the same periodicity as the crystal lattice. Substitute equation (2–2) and equation (2–3) into equation (2–1), we obtain a differential equation for $u_{\boldsymbol{k}}(\boldsymbol{r})$, the periodic part of the wave function:

$$\left[\frac{\boldsymbol{p}^2}{2m_0} + V_0(\boldsymbol{r}) + \frac{\hbar}{m_0}\boldsymbol{k}\cdot\boldsymbol{p}\right]u_{\boldsymbol{k}}(\boldsymbol{r}) = \left[E(\boldsymbol{k}) - \frac{\hbar^2 k^2}{2m_0}\right]u_{\boldsymbol{k}}(\boldsymbol{r}). \tag{2–4}$$

The third term in the above equation is proportional to $\boldsymbol{k}\cdot\boldsymbol{p}$, hence the name "$\boldsymbol{k}\cdot\boldsymbol{p}$" method.

To solve equation (2–4) for an arbitrary $\boldsymbol{k}$, we assume that the solutions for a particular point $\boldsymbol{k_0}$ are known, and denote them as $\{u_{n'\boldsymbol{k_0}}(\boldsymbol{r})\}$, where n' labels the different solutions for the same $\boldsymbol{k}_0$ point. This set of solutions $\{u_{n'\boldsymbol{k_0}}(\boldsymbol{r})\}$ provide a basis for solutions for other $\boldsymbol{k}$ point. In practice, we choose $\boldsymbol{k_0} = \boldsymbol{0}$, i.e., the center of the Brillouin zone. Now $u_{\boldsymbol{k}}(\boldsymbol{r})$ in equation (2–4) can be expressed as a linear combination of the basis functions $\{u_{n'\boldsymbol{0}}(\boldsymbol{r})\}$:

$$u_{\boldsymbol{k}}(\boldsymbol{r}) = \sum_{n'} c_{n'}(\boldsymbol{k})u_{n'\boldsymbol{0}}(\boldsymbol{r}). \tag{2–5}$$

Here $u_{n'\boldsymbol{0}}(\boldsymbol{r})$ satisfy the following two equations

$$\left[\frac{\boldsymbol{p}^2}{2m_0} + V_0(\boldsymbol{r})\right]u_{n'\boldsymbol{0}}(\boldsymbol{r}) = E_{n'}(\boldsymbol{0})u_{n'\boldsymbol{0}}(\boldsymbol{r}) \tag{2–6}$$

and

$$\int_{\text{unit cell}} u_{n\boldsymbol{0}}^*(\boldsymbol{r})u_{n'\boldsymbol{0}}(\boldsymbol{r})d^3\boldsymbol{r} = \delta_{nn'}. \tag{2–7}$$

Substitute equation (2–5) into equation (2–4) and multiply from the left by $u_{n\boldsymbol{0}}^*(\boldsymbol{r})$, and then integrating over the unit cell, by using equation (2–6) and (2–7), we obtain

$$\sum_{n'}\left\{\left[E_{n'}(\boldsymbol{0}) + \frac{\hbar^2 k^2}{2m_0}\right]\delta_{nn'} + \frac{\hbar}{m_0}\boldsymbol{k}\cdot\boldsymbol{P}_{nn'}\right\}c_{n'}(\boldsymbol{k}) = E(\boldsymbol{k})c_n(\boldsymbol{k}), \tag{2–8}$$

where

$$\boldsymbol{P}_{nn'} = \int_{\text{unit cell}} u_{n\boldsymbol{0}}^*(\boldsymbol{r})\boldsymbol{p}u_{n'\boldsymbol{0}}(\boldsymbol{r})d^3\boldsymbol{r}. \tag{2–9}$$

Equation (2–8) can be diagonalized to obtain the energy and wave functions for arbitrary $\mathbf{k}$. So now we have a working routine to solve the electronic states near the band edge. However equation (2–8) will not give us reasonable results since we have not considered the spin-orbit interaction yet. This is the subject of the next section.

2.2 Spin-Orbit Interaction

As promised, the first correction to the Hamiltonian in equation (2–2) is a term coming from the spin-orbit interaction:

$$H_{SO} = \frac{\hbar}{4m_0^2 c^2} \mathbf{p} \cdot \boldsymbol{\sigma} \times (\nabla V_0). \tag{2–10}$$

where c is the speed of light and $\boldsymbol{\sigma}$ is the Pauli spin matrix that acting on the spinor states. The origin of this term can be traced back to the non-relativistic approximation to the Dirac equation which can be found on any standard quantum mechanic text book such as [12]. The importance of this term is discussed by Elliott[13], Dresselhaus[14, 15] and Parmenter[16]. When this term is included in the original Hamiltonian, we have the Schrödinger equation:

$$\left[\frac{\mathbf{p}^2}{2m_0} + V_0(\mathbf{r}) + \frac{\hbar}{4m_0^2 c^2} \mathbf{p} \cdot \boldsymbol{\sigma} \times (\nabla V_0) \right] e^{i\mathbf{k}\cdot\mathbf{r}} u_{\mathbf{k}}(\mathbf{r}) = E(\mathbf{k}) e^{i\mathbf{k}\cdot\mathbf{r}} u_{\mathbf{k}}(\mathbf{r}), \tag{2–11}$$

here we already write the wave function in terms of the Bloch function, $\psi_{\mathbf{k}}(\mathbf{r}) = e^{i\mathbf{k}\cdot\mathbf{r}} u_{\mathbf{k}}(\mathbf{r})$. Note that $u_{\mathbf{k}}(\mathbf{r})$ is a compact notation of the two-component column spinor function

$$u_{\mathbf{k}}(\mathbf{r}) = \begin{bmatrix} u_{\mathbf{k}}^{(1)}(\mathbf{r}) \\ u_{\mathbf{k}}^{(2)}(\mathbf{r}) \end{bmatrix} = u_{\mathbf{k}}^{(1)}(\mathbf{r})|\uparrow\rangle + u_{\mathbf{k}}^{(2)}(\mathbf{r})|\downarrow\rangle. \tag{2–12}$$

Now evaluating the Hamiltonian operator acting on the plane wave part $e^{i\mathbf{k}\cdot\mathbf{r}}$, we got a equation for the two component spinor part of the wave function

$$\left[\frac{\mathbf{p}^2}{2m_0} + V_0(\mathbf{r}) + \frac{\hbar^2 k^2}{2m_0} + \frac{\hbar}{m_0} \mathbf{k} \cdot \boldsymbol{\pi} + \frac{\hbar}{4m_0^2 c^2} \mathbf{p} \cdot \boldsymbol{\sigma} \times (\nabla V_0) \right] u_{\mathbf{k}}(\mathbf{r}) = E(\mathbf{k}) u_{\mathbf{k}}(\mathbf{r}) \tag{2–13}$$

where

$$\pi = p + \frac{\hbar}{4m_0 c^2} \sigma \times \nabla V_0,$$ (2–14)

This is the equation we want to solve in the presence of spin-orbit interaction.

Like the case when there is no spin-orbit interaction, the general solutions for equation (2–13) can still be expanded in terms of the zone center solutions. We can still write them as

$$u_{\boldsymbol{k}}(\boldsymbol{r}) = \sum_{n'} c_{n'}(\boldsymbol{k}) u_{n'\boldsymbol{0}}(\boldsymbol{r}).$$ (2–15)

Here $u_{n'\boldsymbol{0}}(\boldsymbol{r})$ satisfy the following two equations

$$\left[\frac{\boldsymbol{p}^2}{2m_0} + V_0(\boldsymbol{r})\right] u_{n'\boldsymbol{0}}(\boldsymbol{r}) = E_{n'}(\boldsymbol{0}) u_{n'\boldsymbol{0}}(\boldsymbol{r})$$ (2–16)

and

$$\int_{\text{unit cell}} u_{n\boldsymbol{0}}^{\dagger}(\boldsymbol{r}) u_{n'\boldsymbol{0}}(\boldsymbol{r}) d^3\boldsymbol{r} = \delta_{nn'}.$$ (2–17)

Substitute this expansion of $u_{\boldsymbol{k}}(\boldsymbol{r})$ into equation (2–13) and multiply from the left by $u_{n\boldsymbol{0}}^{\dagger}(\boldsymbol{r})$, and then integrate over a unit cell, by using equation (2–16) and (2–17), we got the matrix eigenvalue equation for the expansion coefficient $c_{n'}(\boldsymbol{k})$

$$\sum_{n'} \left\{ E_{n'}(\boldsymbol{0})\delta_{nn'} + \frac{\hbar}{m_0} \boldsymbol{k} \cdot \pi_{nn'} + \Delta_{nn'} \right\} c_{n'}(\boldsymbol{k}) = E'(\boldsymbol{k})c_n(\boldsymbol{k}),$$ (2–18)

where

$$E'(\boldsymbol{k}) = E(\boldsymbol{k}) - \frac{\hbar^2 k^2}{2m_0}$$ (2–19)

$$\pi_{nn'} = \int_{\text{cell}} u_{n\boldsymbol{0}}^{\dagger}(\boldsymbol{r})\pi u_{n'\boldsymbol{0}}(\boldsymbol{r})d^3\boldsymbol{r}$$ (2–20)

$$\Delta_{nn'} = \frac{\hbar}{4m_0^2 c^2} \int_{\text{cell}} u_{n\boldsymbol{0}}^{\dagger}(\boldsymbol{r})[\boldsymbol{p} \cdot \sigma \times \nabla V_0] u_{n'\boldsymbol{0}}(\boldsymbol{r})d^3\boldsymbol{r}.$$ (2–21)

Note that $\pi_{nn'}$ has two contributions

$$\pi_{nn'} = \int_{\text{cell}} u_{n\boldsymbol{0}}^{\dagger}(\boldsymbol{r})\boldsymbol{p}u_{n'\boldsymbol{0}}(\boldsymbol{r})d^3\boldsymbol{r} + \frac{\hbar}{4m_0 c^2} \int_{\text{cell}} u_{n\boldsymbol{0}}^{\dagger}(\boldsymbol{r})[\sigma \times \nabla V_0]u_{n'\boldsymbol{0}}(\boldsymbol{r})d^3\boldsymbol{r}$$ (2–22)

the second contribution is very small compared with the $\Delta_{nn'}$ term[7], thus can be neglected. In this approximation the matrix element $\pi_{nn'}$ is given by

$$\pi_{nn'} = \boldsymbol{p}_{nn'} = \int_{\text{cell}} u_{n\mathbf{0}}^{\dagger}(\boldsymbol{r})\boldsymbol{p}u_{n'\mathbf{0}}(\boldsymbol{r})d^3\boldsymbol{r}. \qquad (2\text{–}23)$$

Now we can calculating the electron energy and wave functions by solving the eigenvalue problem given by equation (2–18), but note that the matrix arising from equation (2–18) is infinite dimensional, making it in practical unsolvable. Even if we know how to solve an infinite dimensional eigenvalue problem, we still need to know the infinite number of the band edge eigenstates. This is also a daunting task. The good news is that people are usually only interested in a few adjacent bands, either neglecting remote bands completely like the 8-band Kane model[7], or treating them as a perturbation[17, 18]. A systematic approach to reduce the dimensionality to do the perturbation problem is the so called "Löwdin's perturbation theory", and I will introduce this method in the next section.

2.3   Löwdin's Perturbation Theory

The $\boldsymbol{k} \cdot \boldsymbol{p}$ Hamiltonian including the spin-orbit interaction gives us an eigenvalue problem to solve. This eigenvalue problem, given by equation (2–18), involves diagonalizing a infinite dimensional matrix, which make it impossible without further simplifications. One of such simplifications was given by Löwdin[19]. The advantage of Löwdin's perturbation theory over traditional perturbation theories such as Rayleigh-Schrödinger perturbations is that we don't need to differentiate the non-degenerate and degenerate cases, i.e., we can treat both cases together in a systematic way. This advantage make it well suitable to problems such as the valence band spin structures of III-V semiconductors. In this section I will not give a detailed derivation of the theory itself, rather I would summarize the key results of the theory in a form that is readily applicable to our current problems, the problem of solving the $\boldsymbol{k} \cdot \boldsymbol{p}$ eigenvalue and eigenfunctions.

A through treatment of the Löwdin's perturbation theory can be found in the original paper of Löwdin[19], or the book by Roland Winkler[20].

The problem we want to solve is the time-independent Schrödinger equation

$$H|\psi\rangle = E|\psi\rangle, \tag{2–24}$$

where the Hamiltonian H can be divided into two parts: a major contribution H^0, and a small perturbation term H'

$$H = H^0 + H'. \tag{2–25}$$

Like other perturbation methods, we assume that we already know the set of solutions $\{|\psi_n\rangle\}$ to the H^0 part of the problem

$$H^0|\psi_n\rangle = E_n|\psi_n\rangle. \tag{2–26}$$

Our task is to find the solution $|\psi\rangle$ to equation (2–24) in the form of a linear combination of the set of functions $\{|\psi_n\rangle\}$

$$|\psi\rangle = \sum_n c_n|\psi_n\rangle. \tag{2–27}$$

Löwdin assumed that the set of unperturbed eigenstates $\{|\psi_n\rangle\}$ naturally falls into two categories, which we call set A and set B. Each eigenstate of $|\psi_n\rangle$ belongs to one of them. The energy of those states that in set A are different from those in set B. In other words, we may or may not have degenerate states within set A or set B but we are sure that a state from set A will be never degenerate with a state from set B. In doing the linear combination to get the eigenstates of the total Hamiltonian, we are only interested in those states coming from set A, treating contribution from set B as a perturbation. Later on we will see that in our problem of solving the $\boldsymbol{k} \cdot \boldsymbol{p}$ Hamiltonian, we are only interested in the lowest conduction bands and highest valence bands (these bands form set A), treating the distant bands as a perturbation (the distant bands form set B). This method will reduce the dimensionality of the problem from infinity to the number of states in set A.

We use the following notations: m, m' etc are quantum numbers labeling states from set A, and l, l' etc are quantum numbers labeling states from set B. We want to find an approximate solution to equation (2–24) that is valid up to the desired order of the perturbating Hamiltonian H':

$$|\psi\rangle = \sum_{m \in A} c_m |\psi_m\rangle, \qquad (2\text{–}28)$$

note that here $|\psi_m\rangle$ belongs to set A only. If the matrix elements coupling set A and set B vanish, i.e., $\langle \psi_m | H | \psi_l \rangle = 0$ for every $m \in A$ and $l \in B$, we already have set A and set B decoupled and our interested eigenstates are exactly in the form of equation (2–28). If there are non-zero matrix elements $\langle \psi_m | H | \psi_l \rangle$, we want to find a unitary transformation generated by the anti-Hermitian operator S

$$\widetilde{H} = e^{-S} H e^{S}, \qquad (2\text{–}29)$$

so that the transformed Hamiltonian does not have coupling between set A and set B

$$\langle \psi_m | \widetilde{H} | \psi_l \rangle = 0. \qquad (2\text{–}30)$$

Since this is a perturbative theory, what we really mean is $\langle \psi_m | \widetilde{H} | \psi_l \rangle$ vanishes up to the desired order of H'. The generator of the unitary transformation S can be expressed in the asymptotic form

$$S = S^{(1)} + S^{(2)} + S^{(3)} + ... \qquad (2\text{–}31)$$

where $S^{(1)}$ is the 1st-order infinitesimal, $S^{(2)}$ is the 2nd-order infinitesimal, and so on. After some algebra [20] we can show that the first 3 terms of this anti-Hermitian operator S are given by

$$S_{ml}^{(1)} = - \frac{H'_{ml}}{E_m - E_l} \qquad (2\text{–}32a)$$

$$S_{ml}^{(2)} = \frac{1}{E_m - E_l} \left[\sum_{m'} \frac{H'_{mm'} H'_{m'l}}{E_{m'} - E_l} - \sum_{l'} \frac{H'_{ml'} H'_{l'l}}{E_m - E_{l'}} \right] \qquad (2\text{–}32b)$$

$$S_{ml}^{(3)} = \frac{1}{E_m - E_l}$$

20

$$\times \left[-\sum_{m'm''} \frac{H'_{mm''} H'_{m''m'} H'_{m'l}}{(E_{m''} - E_l)(E_{m'} - E_l)} - \sum_{l'l''} \frac{H'_{ml'} H'_{l'l''} H'_{l''l}}{(E_m - E_{l''})(E_m - E_{l'})} \right.$$

$$+ \sum_{l'm'} \frac{H'_{mm'} H'_{m'l'} H'_{l'l}}{(E_{m'} - E_l)(E_{m'} - E_{l'})} + \sum_{l'm'} \frac{H'_{mm'} H'_{m'l'} H'_{l'l}}{(E_m - E_{l'})(E_{m'} - E_{l'})}$$

$$+ \frac{1}{3} \sum_{l'm'} \frac{H'_{ml'} H'_{l'm'} H'_{m'l}}{(E_{m'} - E_{l'})(E_{m'} - E_l)} + \frac{1}{3} \sum_{l'm'} \frac{H'_{ml'} H'_{l'm'} H'_{m'l}}{(E_m - E_{l'})(E_{m'} - E_{l'})}$$

$$+ \left. \frac{2}{3} \sum_{l'm'} \frac{H'_{ml'} H'_{l'm'} H'_{m'l}}{(E_m - E_{l'})(E_{m'} - E_l)} \right], \tag{2–32c}$$

where $H'_{ml} = \langle \psi_m | H' | \psi_l \rangle$. Note that for every j we have $S^{(j)}_{lm} = -S^{(j)^*}_{ml}$, and $S^{(j)}_{mm'} = S^{(j)}_{ll'} = 0$ so that we can actually obtain every elements of S from equation (2–32).

Finally substituting equation (2–32) into equation (2–29) we get the asymptotic form of the transformed Hamiltonian

$$\widetilde{H} = H^{(0)} + H^{(1)} + H^{(2)} + H^{(3)} + ..., \tag{2–33}$$

where

$$H^{(0)}_{mm'} = H^0_{mm'} \tag{2–34a}$$

$$H^{(1)}_{mm'} = H'_{mm'} \tag{2–34b}$$

$$H^{(2)}_{mm'} = \frac{1}{2} \sum_l H'_{ml} H'_{lm'} \left[\frac{1}{E_m - E_l} + \frac{1}{E_{m'} - E_l} \right] \tag{2–34c}$$

$$H^{(3)}_{mm'} = -\frac{1}{2} \sum_{lm''} \left[\frac{H'_{ml} H'_{lm''} H'_{m''m'}}{(E_{m'} - E_l)(E_{m''} - E_l)} + \frac{H'_{mm''} H'_{m''l} H'_{lm'}}{(E_m - E_l)(E_{m''} - E_l)} \right]$$

$$+ \frac{1}{2} \sum_{ll'} H'_{ml} H'_{ll'} H'_{l'm'} \left[\frac{1}{(E_m - E_l)(E_m - E_{l'})} + \frac{1}{(E_{m'} - E_l)(E_{m'} - E_{l'})} \right]. \tag{2–34d}$$

Note that for every j we have $H^{(j)}_{ml} = H^{(j)}_{lm} = 0$, but $H^{(j)}_{ll'}$ need not be zero. Since we are only interested in set A, we do not need the expression for $H^{(j)}_{ll'}$. Now we have reduced our original $(m + l)$ dimensional eigenvalue problem (2–24) to an m dimensional one. The first 4 terms of this m dimensional Hamiltonian is given by equation (2–34).

21

Going back to our original $\mathbf{k} \cdot \mathbf{p}$ eigenvalue problem, if we are only interested in lowest conduction bands and the highest valence bands, then these bands are what we called set *A* and all other distant bands make up the set *B*. Depending on the number of bands we are interested in (the number of bands in set *A*), we may have the 6-band Luttinger model, 8-band Kane model, 14-band extended Kane model etc. The work in this thesis is done using the 8-band Kane model. In the next chapter, we will use the $\mathbf{k} \cdot \mathbf{p}$ method and the Löwdin's perturbation theory together to study the band structure of bulk III-V semiconductor materials in the absence of a external magnetic field. Only after we understand this problem we are able to tackle more complicated problems such as the Landau levels in a magnetic field, quantum confinement potential coming from the semiconductor superlattices, and magneto-optical properties of semiconductor materials, whether it is bulk or low-dimensional.

CHAPTER 3
BAND STRUCTURE OF III-V SEMICONDUCTOR MATERIALS

3.1   Unperturbed Problem—Basis Functions

We have derived a working method to diagonalize the $\boldsymbol{k} \cdot \boldsymbol{p}$ Hamiltonian (2–18), namely, the Lowdin's perturbation theory. Like any other quantum mechanics perturbation theory, the first step is to solve the unperturbed problem. Since we are mostly concerned about a very small volume of $\boldsymbol{k}$-space near the center of the Brillouin zone, $\boldsymbol{k}$ is very small and in equation (2–18) we can treat the term linear in $\boldsymbol{k}$ as a perturbation. We don't need to treat the $\frac{\hbar^2 k^2}{2m_0}$ term as a perturbation because this part of the Hamiltonian is already diagonal. The unperturbed eigenvalue problem is

$$\sum_{n'} [E_{n'}(\boldsymbol{0})\delta_{nn'} + \Delta_{nn'}] \, c_{n'}(\boldsymbol{k}) = E'(\boldsymbol{k})c_n(\boldsymbol{k}), \qquad (3\text{–}1)$$

where

$$E'(\boldsymbol{k}) = E(\boldsymbol{k}) - \frac{\hbar^2 k^2}{2m_0}. \qquad (3\text{–}2)$$

Recall that $c_{n'}(\boldsymbol{k})$ is the expansion coefficient of the general solution $u_{\boldsymbol{k}}(\boldsymbol{r})$:

$$u_{\boldsymbol{k}}(\boldsymbol{r}) = \sum_{n'} c_{n'}(\boldsymbol{k})u_{n'\boldsymbol{0}}(\boldsymbol{r}), \qquad (3\text{–}3)$$

where $u_{n'\boldsymbol{0}}(\boldsymbol{r})$ is the band edge basis function without spin-orbit interaction. Although we do not know the function form of the band edge eigenstates, we know that they transformed according to the irreducible representation of the point group of the crystal. For III-V semiconductors such as GaAs and InSb, the point group is the tetrahedral group (T_d group). Following the notation of Koster [21, 22], the five irreducible representations of T_d are Γ_i for $i = 1, 2, 3, 4, 5$. The lowest conduction band belongs to the Γ_1 representation and its eigenstate transforms as the atomic s-orbital (orbital angular momentum $l = 0$), thus we can label this conduction band edge function as $|S\rangle$. Similarly, the highest valence band belongs to the Γ_5 representation and it has three degenerated eigenstates that transform as the atomic p-orbital (orbital

angular momentum $l = 1$), which can be labeled as $|X\rangle$, $|Y\rangle$ and $|Z\rangle$. Now we have four band edge states near the fundamental gap: $|S\rangle$, $|X\rangle$, $|Y\rangle$ and $|Z\rangle$. Including spin degree of freedom but not spin-orbit interaction, we have 8 band edge states:

$$|\nu'\sigma'\rangle = \{|S\uparrow\rangle, |X\uparrow\rangle, |Y\uparrow\rangle, |Z\uparrow\rangle, |S\downarrow\rangle, |X\downarrow\rangle, |Y\downarrow\rangle, |Z\downarrow\rangle\} \qquad (3\text{–}4)$$

When spin-orbit interaction is considered as in equation (3–1), the band edge eigenstates are classified according to the double group for the T_d group. The irreducible representation of the double group can be obtained from taking the direct product of the corresponding single group representation with the irreducible representation of the spinor which we call Γ_6. Group theory tell us that

$$\Gamma_1 \otimes \Gamma_6 = \Gamma_6 \qquad (3\text{–}5a)$$

$$\Gamma_5 \otimes \Gamma_6 = \Gamma_7 + \Gamma_8 \qquad (3\text{–}5b)$$

So the original conduction band of Γ_1 representation becomes Γ_6 and the valence band of Γ_5 representation becomes Γ_7 and Γ_8. This will split the 6-fold degenerate valence band at $\mathbf{k} = 0$ into two sets: the 4-fold degenerate Γ_8 band and the 2-fold degenerate Γ_7 band. As expected the conduction band remains the same as if there is no spin-orbit interaction because the conduction band is "s like" and the orbit angular momentum $l = 0$.

Although the functions given in equation (3–4) can serve as a basis when spin-orbit interaction is included, they are not the eigenstates for total angular momentum $J = L+S$, and the matrix $\Delta_{\nu\sigma,\nu'\sigma'}$ in equation (3–1) is not diagonal. It is better to choose a new set of basis functions that can diagonalize the spin-orbit interaction Hamiltonian. Such a set of basis functions can be obtained by doing the problem of the addition of angular momenta. The four eigenstates of the orbit angular momentum $|l, m_l\rangle$ can be defined as

(similar to the spherical harmonics)

$$|0, 0\rangle = |iS\rangle \tag{3–6a}$$

$$|1, 1\rangle = -|X + iY\rangle/\sqrt{2} \tag{3–6b}$$

$$|1, 0\rangle = |Z\rangle \tag{3–6c}$$

$$|1, -1\rangle = |X - iY\rangle/\sqrt{2}, \tag{3–6d}$$

and the two spin eigenstates $|s, m_s\rangle$ can be written as

$$\left|\frac{1}{2}, +\frac{1}{2}\right\rangle = |\uparrow\rangle \tag{3–7a}$$

$$\left|\frac{1}{2}, -\frac{1}{2}\right\rangle = |\downarrow\rangle. \tag{3–7b}$$

For the $l = 0$ conduction bands, the total angular momentum $j = 0 + 1/2$, and for the $l = 1$ valence bands, the total angular momentum $j = 1 \pm 1/2$. Using the standard technique of addition of angular momentum we can obtain the basis functions $|j, m_j\rangle$ from equation (3–6) and (3–7),

$$\left|\frac{1}{2}, +\frac{1}{2}\right\rangle_c = |iS \uparrow\rangle \tag{3–8a}$$

$$\left|\frac{1}{2}, -\frac{1}{2}\right\rangle_c = |iS \downarrow\rangle \tag{3–8b}$$

$$\left|\frac{3}{2}, +\frac{3}{2}\right\rangle_v = -\frac{1}{\sqrt{2}}|(X + iY) \uparrow\rangle \tag{3–8c}$$

$$\left|\frac{3}{2}, +\frac{1}{2}\right\rangle_v = -\frac{1}{\sqrt{6}}|(X + iY) \downarrow -2Z \uparrow\rangle \tag{3–8d}$$

$$\left|\frac{3}{2}, -\frac{1}{2}\right\rangle_v = \frac{1}{\sqrt{6}}|(X - iY) \uparrow +2Z \downarrow\rangle \tag{3–8e}$$

$$\left|\frac{3}{2}, -\frac{3}{2}\right\rangle_v = \frac{1}{\sqrt{2}}|(X - iY) \downarrow\rangle \tag{3–8f}$$

$$\left|\frac{1}{2}, +\frac{1}{2}\right\rangle_v = -\frac{1}{\sqrt{3}}|(X + iY) \downarrow +Z \uparrow\rangle \tag{3–8g}$$

$$\left|\frac{1}{2}, -\frac{1}{2}\right\rangle_v = -\frac{1}{\sqrt{3}}|(X - iY) \uparrow -Z \downarrow\rangle. \tag{3–8h}$$

25

The phase convention in equation (3–8) is chosen to be agree with the Clebsch-Gordan coefficients. We have a slightly different phase convention and re-order these 8 states to form a basis which we use in our calculations. Our basis functions from now on read as the following:

$$|1\rangle = |CB\uparrow\rangle = \left|\frac{1}{2}, +\frac{1}{2}\right\rangle_c = |S\uparrow\rangle \tag{3–9a}$$

$$|2\rangle = |HH\uparrow\rangle = \left|\frac{3}{2}, +\frac{3}{2}\right\rangle_v = \frac{1}{\sqrt{2}}|(X+iY)\uparrow\rangle \tag{3–9b}$$

$$|3\rangle = |LH\downarrow\rangle = \left|\frac{3}{2}, -\frac{1}{2}\right\rangle_v = \frac{1}{\sqrt{6}}|(X-iY)\uparrow +2Z\downarrow\rangle \tag{3–9c}$$

$$|4\rangle = |SO\downarrow\rangle = \left|\frac{1}{2}, -\frac{1}{2}\right\rangle_v = \frac{i}{\sqrt{3}}|-(X-iY)\uparrow +Z\downarrow\rangle \tag{3–9d}$$

$$|5\rangle = |CB\downarrow\rangle = \left|\frac{1}{2}, -\frac{1}{2}\right\rangle_c = |S\downarrow\rangle \tag{3–9e}$$

$$|6\rangle = |HH\downarrow\rangle = \left|\frac{3}{2}, -\frac{3}{2}\right\rangle_v = \frac{i}{\sqrt{2}}|(X-iY)\downarrow\rangle \tag{3–9f}$$

$$|7\rangle = |LH\uparrow\rangle = \left|\frac{3}{2}, +\frac{1}{2}\right\rangle_v = \frac{i}{\sqrt{6}}|(X+iY)\downarrow -2Z\uparrow\rangle \tag{3–9g}$$

$$|8\rangle = |SO\uparrow\rangle = \left|\frac{1}{2}, +\frac{1}{2}\right\rangle_v = \frac{1}{\sqrt{3}}|(X+iY)\downarrow +Z\uparrow\rangle. \tag{3–9h}$$

We can directly verify that, using the basis functions in (3–9), the unperturbed Hamiltonian is diagonalized and its matrix form in equation (3–1) is

$$H^{(0)} = \begin{bmatrix} A & 0 \\ 0 & A \end{bmatrix} \tag{3–10}$$

where

$$A = \begin{bmatrix} E_s & 0 & 0 & 0 \\ 0 & E_p + \Delta/3 & 0 & 0 \\ 0 & 0 & E_p + \Delta/3 & 0 \\ 0 & 0 & 0 & E_p - 2\Delta/3. \end{bmatrix} \tag{3–11}$$

Here E_s and E_p are the band edge energy without spin-orbit interaction

$$E_s = \langle S| \left[\frac{\mathbf{p}^2}{2m_0} + V_0(\mathbf{r}) \right] |S\rangle \tag{3–12a}$$

$$E_p = \langle Z| \left[\frac{\mathbf{p}^2}{2m_0} + V_0(\mathbf{r}) \right] |Z\rangle, \tag{3–12b}$$

and the spin-orbit split-off energy Δ is defined as

$$\Delta = \frac{3i\hbar}{4m_0^2 c^2} \left\langle X \left| \frac{\partial V_0}{\partial x} p_y - \frac{\partial V_0}{\partial y} p_x \right| Y \right\rangle. \tag{3–13}$$

Choosing the energy reference point of V_0, we can let $E_p = -\Delta/3$ and define $E_g = E_s$, so that the 4×4 matrix A in equation (3–10) can be written as

$$A = \begin{bmatrix} E_g & 0 & 0 & 0 \\ 0 & 0 & 0 & 0 \\ 0 & 0 & 0 & 0 \\ 0 & 0 & 0 & -\Delta \end{bmatrix}. \tag{3–14}$$

We have already solved the eigenvalue problem for the unperturbed Hamiltonian, the eigenstates of which are given by equation (3–9). The first 4 states are degenerate with the last 4 states, respectively, and the energy for them are: E_g (for conduction band), 0 (for heavy and light hole bands) and $-\Delta$ (for spin-orbit band). This concludes our first step in Löwdin perturbations. In the following sections we will go to the next step in Löwdin perturbations.

3.2 $k \cdot p$ Perturbation Without Coupling to Distant Bands

In the previous section we diagonalized the zeroth order Hamiltonian and obtained the band edge energy and basis states in the presence of spin-orbit interaction but without the $\mathbf{k} \cdot \mathbf{p}$ coupling between different bands. In the next level of Löwdin perturbation theory the perturbating Hamiltonian is given by equation (2–34b). In the context of our eigenvalue problem given by equation (2–18), the perturbating Hamiltonian is just the term $\frac{\hbar}{m_0}\mathbf{k} \cdot \boldsymbol{\pi}_{nn'}$ or $\frac{\hbar}{m_0}\mathbf{k} \cdot \mathbf{p}_{nn'}$. Note that at this level of perturbation,

the $\boldsymbol{k} \cdot \boldsymbol{p}$ term only couples those states coming from "set A", i.e., n and n' are chosen from the eight basis states in equation (3–9). Coupling to distant bands will be treated in the higher order perturbation.

Group theory shows that the only non-zero momentum matrix elements within our basis states in (3–4) are of the form $\langle S|p_z|Z \rangle$, and all the other ones such as $\langle S|p_x|Y \rangle$ and $\langle X|p_z|Z \rangle$ vanish. We only have three non-zero momentum matrix elements and they are all equal, so we can define the Kane's parameter V as

$$V = -i\frac{\hbar}{m_0}\langle S|p_x|X \rangle = -i\frac{\hbar}{m_0}\langle S|p_y|Y \rangle = -i\frac{\hbar}{m_0}\langle S|p_z|Z \rangle. \tag{3–15}$$

It is also convenient to define the "plus" and "minus" wave vector

$$k_{\pm} = k_x \pm ik_y. \tag{3–16}$$

Now our first order perturbation Hamiltonian in the matrix form is

$$H^{(1)} = \begin{bmatrix} 0 & \frac{i}{\sqrt{2}}Vk_+ & \frac{i}{\sqrt{6}}Vk_- & \frac{1}{\sqrt{3}}Vk_- & 0 & 0 & \sqrt{\frac{2}{3}}Vk_z & \frac{i}{\sqrt{3}}Vk_z \\ -\frac{i}{\sqrt{2}}Vk_- & 0 & 0 & 0 & 0 & 0 & 0 & 0 \\ -\frac{i}{\sqrt{6}}Vk_+ & 0 & 0 & 0 & -i\sqrt{\frac{2}{3}}Vk_z & 0 & 0 & 0 \\ \frac{1}{\sqrt{3}}Vk_+ & 0 & 0 & 0 & -\frac{1}{\sqrt{3}}Vk_z & 0 & 0 & 0 \\ 0 & 0 & i\sqrt{\frac{2}{3}}Vk_z & -\frac{1}{\sqrt{3}}Vk_z & 0 & -\frac{1}{\sqrt{2}}Vk_- & -\frac{1}{\sqrt{6}}Vk_+ & \frac{i}{\sqrt{3}}Vk_+ \\ 0 & 0 & 0 & 0 & -\frac{1}{\sqrt{2}}Vk_+ & 0 & 0 & 0 \\ \sqrt{\frac{2}{3}}Vk_z & 0 & 0 & 0 & -\frac{1}{\sqrt{6}}Vk_- & 0 & 0 & 0 \\ -\frac{i}{\sqrt{3}}Vk_z & 0 & 0 & 0 & -\frac{i}{\sqrt{3}}Vk_- & 0 & 0 & 0 \end{bmatrix}. \tag{3–17}$$

We can add $H^{(0)}$ and $H^{(1)}$ together to obtain our Hamiltonian H: $H = H^{(0)} + H^{(1)}$. The explicit form of the matrix H is given by

$$H = \begin{bmatrix} E_g & \frac{i}{\sqrt{2}}Vk_+ & \frac{i}{\sqrt{6}}Vk_- & \frac{1}{\sqrt{3}}Vk_- & 0 & 0 & \sqrt{\frac{2}{3}}Vk_z & \frac{i}{\sqrt{3}}Vk_z \\ -\frac{i}{\sqrt{2}}Vk_- & 0 & 0 & 0 & 0 & 0 & 0 & 0 \\ -\frac{i}{\sqrt{6}}Vk_+ & 0 & 0 & 0 & -i\sqrt{\frac{2}{3}}Vk_z & 0 & 0 & 0 \\ \frac{1}{\sqrt{3}}Vk_+ & 0 & 0 & -\Delta & -\frac{1}{\sqrt{3}}Vk_z & 0 & 0 & 0 \\ 0 & 0 & i\sqrt{\frac{2}{3}}Vk_z & -\frac{1}{\sqrt{3}}Vk_z & E_g & -\frac{1}{\sqrt{2}}Vk_- & -\frac{1}{\sqrt{6}}Vk_+ & \frac{i}{\sqrt{3}}Vk_+ \\ 0 & 0 & 0 & 0 & -\frac{1}{\sqrt{2}}Vk_+ & 0 & 0 & 0 \\ \sqrt{\frac{2}{3}}Vk_z & 0 & 0 & 0 & -\frac{1}{\sqrt{6}}Vk_- & 0 & 0 & 0 \\ -\frac{i}{\sqrt{3}}Vk_z & 0 & 0 & 0 & -\frac{i}{\sqrt{3}}Vk_- & 0 & 0 & -\Delta \end{bmatrix}.$$

$$(3\text{--}18)$$

For any wave vector k that is in the first Brillouin (but not need to be small), we can diagonalize the matrix H in equation (3–18) to obtain the electron energy and their wave function in terms of the linear combination of the eight basis states. Numerically diagonalizing a 8×8 matrix can be done very easily but it is hard to do it analytically. However if the wave vector k is restricted near the band edge, i.e., k is small compared with the size of the Brillouin zone, then we can diagonalize H in equation (3–18) using the two-step procedure: [7] first consider the special case when k is in the $\hat{z}$ direction, $k = k\hat{z}$ and diagonalize H in this special case; then using the appropriate unitary transformation to rotate the basis function to handle the general case when k is in a general direction.

In the special case when $\boldsymbol{k} = k\hat{z}$, we have $k_\pm = 0$ and k_z is replaced by the magnitude k, the Hamiltonian H becomes

$$H = \begin{bmatrix} E_g & 0 & 0 & 0 & 0 & 0 & \sqrt{\frac{2}{3}}Vk & \frac{i}{\sqrt{3}}Vk \\ 0 & 0 & 0 & 0 & 0 & 0 & 0 & 0 \\ 0 & 0 & 0 & 0 & -i\sqrt{\frac{2}{3}}Vk & 0 & 0 & 0 \\ 0 & 0 & 0 & -\Delta & -\frac{1}{\sqrt{3}}Vk & 0 & 0 & 0 \\ 0 & 0 & i\sqrt{\frac{2}{3}}Vk & -\frac{1}{\sqrt{3}}Vk & E_g & 0 & 0 & 0 \\ 0 & 0 & 0 & 0 & 0 & 0 & 0 & 0 \\ \sqrt{\frac{2}{3}}Vk & 0 & 0 & 0 & 0 & 0 & 0 & 0 \\ -\frac{i}{\sqrt{3}}Vk & 0 & 0 & 0 & 0 & 0 & 0 & -\Delta \end{bmatrix}. \tag{3–19}$$

We can immediately see that the heavy hole states $|HH\uparrow\rangle$ and $|HH\downarrow\rangle$ decouple from the rest of the states. So we have the doubly degenerate energy $E' = 0$. The rest of the states also decouple into two different blocks which we will call the "upper" block and the "lower" block. The upper block corresponding to states $|CB\uparrow\rangle$, $|LH\uparrow\rangle$ and $|SO\uparrow\rangle$ is

$$\begin{bmatrix} E_g & \sqrt{\frac{2}{3}}Vk & \frac{i}{\sqrt{3}}Vk \\ \sqrt{\frac{2}{3}}Vk & 0 & 0 \\ -\frac{i}{\sqrt{3}}Vk & 0 & -\Delta \end{bmatrix}, \tag{3–20}$$

and the lower block corresponding the states $|CB\downarrow\rangle$, $|LH\downarrow\rangle$ and $|SO\downarrow\rangle$ is

$$\begin{bmatrix} E_g & i\sqrt{\frac{2}{3}}Vk & -\frac{1}{\sqrt{3}}Vk \\ -i\sqrt{\frac{2}{3}}Vk & 0 & 0 \\ -\frac{1}{\sqrt{3}}Vk & 0 & -\Delta \end{bmatrix}. \tag{3–21}$$

We have simplify the original 8×8 dimensional problem into two 3×3 ones and two 1-dimensional ones. Although the upper and lower block matrix are different, they lead to the same secular equation

$$E'(E' - E_g)(E' + \Delta) - V^2 k^2 \left(E' + \frac{2}{3}\Delta\right) = 0. \tag{3–22}$$

This is a cubic equation which we can solve by using the standard cubic formula, but it is too tedious. Since we know that k is small, the three solutions to equation (3–22) will be close to $E' = E_g$, $E' = 0$ and $E' = -\Delta$. Assume one of the three roots is $E' = E_g + \epsilon$, we can replace in equation (3–22) $(E' - E_g)$ with ϵ and every other E' with E_g. This will give us

$$\epsilon = \frac{V^2 k^2 (E_g + 2\Delta/3)}{E_g (E_g + \Delta)}, \tag{3–23}$$

so the first root is

$$E' = E_g + \frac{V^2 k^2 (E_g + 2\Delta/3)}{E_g (E_g + \Delta)}. \tag{3–24}$$

Similar tricks give us the other two roots for E'

$$E' = -\frac{2 V^2 k^2}{3 E_g}, \tag{3–25}$$

$$E' = -\Delta - \frac{V^2 k^2}{3(E_g + \Delta)}. \tag{3–26}$$

Because the actual energy $E(\mathbf{k})$ is given by $E(\mathbf{k}) = E'(\mathbf{k}) + \hbar^2 k^2 / 2m_0$, we can summarize our results at this point that we have four different energy bands, each is two-fold degenerate, and they are given by (in the order of conduction band, heavy hole band, light hole band and spin-orbit split-off band)

$$E_{cb}(\mathbf{k}) = E_g + \frac{\hbar^2 k^2}{2m_0} + \frac{V^2 k^2 (E_g + 2\Delta/3)}{E_g (E_g + \Delta)} \tag{3–27a}$$

$$E_{hh}(\mathbf{k}) = \frac{\hbar^2 k^2}{2m_0} \tag{3–27b}$$

$$E_{lh}(\mathbf{k}) = \frac{\hbar^2 k^2}{2m_0} - \frac{2 V^2 k^2}{3 E_g} \tag{3–27c}$$

$$E_{so}(\mathbf{k}) = -\Delta + \frac{\hbar^2 k^2}{2m_0} - \frac{V^2 k^2}{3(E_g + \Delta)}. \tag{3–27d}$$

If the wave vector $\mathbf{k}$ is in a general direction specified by two polar angles θ and ϕ,

$$\mathbf{k} = k \sin\theta \cos\phi \hat{x} + k \sin\theta \sin\phi \hat{y} + k \cos\theta \hat{z}, \tag{3–28}$$

we can rotate to a new basis so that in the new basis the wave vector is in the $\hat{z}'$
direction, $\boldsymbol{k} = k\hat{z}'$. The band edge functions are also rotated to the new primed states

$$
\begin{bmatrix} X' \\ Y' \\ Z' \end{bmatrix} = \begin{bmatrix} \cos\theta\cos\phi & \cos\theta\sin\phi & -\sin\theta \\ -\sin\phi & \cos\phi & 0 \\ \sin\theta\cos\phi & \sin\theta\sin\phi & \cos\theta \end{bmatrix} \begin{bmatrix} X \\ Y \\ Z \end{bmatrix}
\tag{3–29a}
$$

$$
\begin{bmatrix} \uparrow' \\ \downarrow' \end{bmatrix} = \begin{bmatrix} e^{-i\phi/2}\cos\theta/2 & e^{i\phi/2}\sin\theta/2 \\ -e^{-i\phi/2}\sin\theta/2 & e^{i\phi/2}\cos\theta/2 \end{bmatrix} \begin{bmatrix} \uparrow \\ \downarrow \end{bmatrix} .
\tag{3–29b}
$$

Next we define the 8 primed angular momentum basis states similar to those in equation
(3–9), for example

$$
\left| \frac{3}{2}, +\frac{3}{2} \right\rangle_v' = \frac{1}{\sqrt{2}} |(X' + iY')\uparrow'\rangle .
\tag{3–30}
$$

We can directly calculate the matrix element of $H^{(0)}$ and $H^{(1)}$ with respect to the primed
basis, after a very tedious algebra we will see that both $H^{(0)}$ and $H^{(1)}$ still take the same
form as in equations (3–10) and (3–17). The reason for this can be understand from
two point of view: mathematically, the transformation matrix connecting the old and new
basis is unitary, physically, both the spin-orbit interaction and the $\boldsymbol{k} \cdot \boldsymbol{p}$ coupling term
are isotropic [23]. Since $H^{(0)}$ and $H^{(1)}$ stay the same in the new primed basis, the energy
dispersion relation in equation (3–27) still holds for the general $\boldsymbol{k}$ direction.

Equation (3–27) give us four isotropic, parabolic bands near the Brillouin zone
center, each of which is doubly degenerate. We can define a scalar effective mass for
each band. Note that in the current model the heavy hole dispersion is still the same
as a free electron, which is certainly wrong. This is because we have not include the
coupling between our 8 basis states from set A and remote bands in set B. Once
coupling with remote bands is considered, we will get a better approximation for the
effective mass, and we will also find that the bands are anisotropic [24].

3.3   Coupling to Distant Bands

In order to get the more accurate band dispersion relation near the zone center, and to account for the anisotropic properties of the bands, we need to consider the coupling effects generated by the $\frac{\hbar}{m_0} \boldsymbol{k} \cdot \boldsymbol{p}$ term between our 8 basis states in the set A and the remote bands from set B. Thus we need to go to the next order in the Löwdin's perturbation procedure. The next order correction to the Hamiltonian is given by equation (2–34c), which I will rewrite it here:

$$H^{(2)}_{mm'} = \frac{1}{2} \sum_l H'_{ml} H'_{lm'} \left[\frac{1}{E_m - E_l} + \frac{1}{E_{m'} - E_l} \right]. \tag{3–31}$$

The perturbating Hamiltonian is still $H' = \frac{\hbar}{m_0} \boldsymbol{k} \cdot \boldsymbol{p}$. Note that $H^{(2)}_{mm'}$ depends on the energy E_m and $E_{m'}$, which are the eigen energies of the band edge basis states in set A. This energy dependence will make the number of independent parameters due to coupling to the distant bands much large than if their is no energy dependence. To simplify our problem, we make the approximation that all the energies E_m and $E_{m'}$ in equation (3–31) can be replaced by an average energy $\bar{E}$, since E_l are the energy of the distant band so that the energy difference between E_m and $E_{m'}$ is small compared with the difference between E_m (or $E_{m'}$) and E_l. Now our perturbation is

$$H^{(2)}_{mm'} = \sum_l \frac{H'_{ml} H'_{lm'}}{\bar{E} - E_l}. \tag{3–32}$$

Group theory can help us to reduce the number of the independent parameters arise from the coupling due to the perturbation $H^{(2)}_{mm'}$. It turns out that, with our choice of the basis states in equation (3–9), we need four additional coupling parameters,

$$A_0 = \frac{\hbar^2}{2m_0} + \frac{\hbar^2}{m_0^2} \sum_\alpha \frac{p^x_{X\alpha} p^x_{\alpha X}}{\bar{E} - E_\alpha} \tag{3–33a}$$

$$B_0 = \frac{\hbar^2}{2m_0} + \frac{\hbar^2}{m_0^2} \sum_\alpha \frac{p^y_{X\alpha} p^y_{\alpha X}}{\bar{E} - E_\alpha} \tag{3–33b}$$

$$C_0 = \frac{\hbar^2}{m_0^2} \sum_\alpha \frac{p^x_{X\alpha} p^y_{\alpha Y} + p^y_{X\alpha} p^x_{\alpha Y}}{\bar{E} - E_\alpha} \tag{3–33c}$$

$$F_0 = \frac{1}{m_0} \sum_{\alpha} \frac{p_{S\alpha}^x p_{\alpha S}^x}{\bar{E} - E_{\alpha}}. \tag{3–33d}$$

Parameters A_0, B_0 and C_0 describe the coupling between the valence band components $|X\rangle$, $|Y\rangle$, and $|Z\rangle$, with the remote bands labeled by α. They are similar to the parameters A, B and C defined by Luttinger and Kohn in their original paper [17]. The only difference is that our parameters do not have the contribution that comes from the coupling between the lowest conduction band with the highest valence bands, because our model is 8-dimensional which already include this contribution. We have to define one more parameter F_0 because we need to consider the coupling between lowest conduction band with remote bands. Next we define the renormalized Luttinger parameter

$$\frac{\hbar^2}{2m_0}\gamma_1 = -\frac{1}{3}(A_0 + 2B_0) \tag{3–34a}$$

$$\frac{\hbar^2}{2m_0}\gamma_2 = -\frac{1}{6}(A_0 - B_0) \tag{3–34b}$$

$$\frac{\hbar^2}{2m_0}\gamma_3 = -\frac{1}{6}C_0 \tag{3–34c}$$

$$\gamma_4 = 1 + 2F_0. \tag{3–34d}$$

Our renormalized Luttinger parameters are related to the original Luttinger parameters γ_1^L, γ_2^L and γ_3^L through the following equations

$$\gamma_1 = \gamma_1^L - E_p/3E_g \tag{3–35a}$$

$$\gamma_2 = \gamma_2^L - E_p/6E_g \tag{3–35b}$$

$$\gamma_3 = \gamma_3^L - E_p/6E_g, \tag{3–35c}$$

where

$$E_P = \frac{2m_0 V^2}{\hbar^2} \tag{3–36}$$

is a measure of the coupling strength between conduction and valence bands.

Now we can calculate the matrix element of the second order perturbating Hamiltonian $H^{(2)}_{mm'}$,

$$H^{(2)}_{mm'} + \frac{\hbar^2 k^2}{2m_0}\delta_{mm'} = \begin{bmatrix} A & 0 & 0 & 0 & 0 & 0 & 0 & 0 \\ 0 & -P-Q & -M & i\sqrt{2}M & 0 & 0 & -L & -\frac{i}{\sqrt{2}}L \\ 0 & -M^* & -P+Q & i\sqrt{2}Q & 0 & L & 0 & i\sqrt{\frac{3}{2}}L^* \\ 0 & -i\sqrt{2}M^* & -i\sqrt{2}Q & -P & 0 & -\frac{i}{\sqrt{2}}L & i\sqrt{\frac{3}{2}}L^* & 0 \\ 0 & 0 & 0 & 0 & A & 0 & 0 & 0 \\ 0 & 0 & L^* & \frac{i}{\sqrt{2}}L^* & 0 & -P-Q & -M^* & i\sqrt{2}M^* \\ 0 & -L^* & 0 & -i\sqrt{\frac{3}{2}}L & 0 & -M & -P+Q & i\sqrt{2}Q \\ 0 & \frac{i}{\sqrt{2}}L^* & -i\sqrt{\frac{3}{2}}L & 0 & 0 & -i\sqrt{2}M & -i\sqrt{2}Q & -P \end{bmatrix},$$

$$(3\text{–}37)$$

where

$$A = \gamma_4 \frac{\hbar^2 k^2}{2m_0} \tag{3–38a}$$

$$P = \gamma_1 \frac{\hbar^2 k^2}{2m_0} \tag{3–38b}$$

$$Q = \gamma_2 \frac{\hbar^2}{2m_0}(k_x^2 + k_y^2 - 2k_z^2) \tag{3–38c}$$

$$L = -i\sqrt{3}\gamma_3 \frac{\hbar^2}{m_0}k_- k_z \tag{3–38d}$$

$$M = \sqrt{3}\frac{\hbar^2}{2m_0}[\gamma_2(k_x^2 - k_y^2) - 2i\gamma_3 k_x k_y]. \tag{3–38e}$$

35

By adding $H^{(0)}$, $H^{(1)}$, $H^{(2)}$ and the diagonal term $\frac{\hbar^2 k^2}{2m_0}$ together we can get the total Hamiltonian H

$$
H = \begin{bmatrix}
E_g + A & \frac{i}{\sqrt{2}}Vk_+ & \frac{i}{\sqrt{6}}Vk_- & \frac{1}{\sqrt{3}}Vk_- & 0 & 0 & \sqrt{\frac{2}{3}}Vk_z & \frac{i}{\sqrt{3}}Vk_z \\
-\frac{i}{\sqrt{2}}Vk_- & -P - Q & -M & i\sqrt{2}M & 0 & 0 & -L & -\frac{i}{\sqrt{2}}L \\
-\frac{i}{\sqrt{6}}Vk_+ & -M^* & -P + Q & i\sqrt{2}Q & -i\sqrt{\frac{2}{3}}Vk_z & L & 0 & i\sqrt{\frac{3}{2}}L^* \\
\frac{1}{\sqrt{3}}Vk_+ & -i\sqrt{2}M^* & -i\sqrt{2}Q & -P - \Delta & -\frac{1}{\sqrt{3}}Vk_z & -\frac{i}{\sqrt{2}}L & i\sqrt{\frac{3}{2}}L^* & 0 \\
0 & 0 & i\sqrt{\frac{2}{3}}Vk_z & -\frac{1}{\sqrt{3}}Vk_z & E_g + A & -\frac{1}{\sqrt{2}}Vk_- & -\frac{1}{\sqrt{6}}Vk_+ & \frac{i}{\sqrt{3}}Vk_+ \\
0 & 0 & L^* & \frac{i}{\sqrt{2}}L^* & -\frac{1}{\sqrt{2}}Vk_+ & -P - Q & -M^* & i\sqrt{2}M^* \\
\sqrt{\frac{2}{3}}Vk_z & -L^* & 0 & -i\sqrt{\frac{3}{2}}L & -\frac{1}{\sqrt{6}}Vk_- & -M & -P + Q & i\sqrt{2}Q \\
-\frac{i}{\sqrt{3}}Vk_z & \frac{i}{\sqrt{2}}L^* & -i\sqrt{\frac{3}{2}}L & 0 & -\frac{i}{\sqrt{3}}Vk_- & -i\sqrt{2}M & -i\sqrt{2}Q & -P - \Delta
\end{bmatrix} .
$$

$$(3\text{–}39)$$

Here I want to emphasize that this Hamiltonian in equation (3–39) have already taken into account the crystal periodic potential, the spin-orbit interactions, the $\boldsymbol{k} \cdot \boldsymbol{p}$ coupling effects with the remote bands, and finally the diagonal term $\frac{\hbar^2 k^2}{2m_0}$. So we can get the energy of the electron by diagonalizing this H. This is a much complicated Hamiltonian than the one in equation (3–18) and it is impossible to solve analytically without further simplifications. It is possible to solve this eigenvalue problems analytically for some special cases for example if k_z vanishes. In this case the Hamiltonian in equation (3–39) has a block diagonal form, decoupling into two 4×4 problems. However we will not go further in this direction since we can solve the full 8×8 problems numerically anyway. The real problem we are interested in is when there is an external magnetic field, what is the band structure look like.

CHAPTER 4
LANDAU LEVELS OF GALLIUM ARSENIDE

4.1   The Envelope Function Approximation

When there is an external magnetic field applied to the bulk III-V semiconductor sample such as GaAs, the Schrödinger equation does not take the form of equation (2–11) any more. Instead we need to go back to the Dirac equation for the electron in the periodic potential in the presence of the external field. The non-relativistic approximation of the Dirac equation for the large component spinor wave function becomes

$$\left[\frac{(-i\hbar\nabla + \frac{e}{c}\boldsymbol{A})^2}{2m_0} + V_0(\boldsymbol{r}) + \frac{\hbar}{4m_0^2 c^2}(-i\hbar\nabla + \frac{e}{c}\boldsymbol{A}) \cdot \boldsymbol{\sigma} \times (\nabla V_0) + \mu_B \boldsymbol{\sigma} \cdot \boldsymbol{B} \right] \Psi(\boldsymbol{r}) = E\Psi(\boldsymbol{r}) \quad (4\text{–}1)$$

where A is the vector potential and μ_B is the Bohr magneton $\mu_B = e\hbar/2m_0 c$. We have already assumed the scalar potential is zero since we are only interested in the case of a static magnetic field. The magnetic field is given by $B = \nabla \times A(\boldsymbol{r})$.

We know that wave function for the Bloch electron can be expressed as a plain wave times a function with the same periodicity as the crystal lattice. Similarly, the solution to equation (4–1) can be written as

$$\Psi(\boldsymbol{r}) = \sum_{n'} \psi_{n'}(\boldsymbol{r}) u_{n'\boldsymbol{0}}(\boldsymbol{r}), \quad (4\text{–}2)$$

where the $u_{n'\boldsymbol{0}}(\boldsymbol{r})$ are still the band edge spinor functions including both the set A and set B. The spinor functions in set A are still given by equation (3–9). The functions $\psi_{n'}(\boldsymbol{r})$ are called envelope functions. Substitute equation (4–2) into equation (4–1), multiply from the left by $u_{n\boldsymbol{0}}^{\dagger}(\boldsymbol{r})$, and then integrate over a unit cell, we obtain

$$\sum_{n'} \left\{ \left[E_{n'}(\boldsymbol{0}) + \frac{(-i\hbar\nabla + e\boldsymbol{A}/c)^2}{2m_0} \right] \delta_{nn'} + \frac{1}{m_0}(-i\hbar\nabla + e\boldsymbol{A}/c) \cdot \boldsymbol{\pi}_{nn'} \right.$$

$$\left. + \Delta_{nn'} + \mu_B \langle n|\boldsymbol{\sigma} \cdot \boldsymbol{B}|n'\rangle \right\} \psi_{n'}(\boldsymbol{r}) = E\psi_n(\boldsymbol{r}), \quad (4\text{–}3)$$

which is a system of coupled differential equations. We can still using the Löwdin's perturbation method to reduce the infinite numbers of equations to a tractable set, for example by using the basis given by equation (3–9) we can obtain a 8 dimensional eigenvalue problem. The Hamiltonian in equation (4–3) is called EFA (Envelope Function Approximation) Hamiltonian. The eigenvector of the EFA Hamiltonian is the set of envelope functions. The electronic wave function is obtained by using equation (4–2) once we know those envelope functions.

4.2 Explicit Form of the EFA Hamiltonian

We have already derived the explicit form of the Hamiltonian when there is no magnetic field. In the presence of an external magnetic field, we want to derive a similar matrix from which we can obtain the eigenenergy and the envelope functions. Comparing equation (2–18) and (4–3) we can see that the magnetic field effect is built into the set of coupled differential equations through replacing the wave vector $\hbar\boldsymbol{k}$ with the operator $-i\hbar\nabla + e\boldsymbol{A}/c$, and adding the $\mu_B\boldsymbol{\sigma} \cdot \boldsymbol{B}$ term explicitly. This similarity can help us to derive the EFA matrix in a similar way to the case when there is no magnetic field. Instead of deriving the EFA matrix from equation (4–3) directly from the beginning, we can use the matrix form in equation (3–39) as a starting point. Replacing the wave vector $\hbar\boldsymbol{k}$ in equation (3–39) with the operator $-i\hbar\nabla + e\boldsymbol{A}/c$, and adding the matrix element $\mu_B\langle n|\boldsymbol{\sigma} \cdot \boldsymbol{B}|n'\rangle$, we arrive at the matrix form of the EFA Hamiltonian. However there is a subtle point that we must pay special attention to during this process. In what follows I will explain this subtle point in a little bit detail.

In the absence of the magnetic field, the different component of the wave vector commute with each other ($[k_x, k_y] = 0$ etc.). When there is a magnetic field around, the different components of the mechanic momentum $\hbar\boldsymbol{k}(= -i\hbar\nabla + e\boldsymbol{A}/c)$ vector do not commute. We can directly calculate the commutator using the definition of the mechanic momentum operator to get

$$[k_i, k_j] = \frac{e}{i\hbar c}\epsilon_{ijk}B_k, \tag{4–4}$$

or in terms of the vector product

$$k \times k = \frac{e}{i\hbar c}B.$$ (4–5)

In our original derivation of the matrix $H^{(2)}_{mm'}$ in equation (3–37), we will typically encounter the term that containing the product of the two components of the wave vector

$$
\begin{aligned}
H^{(2)}_{mm'} &= \sum_l \frac{H'_{ml}H'_{lm'}}{\bar{E} - E_l} \\
&= \frac{\hbar^2}{m_0^2} \sum_{\alpha\beta} \sum_l k_\alpha k_\beta \frac{p^\alpha_{ml} p^\beta_{lm'}}{\bar{E} - E_l} \\
&= \sum_{\alpha\beta} D^{\alpha\beta}_{mm'} k_\alpha k_\beta.
\end{aligned}
$$ (4–6)

where the definition of $D^{\alpha\beta}_{mm'}$ is given by

$$D^{\alpha\beta}_{mm'} = \frac{\hbar^2}{m_0^2} \sum_l \frac{p^\alpha_{ml} p^\beta_{lm'}}{\bar{E} - E_l}$$ (4–7)

If the two components of the wave vector commute, we can construct the coefficients to be symmetric about interchanging the α and β indices,

$$H^{(2)}_{mm'} = \sum_{\alpha\beta} D^{(S)\alpha\beta}_{mm'} k_\alpha k_\beta$$ (4–8a)

$$D^{(S)\alpha\beta}_{mm'} = \frac{1}{2} D^{\alpha\beta}_{mm'} + \frac{1}{2} D^{\beta\alpha}_{mm'}.$$ (4–8b)

In the presence of a magnetic field, the two components of the k operator do not commute, $k_\alpha k_\beta \neq k_\beta k_\alpha$, and we can write $k_\alpha k_\beta$ as

$$k_\alpha k_\beta = \frac{1}{2}\{k_\alpha, k_\beta\} + \frac{1}{2}[k_\alpha, k_\beta]$$ (4–9)

where the commutator is $[k_\alpha, k_\beta] = k_\alpha k_\beta - k_\beta k_\alpha$ and the anticommutator is $\{k_\alpha, k_\beta\} = k_\alpha k_\beta + k_\beta k_\alpha$. Now the matrix elements $H^{(2)}_{mm'}$ can be written as

$$H^{(2)}_{mm'} = \frac{1}{2} \sum_{\alpha\beta} D^{\alpha\beta}_{mm'} \{k_\alpha, k_\beta\} + \frac{1}{2} \sum_{\alpha\beta} D^{\alpha\beta}_{mm'} [k_\alpha, k_\beta].$$ (4–10)

Again we can define the symmetric and antisymmetric part of the $D_{mm'}^{\alpha\beta}$ coefficients to be

$$D^{(S)\alpha\beta}_{mm'} = \frac{1}{2}D^{\alpha\beta}_{mm'} + \frac{1}{2}D^{\beta\alpha}_{mm'} \tag{4–11a}$$

$$D^{(A)\alpha\beta}_{mm'} = \frac{1}{2}D^{\alpha\beta}_{mm'} - \frac{1}{2}D^{\beta\alpha}_{mm'}, \tag{4–11b}$$

and write $H_{mm'}^{(2)}$ as

$$H_{mm'}^{(2)} = \frac{1}{2}\sum_{\alpha\beta} D^{(S)\alpha\beta}_{mm'}\{k_\alpha, k_\beta\} + \frac{1}{2}\sum_{\alpha\beta} D^{(A)\alpha\beta}_{mm'}[k_\alpha, k_\beta]. \tag{4–12}$$

We can see that the matrix elements $H_{mm'}^{(2)}$ has two part of contributions: a symmetric part given by the first term in equation (4–12) and an antisymmetric part given by the second term in equation (4–12). The symmetric term require us to define four independent coupling parameters A_0, B_0, C_0, and F_0 as we did in equation (3–33). We will see later that the antisymmetric term require us to define one more coupling parameter.

If we simply replace the $\hbar\mathbf{k}$ vector with the operator $-i\hbar\nabla + e\mathbf{A}/c$ in the matrix given in equation (3–37), and interpret any product of the wave vector $k_\alpha k_\beta$ as the symmetrized product $\frac{1}{2}\{k_\alpha, k_\beta\}$, we will obtain the symmetric part $H^{(S)}$ of the $H^{(2)}$ matrix. This $H^{(S)}$ matrix, together with the $H^{(0)}$, $H^{(1)}$ and the diagonal term $\frac{\hbar^2 k^2}{2m_0}\delta_{mm'}$ give us the so called Landau Hamiltonian H^L. The second term in equation (4–12) will give us the antisymmetric part $H^{(A)}$ of the $H^{(2)}$ matrix, which did not show up when there was no magnetic field applied. This $H^{(A)}$ matrix, together with the $\mu_B\boldsymbol{\sigma}\cdot\mathbf{B}$ term will give us the so-called Zeeman Hamiltonian H^Z. So we have

$$H_{mm'}^{(2)} = H_{mm'}^{(S)} + H_{mm'}^{(A)} \tag{4–13a}$$

$$H_{mm'} = \underbrace{H_{mm'}^{(0)} + H_{mm'}^{(1)} + \frac{\hbar^2 k^2}{2m_0}\delta_{mm'} + H_{mm'}^{(S)}}_{H^L} + \underbrace{H_{mm'}^{(A)} + \mu_B\langle m|\boldsymbol{\sigma}\cdot\mathbf{B}|m'\rangle}_{H^Z}. \tag{4–13b}$$

We will discuss the Landau and Zeeman Hamiltonian one by one.

4.2.1 Landau Hamiltonian

The Landau part of the Hamiltonian is given by four terms:

$$H^L = H^{(0)} + H^{(1)} + H^{(S)} + \frac{\hbar^2 k^2}{2m_0} I_{8\times 8}. \tag{4--14}$$

We can obtain the Landau Hamiltonian H^L from equation (3–39), by replacing the $\boldsymbol{k}$ wave vector with the operator

$$\hat{\boldsymbol{k}} = \frac{1}{\hbar}(-i\hbar\nabla + e\boldsymbol{A}/c), \tag{4--15}$$

and treating the wave vector product $k_\alpha k_\beta$ as the symmetrized product $\frac{1}{2}\{k_\alpha, k_\beta\}$. Note that in the original matrix in equation (3–39), the $H^{(0)}$ and $H^{(1)}$ do not contain a term like $k_\alpha k_\beta$, and the diagonal term is already symmetrized in the form of $k_\alpha k_\alpha$, so we only need to be careful about the $H^{(2)}$ contribution.

Now we can rewrite the matrix in equation (3–39), using the operators $\hat{k}_x$, $\hat{k}_y$ and $\hat{k}_z$ instead of the wave vector components k_x, k_y and k_z, to obtain the Landau part of the Hamiltonian. The explicit form of Landau Hamiltonian matrix is thus

$$H^L = \begin{bmatrix} E_g + A & \frac{i}{\sqrt{2}}V\hat{k}_+ & \frac{i}{\sqrt{6}}V\hat{k}_- & \frac{1}{\sqrt{3}}V\hat{k}_- & 0 & 0 & \sqrt{\frac{2}{3}}V\hat{k}_z & \frac{i}{\sqrt{3}}V\hat{k}_z \\ -\frac{i}{\sqrt{2}}V\hat{k}_- & -P-Q & -M & i\sqrt{2}M & 0 & 0 & -L & -\frac{i}{\sqrt{2}}L \\ -\frac{i}{\sqrt{6}}V\hat{k}_+ & -M^\dagger & -P+Q & i\sqrt{2}Q & -i\sqrt{\frac{2}{3}}V\hat{k}_z & L & 0 & i\sqrt{\frac{3}{2}}L^\dagger \\ \frac{1}{\sqrt{3}}V\hat{k}_+ & -i\sqrt{2}M^\dagger & -i\sqrt{2}Q & -P-\Delta & -\frac{1}{\sqrt{3}}V\hat{k}_z & -\frac{i}{\sqrt{2}}L & i\sqrt{\frac{3}{2}}L^\dagger & 0 \\ 0 & 0 & i\sqrt{\frac{2}{3}}V\hat{k}_z & -\frac{1}{\sqrt{3}}V\hat{k}_z & E_g+A & -\frac{1}{\sqrt{2}}V\hat{k}_- & -\frac{1}{\sqrt{6}}V\hat{k}_+ & \frac{i}{\sqrt{3}}V\hat{k}_+ \\ 0 & 0 & L^\dagger & \frac{i}{\sqrt{2}}L^\dagger & -\frac{1}{\sqrt{2}}V\hat{k}_+ & -P-Q & -M^\dagger & i\sqrt{2}M^\dagger \\ \sqrt{\frac{2}{3}}V\hat{k}_z & -L^\dagger & 0 & -i\sqrt{\frac{3}{2}}L & -\frac{1}{\sqrt{6}}V\hat{k}_- & -M & -P+Q & i\sqrt{2}Q \\ -\frac{i}{\sqrt{3}}V\hat{k}_z & \frac{i}{\sqrt{2}}L^\dagger & -i\sqrt{\frac{3}{2}}L & 0 & -\frac{i}{\sqrt{3}}V\hat{k}_- & -i\sqrt{2}M & -i\sqrt{2}Q & -P-\Delta \end{bmatrix}. \tag{4--16}$$

where the operators A, P, Q, L and M are given by

$$A = \gamma_4 \frac{\hbar^2 \hat{k}^2}{2m_0} \tag{4--17a}$$

$$P = \gamma_1 \frac{\hbar^2 \hat{k}^2}{2m_0} \tag{4–17b}$$

$$Q = \gamma_2 \frac{\hbar^2}{2m_0}(\hat{k}_x^2 + \hat{k}_y^2 - 2\hat{k}_z^2) \tag{4–17c}$$

$$L = -i\sqrt{3}\gamma_3 \frac{\hbar^2}{2m_0}(\hat{k}_-\hat{k}_z + \hat{k}_z\hat{k}_-) \tag{4–17d}$$

$$M = \sqrt{3}\frac{\hbar^2}{2m_0}[\gamma_2(\hat{k}_x^2 - \hat{k}_y^2) - i\gamma_3(\hat{k}_x\hat{k}_y + \hat{k}_y\hat{k}_x)]. \tag{4–17e}$$

4.2.2 Zeeman Hamiltonian

To be specific we will assume the magnetic field is in the $\hat{z}$ direction from now on, and we choose the Landau gauge

$$\mathbf{A} = -By\hat{x} \tag{4–18}$$

so that the magnetic field is given by

$$\mathbf{B} = \nabla \times \mathbf{A} = B\hat{z}. \tag{4–19}$$

The three operators $\hat{k}_x$, $\hat{k}_y$ and $\hat{k}_z$ are given by

$$\hat{k}_x = -i\nabla_x - \frac{y}{\lambda^2} \tag{4–20a}$$

$$\hat{k}_y = -i\nabla_y \tag{4–20b}$$

$$\hat{k}_z = -i\nabla_z \tag{4–20c}$$

where λ is the magnetic length defined by

$$\lambda^2 = \frac{\hbar c}{eB}. \tag{4–21}$$

The non-zero commutator between different components of the $\mathbf{k}$ operator is of the form

$$[\hat{k}_x, \hat{k}_y] = \frac{eB}{i\hbar c} = \frac{1}{i\lambda^2}, \tag{4–22}$$

and both $\hat{k}_x$ and $\hat{k}_y$ operators still commute with $\hat{k}_z$.

Next we want to derive the explict form of the Zeeman Hamiltonian. The Zeeman Hamiltonian has two contributions:

$$H_{mm'}^Z = H_{mm'}^{(A)} + \mu_B \langle m | \boldsymbol{\sigma} \cdot \boldsymbol{B} | m' \rangle, \tag{4–23}$$

we begin with the first one:

The definition of the antisymmetric Hamiltonian is given by the second term of equation (4–12),

$$H_{mm'}^{(A)} = \frac{1}{2} \sum_{\alpha\beta} D_{mm'}^{(A)\alpha\beta} [\hat{k}_\alpha, \hat{k}_\beta]. \tag{4–24}$$

When the magnetic field is in the $\hat{z}$ direction, the only non-zero commutator is $[\hat{k}_x, \hat{k}_y] = -[\hat{k}_y, \hat{k}_x]$, and both $\hat{k}_x$ and $\hat{k}_y$ still commute with $\hat{k}_z$, so we have two terms survive from the summation:

$$\begin{aligned}
H_{mm'}^{(A)} &= \frac{1}{2} D_{mm'}^{(A)xy} [\hat{k}_x, \hat{k}_y] + \frac{1}{2} D_{mm'}^{(A)yx} [\hat{k}_y, \hat{k}_x] \\
&= D_{mm'}^{(A)xy} [\hat{k}_x, \hat{k}_y] \\
&= \frac{1}{2} (D_{mm'}^{xy} - D_{mm'}^{yx})[\hat{k}_x, \hat{k}_y].
\end{aligned} \tag{4–25}$$

Using the definition of the $D_{mm'}^{\alpha\beta}$ coefficients in equation (4–7) and the commutation relation given in equation (4–22), we can write $H_{mm'}^{(A)}$ as

$$H_{mm'}^{(A)} = \frac{1}{2} \frac{eB}{i\hbar c} \frac{\hbar^2}{m_0^2} \sum_\alpha \frac{p_{m\alpha}^x p_{\alpha m'}^y - p_{m\alpha}^y p_{\alpha m'}^x}{\bar{E} - E_\alpha}. \tag{4–26}$$

We can immediately see that we need another coupling constant K_0 besides the already defined constants A_0, B_0, C_0 and F_0 in equation (3–33). The coupling constant K_0 is defined as

$$K_0 = \frac{\hbar^2}{m_0^2} \sum_\alpha \frac{p_{X\alpha}^x p_{\alpha Y}^y - p_{X\alpha}^y p_{\alpha Y}^x}{\bar{E} - E_\alpha}. \tag{4–27}$$

We also define the renormalized Luttinger parameter κ through the relation

$$\frac{\hbar^2}{m_0}(3\kappa + 1) = -K_0 \tag{4–28}$$

where κ is related to the original Luttinger parameter κ^L through $\kappa = \kappa^L - E_p/6E_g$. For the Luttinger parameter κ^L, we use the approximation[14, 15, 25]

$$\kappa^L = \gamma_3^L + \frac{2}{3}\gamma_2^L - \frac{1}{3}\gamma_1^L - \frac{2}{3}. \tag{4-29}$$

With these definitions we can calculate the explict form of the $H^{(A)}$ matrix from equation (4-26), the result is

$$H^{(A)} = \mu_B B \begin{bmatrix} 0 & 0 & 0 & 0 & 0 & 0 & 0 & 0 \\ 0 & -3\kappa - 1 & 0 & 0 & 0 & 0 & 0 & 0 \\ 0 & 0 & \kappa + \frac{1}{3} & -i\sqrt{2}(\kappa + \frac{1}{3}) & 0 & 0 & 0 & 0 \\ 0 & 0 & i\sqrt{2}(\kappa + \frac{1}{3}) & 2\kappa + \frac{2}{3} & 0 & 0 & 0 & 0 \\ 0 & 0 & 0 & 0 & 0 & 0 & 0 & 0 \\ 0 & 0 & 0 & 0 & 0 & 3\kappa + 1 & 0 & 0 \\ 0 & 0 & 0 & 0 & 0 & 0 & -\kappa - \frac{1}{3} & i\sqrt{2}(\kappa + \frac{1}{3}) \\ 0 & 0 & 0 & 0 & 0 & 0 & -i\sqrt{2}(\kappa + \frac{1}{3}) & -2\kappa - \frac{2}{3} \end{bmatrix}. \tag{4-30}$$

Next we calculate the matrix element of $\mu_B\langle m|\boldsymbol{\sigma} \cdot \boldsymbol{B}|m'\rangle$. Noting that the magnetic field is in the $\hat{z}$ direction we have $\boldsymbol{\sigma} \cdot \boldsymbol{B} = \sigma_z B$. The result of the $\mu_B\langle m|\boldsymbol{\sigma} \cdot \boldsymbol{B}|m'\rangle$ matrix takes the form

$$\mu_B\langle m|\boldsymbol{\sigma} \cdot \boldsymbol{B}|m'\rangle = \mu_B B \begin{bmatrix} 1 & 0 & 0 & 0 & 0 & 0 & 0 & 0 \\ 0 & 1 & 0 & 0 & 0 & 0 & 0 & 0 \\ 0 & 0 & -\frac{1}{3} & -\frac{2\sqrt{2}}{3}i & 0 & 0 & 0 & 0 \\ 0 & 0 & \frac{2\sqrt{2}}{3}i & \frac{1}{3} & 0 & 0 & 0 & 0 \\ 0 & 0 & 0 & 0 & -1 & 0 & 0 & 0 \\ 0 & 0 & 0 & 0 & 0 & -1 & 0 & 0 \\ 0 & 0 & 0 & 0 & 0 & 0 & \frac{1}{3} & \frac{2\sqrt{2}}{3}i \\ 0 & 0 & 0 & 0 & 0 & 0 & -\frac{2\sqrt{2}}{3}i & -\frac{1}{3} \end{bmatrix}. \tag{4-31}$$

44

Now we can add equation (4–30) and (4–31) together to get the explicit form of the Zeeman Hamiltonian

$$
H^Z = 2\mu_B B
\begin{bmatrix}
\frac{1}{2} & 0 & 0 & 0 & 0 & 0 & 0 & 0 \\
0 & -\frac{3}{2}\kappa & 0 & 0 & 0 & 0 & 0 & 0 \\
0 & 0 & \frac{1}{2}\kappa & -i\sqrt{\frac{1}{2}}(\kappa+1) & 0 & 0 & 0 & 0 \\
0 & 0 & i\sqrt{\frac{1}{2}}(\kappa+1) & \kappa+\frac{1}{2} & 0 & 0 & 0 & 0 \\
0 & 0 & 0 & 0 & -\frac{1}{2} & 0 & 0 & 0 \\
0 & 0 & 0 & 0 & 0 & \frac{3}{2}\kappa & 0 & 0 \\
0 & 0 & 0 & 0 & 0 & 0 & -\frac{1}{2}\kappa & i\sqrt{\frac{1}{2}}(\kappa+1) \\
0 & 0 & 0 & 0 & 0 & 0 & -i\sqrt{\frac{1}{2}}(\kappa+1) & -\kappa-\frac{1}{2}
\end{bmatrix}.
$$

$$(4\text{--}32)$$

Now we have the explicit matrix for both the Landau and Zeeman part of the Hamiltonian, we can add them together to get the total EFA Hamiltonian for semiconductors in an external magnetic field.

4.3   Energy and Envelope Functions

According to the envelope function approximation, our eigenvalue problem for the Bloch electron in an external magnetic field can be phrased as

$$
\sum_{m'=1}^{8} H_{mm'}^{EFA}\psi_{m'}(\boldsymbol{r}) = E\psi_m(\boldsymbol{r}),
\tag{4–33}
$$

where m and m' are integers from 1 to 8, and the EFA Hamiltonian is the sum of the Landau Hamiltonian and the Zeeman Hamiltonian:

$$
H^{EFA} = H^L + H^Z.
\tag{4–34}
$$

The electron wave function

$$
\Psi(\boldsymbol{r}) = \sum_{m=1}^{8} \psi_m(\boldsymbol{r})u_{m\mathbf{0}}(\boldsymbol{r}),
\tag{4–35}
$$

where $\psi_m(\boldsymbol{r})$ is the envelope function and $u_{m\mathbf{0}}(\boldsymbol{r})$ is the basis function given by equation (3–9). Note that equation (4–33) is a system of coupled differential equations since

the elements of the EFA Hamiltonian contains the differential operators $\hat{k}_x$, $\hat{k}_y$ and $\hat{k}_z$. Therefore the Hamiltonian H^{EFA} is not readily to be diagonalized. What we want is an algebraic matrix eigenvalue problem, the matrix elements of which are just numbers instead of operators. To achieve this purpose we can proceed as follows:

First we separate variables in our envelope functions $\psi_m(\boldsymbol{r})$

$$\psi_m(\boldsymbol{r}) = e^{i(k_x x + k_z z)} f_m(y). \tag{4–36}$$

This separation of variable is possible because of our particular choice of the vector potential in equation (4–18): since the vector potential is only depend on y but not x and z, the k_x and k_z are good quantum numbers. We then substitute equation (4–36) into equation (4–33) to get

$$\sum_{m'=1}^{8} H_{mm'}^{EFA} e^{i(k_x x + k_z z)} f_{m'}(y) = E e^{i(k_x x + k_z z)} f_m(y). \tag{4–37}$$

Note that the EFA Hamiltonian is the sum of Landau Hamiltonian and Zeeman Hamiltonian, so the left hand side of equation (4–37) can be written as

$$\sum_{m'=1}^{8} H_{mm'}^{EFA} e^{i(k_x x + k_z z)} f_{m'}(y) = \sum_{m'=1}^{8} H_{mm'}^{L} e^{i(k_x x + k_z z)} f_{m'}(y) + \sum_{m'=1}^{8} H_{mm'}^{Z} e^{i(k_x x + k_z z)} f_{m'}(y) \tag{4–38}$$

The next step is to evaluate the effect of Landau Hamiltonian acting on the envelope functions. Since we know every elements, $H_{mm'}^{L}$, of Landau Hamiltonian $H_{mm'}^{EFA}$, we can evaluate the operator acting on the plane wave part of the envelope functions one by one for every m and m', the result is

$$H_{mm'}^{L} e^{i(k_x x + k_z z)} f_{m'}(y) = e^{i(k_x x + k_z z)} G_{mm'}^{L} f_{m'}(y), \tag{4–39}$$

where the $G^L_{mm'}$ matrix is given by

$$
G^L =
\begin{bmatrix}
E_g + A & \frac{i}{\sqrt{2}}V\hat{k}_+ & \frac{i}{\sqrt{6}}V\hat{k}_- & \frac{1}{\sqrt{3}}V\hat{k}_- & 0 & 0 & \sqrt{\frac{2}{3}}Vk_z & \frac{i}{\sqrt{3}}Vk_z \\
-\frac{i}{\sqrt{2}}V\hat{k}_- & -P-Q & -M & i\sqrt{2}M & 0 & 0 & -L & -\frac{i}{\sqrt{2}}L \\
-\frac{i}{\sqrt{6}}V\hat{k}_+ & -M^\dagger & -P+Q & i\sqrt{2}Q & -i\sqrt{\frac{2}{3}}Vk_z & L & 0 & i\sqrt{\frac{3}{2}}L^\dagger \\
\frac{1}{\sqrt{3}}V\hat{k}_+ & -i\sqrt{2}M^\dagger & -i\sqrt{2}Q & -P-\Delta & -\frac{1}{\sqrt{3}}Vk_z & -\frac{i}{\sqrt{2}}L & i\sqrt{\frac{3}{2}}L^\dagger & 0 \\
0 & 0 & i\sqrt{\frac{2}{3}}Vk_z & -\frac{1}{\sqrt{3}}Vk_z & E_g + A & -\frac{1}{\sqrt{2}}V\hat{k}_- & -\frac{1}{\sqrt{6}}V\hat{k}_+ & \frac{i}{\sqrt{3}}V\hat{k}_+ \\
0 & 0 & L^\dagger & \frac{i}{\sqrt{2}}L^\dagger & -\frac{1}{\sqrt{2}}V\hat{k}_+ & -P-Q & -M^\dagger & i\sqrt{2}M^\dagger \\
\sqrt{\frac{2}{3}}Vk_z & -L^\dagger & 0 & -i\sqrt{\frac{3}{2}}L & -\frac{1}{\sqrt{6}}V\hat{k}_- & -M & -P+Q & i\sqrt{2}Q \\
-\frac{i}{\sqrt{3}}Vk_z & \frac{i}{\sqrt{2}}L^\dagger & -i\sqrt{\frac{3}{2}}L & 0 & -\frac{i}{\sqrt{3}}V\hat{k}_- & -i\sqrt{2}M & -i\sqrt{2}Q & -P-\Delta
\end{bmatrix} .
$$

$$(4\text{--}40)$$

where the redefined operators $\hat{k}_\pm = k_x - \frac{y}{\lambda^2} \pm i\hat{k}_y$ and the operators A, P, Q, L and M are given by

$$A = \gamma_4 \frac{\hbar^2}{2m_0}[(k_x - \frac{y}{\lambda^2})^2 + \hat{k}_y^2 + k_z^2] \tag{4--41a}$$

$$P = \gamma_1 \frac{\hbar^2}{2m_0}[(k_x - \frac{y}{\lambda^2})^2 + \hat{k}_y^2 + k_z^2] \tag{4--41b}$$

$$Q = \gamma_2 \frac{\hbar^2}{2m_0}[(k_x - \frac{y}{\lambda^2})^2 + \hat{k}_y^2 - 2k_z^2] \tag{4--41c}$$

$$L = -i\sqrt{3}\gamma_3 \frac{\hbar^2}{m_0} k_z(k_x - \frac{y}{\lambda^2} - i\hat{k}_y) \tag{4--41d}$$

$$M = \sqrt{3}\frac{\hbar^2}{2m_0}\left\{ \gamma_2\left[(k_x - \frac{y}{\lambda^2})^2 - \hat{k}_y^2\right] - i\gamma_3\left[(k_x - \frac{y}{\lambda^2})\hat{k}_y + \hat{k}_y(k_x - \frac{y}{\lambda^2})\right] \right\}. \tag{4--41e}$$

This new matrix G^L only contains operator $\hat{k}_y$ and the wave vector quantum number k_x and k_z but not operator $\hat{k}_x$ and $\hat{k}_z$, since we have already evaluated the effects of operators $\hat{k}_x$ and $\hat{k}_z$ acting on the plane wave part of the envelope functions.

To further simply the expression of the G^L matrix, it is convenient to define the operator

$$a = \frac{1}{\sqrt{2}\lambda}(\lambda^2 k_x - y) - i\frac{\lambda}{\sqrt{2}}\hat{k}_y \tag{4--42}$$

and its Hermitian conjugate

$$a^\dagger = \frac{1}{\sqrt{2}\lambda}(\lambda^2 k_x - y) + i\frac{\lambda}{\sqrt{2}}\hat{k}_y. \tag{4–43}$$

It can be directly verified that the commutation relation

$$[a, a^\dagger] = 1, \tag{4–44}$$

so that we can think of operators a and $a^\dagger$ as annihilation and creation operators and define the number operator

$$N = a^\dagger a. \tag{4–45}$$

Using the annihilation and creation operators a and $a^\dagger$, the matrix G^L can be written as

$$G^L = \begin{bmatrix} E_g + A & i\frac{V}{\lambda}a^\dagger & i\sqrt{\frac{1}{3}\frac{V}{\lambda}}a & \sqrt{\frac{2}{3}\frac{V}{\lambda}}a & 0 & 0 & \sqrt{\frac{2}{3}}Vk_z & i\sqrt{\frac{1}{3}}Vk_z \\ -i\frac{V}{\lambda}a & -P - Q & -M & i\sqrt{2}M & 0 & 0 & -L & -i\sqrt{\frac{1}{2}}L \\ -i\sqrt{\frac{1}{3}\frac{V}{\lambda}}a^\dagger & -M^\dagger & -P + Q & i\sqrt{2}Q & -i\sqrt{\frac{2}{3}}Vk_z & L & 0 & i\sqrt{\frac{3}{2}}L^\dagger \\ \sqrt{\frac{2}{3}\frac{V}{\lambda}}a^\dagger & -i\sqrt{2}M^\dagger & -i\sqrt{2}Q & -P - \Delta & -\sqrt{\frac{1}{3}}Vk_z & -i\sqrt{\frac{1}{2}}L & i\sqrt{\frac{3}{2}}L^\dagger & 0 \\ 0 & 0 & i\sqrt{\frac{2}{3}}Vk_z & -\sqrt{\frac{1}{3}}Vk_z & E_g + A & -\frac{V}{\lambda}a & -\sqrt{\frac{1}{3}\frac{V}{\lambda}}a^\dagger & i\sqrt{\frac{2}{3}\frac{V}{\lambda}}a^\dagger \\ 0 & 0 & L^\dagger & i\sqrt{\frac{1}{2}}L^\dagger & -\frac{V}{\lambda}a^\dagger & -P - Q & -M^\dagger & i\sqrt{2}M^\dagger \\ \sqrt{\frac{2}{3}}Vk_z & -L^\dagger & 0 & -i\sqrt{\frac{3}{2}}L & -\sqrt{\frac{1}{3}\frac{V}{\lambda}}a & -M & -P + Q & i\sqrt{2}Q \\ -i\sqrt{\frac{1}{3}}Vk_z & i\sqrt{\frac{1}{2}}L^\dagger & -i\sqrt{\frac{3}{2}}L & 0 & -i\sqrt{\frac{2}{3}\frac{V}{\lambda}}a & -i\sqrt{2}M & -i\sqrt{2}Q & -P - \Delta \end{bmatrix}, \tag{4–46}$$

and the operators A, P, Q, L and M are given by

$$A = \frac{\hbar^2}{m_0}\frac{\gamma_4}{2}\left(\frac{2N + 1}{\lambda^2} + k_z^2\right) \tag{4–47a}$$

$$P = \frac{\hbar^2}{m_0}\frac{\gamma_1}{2}\left(\frac{2N + 1}{\lambda^2} + k_z^2\right) \tag{4–47b}$$

$$Q = \frac{\hbar^2}{m_0}\frac{\gamma_2}{2}\left(\frac{2N + 1}{\lambda^2} - 2k_z^2\right) \tag{4–47c}$$

$$L = -\frac{\hbar^2}{m_0}\gamma_3\left(\frac{i\sqrt{6}k_z a}{\lambda}\right) \tag{4–47d}$$

$$M = \frac{\sqrt{3}\hbar^2}{2m_0\lambda^2}\left[(\gamma_2 + \gamma_3)a^2 + (\gamma_2 - \gamma_3)a^{\dagger 2}\right]. \tag{4–47e}$$

Now that we know the elements of the G^L matrix we can go back to equation (4–37) to obtain

$$\sum_{m'=1}^{8} e^{i(k_x x + k_z z)} G^L_{mm'} f_{m'}(y) + \sum_{m'=1}^{8} H^Z_{mm'} e^{i(k_x x + k_z z)} f_{m'}(y) = E e^{i(k_x x + k_z z)} f_m(y). \tag{4–48}$$

Using the fact that the Zeeman matrix elements $H^Z_{mm'}$ are just numbers we can cancel out the common exponential factor to get

$$\sum_{m'=1}^{8} (G^L_{mm'} + H^Z_{mm'}) f_{m'}(y) = E f_m(y), \tag{4–49}$$

or more compactly

$$\sum_{m'=1}^{8} G_{mm'} f_{m'}(y) = E f_m(y), \tag{4–50}$$

where

$$G = G^L + H^Z. \tag{4–51}$$

Equation (4–50) is a much bigger progress over the original EFA eigenvalue problem in equation (4–33), since we have already separated variables and we only need to focus on the undetermined function $f_m(y)$. The matrix G contains only the y and $\hat{k}_y$ operators, or as we already simplified, the a and $a^{\dagger}$ operators. However this is still not the final form we want because it is still not an algebraic matrix eigenvalue equations due to the existence of the a and $a^{\dagger}$ operators. The last step we take to simplify the problem is using the properties of the harmonic oscillator eigenfunctions to convert equation (4–50) into an algebraic matrix eigenvalue equation. From our definition of the annihilation and creation operators in equation (4–42) and (4–43), we can write the eigenfunctions of the number operator as $\phi_n(y - \lambda^2 k_x)$, with eigenvalue n:

$$N\phi_n(y - \lambda^2 k_x) = n\phi_n(y - \lambda^2 k_x), \tag{4–52}$$

where n is nonnegative integers. We don't need the explict form of this harmonic oscillator eigenfunctions in term of the Hermite polynomials, instead, we will use the following properties of ϕ_n:

$$a\phi_n = \sqrt{n}\phi_{n-1} \tag{4–53a}$$

$$a^\dagger\phi_n = \sqrt{n+1}\phi_{n+1}. \tag{4–53b}$$

Next we expand the $f_m(y)$ functions in terms of these harmonic oscillator eigenfunctions

$$f_1(y) = \sum_{n=1}^{\infty} f_1^n\phi_{n-1} \qquad\qquad f_2(y) = \sum_{n=2}^{\infty} f_2^n\phi_{n-2} \tag{4–54a}$$

$$f_3(y) = \sum_{n=0}^{\infty} f_3^n\phi_n \qquad\qquad f_4(y) = \sum_{n=0}^{\infty} f_4^n\phi_n \tag{4–54b}$$

$$f_5(y) = \sum_{n=0}^{\infty} f_5^n\phi_n \qquad\qquad f_6(y) = \sum_{n=-1}^{\infty} f_6^n\phi_{n+1} \tag{4–54c}$$

$$f_7(y) = \sum_{n=1}^{\infty} f_7^n\phi_{n-1} \qquad\qquad f_8(y) = \sum_{n=1}^{\infty} f_8^n\phi_{n-1} \tag{4–54d}$$

where f_1^n, f_2^n etc. are expansion coefficients independent of y. Note that here we expand the eight components of the envelope function in a slightly different way. This turns to be a better choice than if we expand all eight components in the same form as $\sum_{n=0}^{\infty} f_m^n\phi_n$. The reason for this will be clear shortly.

When we use the already derived operator matrix G acting on the $f_m(y)$ given by equation (4–54), for each line of the operation, we will get an equation of the form

$$\sum_n \left(G_{m1} f_1^n\phi_{n-1} + G_{m2} f_2^n\phi_{n-2} + G_{m3} f_3^n\phi_n + G_{m4} f_4^n\phi_n + G_{m5} f_5^n\phi_n + G_{m6} f_6^n\phi_{n+1} \right.$$
$$\left. + G_{m7} f_7^n\phi_{n-1} + G_{m8} f_8^n\phi_{n-1} \right) = E \sum_n f_m^n\phi_{n_0(n,m)} \tag{4–55}$$

where n_0 is a function of the number n and m:

$$n_0(n, m) = \begin{cases} n - 1, & \text{if } m = 1, 7, 8 \\ n - 2, & \text{if } m = 2 \\ n, & \text{if } m = 3, 4, 5 \\ n + 1, & \text{if } m = 6 \end{cases} \qquad (4\text{--}56)$$

The equation (4–55) can also be written more compactly as

$$\sum_n \sum_{m'} G_{mm'} f_{m'}^n \phi_{n_0(n,m')} = E \sum_n f_m^n \phi_{n_0(n,m)}. \qquad (4\text{--}57)$$

If we neglect the term proportional to $a^{\dagger 2}$ in the definition of the M operator in equation (4–47), we can directly verity that the matrix element $G_{mm'}^L$ and $H_{mm'}^Z$ acting on the $\phi_{n_0(n,m')}$ can be converted into

$$G_{mm'}^L \phi_{n_0(n,m')} = J_{mm'}^n \phi_{n_0(n,m)} \qquad (4\text{--}58a)$$

$$H_{mm'}^Z \phi_{n_0(n,m')} = H_{mm'}^Z \phi_{n_0(n,m)} \qquad (4\text{--}58b)$$

where $J_{mm'}^n$ are just numbers without any operators and the quantum number n_0 are all the same for different m'. The explicit form of the J^n matrix is

$$J^n = \begin{bmatrix} J_a^n & J_c^n \\ J_c^{n\dagger} & J_b^n \end{bmatrix}, \qquad (4\text{--}59)$$

where the submatrices are given by

$$
J_a^n =
\begin{bmatrix}
E_g + \gamma_4\frac{\hbar^2 k_z^2}{2m_0} + \frac{\hbar^2\gamma_4}{m_0\lambda^2}\left(n-\frac{1}{2}\right) & i\frac{V}{\lambda}\sqrt{n-1} & i\frac{V}{\lambda}\sqrt{\frac{n}{3}} & \frac{V}{\lambda}\sqrt{\frac{2}{3}n} \\[2ex]
-i\frac{V}{\lambda}\sqrt{n-1} & \frac{\hbar^2 k_z^2}{m_0}\left(\gamma_2-\frac{\gamma_1}{2}\right) - \frac{\hbar^2}{m_0}\frac{\gamma_1+\gamma_2}{2\lambda^2}(2n-3) & -\frac{\hbar^2}{m_0}\frac{(\gamma_2+\gamma_3)}{2\lambda^2}\sqrt{3n(n-1)} & i\frac{\hbar^2}{m_0}\frac{(\gamma_2+\gamma_3)}{2\lambda^2}\sqrt{6n(n-1)} \\[2ex]
-i\frac{V}{\lambda}\sqrt{\frac{n}{3}} & -\frac{\hbar^2}{m_0}\frac{(\gamma_2+\gamma_3)}{2\lambda^2}\sqrt{3n(n-1)} & \begin{aligned}&-\frac{\hbar^2 k_z^2}{m_0}\left(\frac{\gamma_1}{2}+\gamma_2\right)\\&-\frac{\hbar^2}{m_0}\frac{\gamma_1-\gamma_2}{2\lambda^2}(2n+1)\end{aligned} & \begin{aligned}&i\sqrt{2}\frac{\hbar^2}{m_0}[-\gamma_2 k_z^2\\&+\frac{\gamma_2}{\lambda^2}(n+\tfrac{1}{2})]\end{aligned} \\[2ex]
\frac{V}{\lambda}\sqrt{\frac{2}{3}n} & -i\frac{\hbar^2}{m_0}\frac{(\gamma_2+\gamma_3)}{2\lambda^2}\sqrt{6n(n-1)} & \begin{aligned}&-i\sqrt{2}\frac{\hbar^2}{m_0}[-\gamma_2 k_z^2\\&+\frac{\gamma_2}{\lambda^2}(n+\tfrac{1}{2})]\end{aligned} & \begin{aligned}&-\Delta - \gamma_1\frac{\hbar^2 k_z^2}{2m_0}\\&-\frac{\hbar^2}{m_0}\frac{\gamma_1}{\lambda^2}(n+\tfrac{1}{2})\end{aligned}
\end{bmatrix},
$$

(4–60a)

$$
J_b^n =
\begin{bmatrix}
E_g + \gamma_4\frac{\hbar^2 k_z^2}{2m_0} + \frac{\hbar^2\gamma_4}{m_0\lambda^2}\left(n+\frac{1}{2}\right) & -\frac{V}{\lambda}\sqrt{n+1} & -\frac{V}{\lambda}\sqrt{\frac{n}{3}} & i\frac{V}{\lambda}\sqrt{\frac{2}{3}n} \\[2ex]
-\frac{V}{\lambda}\sqrt{n+1} & \frac{\hbar^2 k_z^2}{m_0}\left(\gamma_2-\frac{\gamma_1}{2}\right) - \frac{\hbar^2}{m_0}\frac{\gamma_1+\gamma_2}{2\lambda^2}(2n+3) & -\frac{\hbar^2}{m_0}\frac{(\gamma_2+\gamma_3)}{2\lambda^2}\sqrt{3n(n+1)} & i\frac{\hbar^2}{m_0}\frac{(\gamma_2+\gamma_3)}{2\lambda^2}\sqrt{6n(n+1)} \\[2ex]
-\frac{V}{\lambda}\sqrt{\frac{n}{3}} & -\frac{\hbar^2}{m_0}\frac{(\gamma_2+\gamma_3)}{2\lambda^2}\sqrt{3n(n+1)} & \begin{aligned}&-\frac{\hbar^2 k_z^2}{m_0}\left(\frac{\gamma_1}{2}+\gamma_2\right)\\&-\frac{\hbar^2}{m_0}\frac{\gamma_1-\gamma_2}{2\lambda^2}(2n-1)\end{aligned} & \begin{aligned}&i\sqrt{2}\frac{\hbar^2}{m_0}[-\gamma_2 k_z^2\\&+\frac{\gamma_2}{\lambda^2}(n-\tfrac{1}{2})]\end{aligned} \\[2ex]
-i\frac{V}{\lambda}\sqrt{\frac{2}{3}n} & -i\frac{\hbar^2}{m_0}\frac{(\gamma_2+\gamma_3)}{2\lambda^2}\sqrt{6n(n+1)} & \begin{aligned}&-i\sqrt{2}\frac{\hbar^2}{m_0}[-\gamma_2 k_z^2\\&+\frac{\gamma_2}{\lambda^2}(n-\tfrac{1}{2})]\end{aligned} & \begin{aligned}&-\Delta - \gamma_1\frac{\hbar^2 k_z^2}{2m_0}\\&-\frac{\hbar^2}{m_0}\frac{\gamma_1}{\lambda^2}(n-\tfrac{1}{2})\end{aligned}
\end{bmatrix},
$$

(4–60b)

$$
J_c^n = k_z
\begin{bmatrix}
0 & 0 & V\sqrt{\frac{3}{2}} & iV\sqrt{\frac{1}{3}} \\[2ex]
0 & 0 & i\frac{\hbar^2}{m_0}\frac{\gamma_3}{\lambda}\sqrt{6(n-1)} & -\frac{\hbar^2}{m_0}\frac{\gamma_3}{\lambda}\sqrt{3(n-1)} \\[2ex]
-iV\sqrt{\frac{2}{3}} & -i\frac{\hbar^2}{m_0}\frac{\gamma_3}{\lambda}\sqrt{6(n+1)} & 0 & -3\frac{\hbar^2}{m_0}\frac{\gamma_3}{\lambda}\sqrt{n} \\[2ex]
-V\sqrt{\frac{1}{3}} & -\frac{\hbar^2}{m_0}\frac{\gamma_3}{\lambda}\sqrt{3(n+1)} & -3\frac{\hbar^2}{m_0}\frac{\gamma_3}{\lambda}\sqrt{n} & 0
\end{bmatrix}.
$$

(4–60c)

This allow us to rewrite equation (4–55) as

$$\sum_n \left[\sum_{m'} (J^n_{mm'} + H^Z_{mm'}) f^n_{m'} \right] \phi_{n_0(n,m)} = E \sum_n f^n_m \phi_{n_0(n,m)}, \qquad (4\text{–}61)$$

At this point it is clear that why we choose the particular expansion form for $f_m(y)$ given in equation (4–54), since this form will give us a quantum number n_0 independent of m' so that we can factor $\phi_{n_0(n,m)}$ out of the summation over m' in the left side of the above equation. Define matrix R^n as

$$R^n = J^n + H^Z \qquad (4\text{–}62)$$

and by using the orthogonality of the harmonic oscillator eigenstates for different quantum number, we arrived

$$\sum_{m'} R^n_{mm'} f^n_{m'} = E f^n_m. \qquad (4\text{–}63)$$

Diagonalizing the above algebraic matrix eigenvalue equation will give us the eigenenergy which depend on the quantum number n and we call this quantum number manifold quantum number. The solutions for different manifold quantum number do not mixed with each other, so that our initially expansion of the $f_m(y)$ in terms of the summation over different manifold quantum number n breaks apart for manifolds. This means that our $f_m(y)$ functions finally take the following form:

$$f_1(y) = f^n_1 \phi_{n-1} \qquad\qquad f_2(y) = f^n_2 \phi_{n-2} \qquad (4\text{–}64a)$$

$$f_3(y) = f^n_3 \phi_n \qquad\qquad f_4(y) = f^n_4 \phi_n \qquad (4\text{–}64b)$$

$$f_5(y) = f^n_5 \phi_n \qquad\qquad f_6(y) = f^n_6 \phi_{n+1} \qquad (4\text{–}64c)$$

$$f_7(y) = f^n_7 \phi_{n-1} \qquad\qquad f_8(y) = f^n_8 \phi_{n-1}, \qquad (4\text{–}64d)$$

or more compactly

$$f_m(y) = f^n_m \phi_{n_0(n,m)}. \qquad (4\text{–}65)$$

Now we can summarize the technique we use to calculate the electronic structures when there is an external magnetic field applied to the III-V semiconductors. When the

magnetic field is in the $\hat{z}$ direction, the electron wave function is given by

$$\Psi(\boldsymbol{r}) = \sum_{m=1}^{8} \psi_m(\boldsymbol{r}) u_{m\mathbf{0}}(\boldsymbol{r}), \tag{4–66}$$

where $u_{m\mathbf{0}}(\boldsymbol{r})$ is the basis function given in equation (3–9), and $\psi_m(\boldsymbol{r})$ is the envelope function given by

$$\psi_m(\boldsymbol{r}) = e^{i(k_x x + k_z z)} f_m^n \phi_{n_0(n,m)}(y - \lambda^2 k_x). \tag{4–67}$$

In equation (4–67), k_x and k_z are wave vector quantum numbers, n is manifold quantum number, and $n_0 = n_0(n, m)$ is Landau quantum number. The coefficients f_m^n and the electron energy can be obtained from the matrix eigenvalue equation

$$\sum_{m'} R_{mm'}^n f_{m'}^n = E f_m^n. \tag{4–68}$$

The matrix R^n is the sum of the J^n matrix and the H^Z matrix, and the explicit form of the matrix J^n and H^Z are given by equation (4–60) and (4–32), respectively. The energy E will depend on n on k_z but not k_x.

4.4 Numerical Calculations of the GaAs Landau Levels

We perform calculations of Landau levels for bulk GaAs at two different magnetic field strength, 4.7T and 7.0T, at a temperature of 6K. Fig. 4-1 and Fig. 4-2 show conduction and valence band diagrams for the two field strength, just to give us an over all idea of what the energy bands look like. We can see here that as the magnetic field increases, the energy spacing between different levels also increases, as expected. The conduction bands have a simple structure but the valence bands are a lot complicated and hard to see clearly in Fig. 4-1 and Fig. 4-2. Fig. 4-3 and Fig. 4-4 give us a closer look at the valence bands near the zone center, at the field strength of 4.7T and 7.0T, respectively.

Besides the energy levels shown here, we also need to investigate the eigenstates of the wave functions, i.e., the break down of the eigenstate in terms of the linear combination of the eight basis states given in equation (3–9), in order to really

understand the band structures of GaAs in the magnetic field. By using the theoretical model developed in the previous section and numerically solving the eigenvalue problem given by equation (4–68), we can obtain each eigenstates manifold by manifold. We list our results for eigenstates in Table 4-1 and Table 4-2 for the cases of B = 4.7T and B = 7.0T, respectively. The interpretation of Table 4-1 and Table 4-2 is the following. Each line (except the first) of the table describes a particular eigenstate while the first line gives the title of each column. The first column assigns each eigenstate a unique ID number which can be used to refer to different eigenstates. The second column is the Pidgeon-Brown manifold number n [25]. The third column labels different eigenstates within each manifold, in the order of increasing energies. The rest eight columns give us the percentage probability of the eigenstate. For example the sixth state in Table 4-1 is the lowest energy state in the n = 1 manifold, and this state is mixed with 0.2% $|CB^0 \uparrow\rangle$ and 99.8% $|SO^1 \downarrow\rangle$. The small number on the shoulder is the Landau quantum number n_0. Note that the Landau quantum number n_0 is different from the Pidgeon-Brown manifold number as we can see from equation (4–56). Table 4-1 and Table 4-2 can be used to explain the features found in the magneto-optical absorption spectra later in this dissertation.

Simple observation of Table 4-1 and Table 4-2 can tell us a lot information. At this point I want to point out several facts. The first fact is that, although our general theory developed in previous sections make us expect the eigenstates is made up with linear combination of the eight components, the zone center, i.e., $\bm{k}$ = 0 states are made up with linear combination of either the first four, or the second four components. The first four components never mix with the second four components at $\bm{k}$ = 0. One can also see this fact directly from the matrix form of J^n and H^Z, as both J^n and H^Z have a block diagonal form when k_z = 0. We will refer the first four components the upper set and the second four components the lower set from now on.

The second fact worth noting is that for both field strengths under investigation, the conduction band components are almost 100% pure states by themselves. See, for example, the conduction band spin-up states $|CB \uparrow\rangle$ with ID= 11, 19, 27, 35, one can tell these states have a large ($> 96\%$) percentage of $|CB \uparrow\rangle$, although this percentage decrease with increasing Landau levels. This can be easily seen from Fig. 4-5 (a) and Fig. 4-6 (a), where the four blue data points are all quite close to 100% and slowly decreasing over Landau level quantume numbers. Similar statements can be made for the conduction band spin-down states $|CB \downarrow\rangle$ with ID= 5, 12, 20, 28, 36, as shown in Fig. 4-5 (b) and Fig. 4-6 (b). One can also tell from Table 4-1 and Table 4-2 that the spin-orbit split-off bands $|SO \uparrow\rangle$ with ID= 7, 14, 22, 30, and $|SO \downarrow\rangle$ with ID= 2, 6, 13, 21, 29 are also almost 100% pure states ($> 99\%$), even purer that the conduction band states. These are illustrated in Fig. 4-5 (c,d) and Fig. 4-6 (c,d). These spin-orbit split-off bands are low lying states whose energies are below the interested range.

Given the fact that the conduction bands and spin-orbit split-off bands are nearly pure states, and the upper set states never mix with the lower set states, the only mixing states that we left are heavy-hole spin-up states $|HH \uparrow\rangle$ mixed with light-hole spin-down states $|LH \downarrow\rangle$ (those with ID= 4, 9, 16, 18, 24, 26, 32, 34), and heavy-hole spin-down states $|HH \downarrow\rangle$ mixed with light-hole spin-up states $|LH \uparrow\rangle$ (those with ID= 1, 3, 8, 10, 15, 17, 23, 25, 31, 33). Fig. 4-5 (e,h) and Fig. 4-6 (e,h) illustrate the mixing between $|HH \uparrow\rangle$ components and $|LH \downarrow\rangle$ components. We can see that in one set of states the $|HH \uparrow\rangle$ components get smaller while the $|LH \downarrow\rangle$ components get bigger; in another set of states the $|LH \downarrow\rangle$ components get smaller while the $|HH \uparrow\rangle$ states get bigger. Similar observations can be made for mixing between the $|HH \downarrow\rangle$ components and the $|LH \uparrow\rangle$ components, which can be seen in Fig. 4-5 (f,g) and Fig. 4-6 (f,g).

4.5 Magneto-Optical Absorption

Once we have known the electronic structure we can compute the transition probabilities under the perturbation of the radiation field using Fermi's golden rule, and

then compute the optical absorption spectra of the GaAs under the external magnetic field. In this section we discuss how we calculate the spin-dependent magneto-optical properties and compare with the magneto-absorption experiments.

We calculate the magneto-optical absorption coefficient at the photon energy $\hbar\omega$ from [26]

$$\alpha(\hbar\omega) = \frac{\hbar\omega}{\hbar c n_r}\epsilon_2(\hbar\omega), \tag{4–69}$$

where $\epsilon_2(\hbar\omega)$ is the imaginary part of the dielectric function and n_r is the index of refraction. The imaginary part of the dielectric function is found using Fermi's golden rule. The result is

$$\epsilon_2(\hbar\omega) = \frac{e^2}{\lambda^2(\hbar\omega)^2}\sum_{n,\nu;n',\nu'}\int_{-\infty}^{\infty}dk_z|\hat{\mathbf{e}}\cdot\mathbf{P}_{n,\nu}^{n',\nu'}(k_z)|^2$$
$$\times[f_{n,\nu}(k_z) - f_{n',\nu'}(k_z)]\delta(\Delta E_{n',\nu'}^{n,\nu}(k_z) - \hbar\omega), \tag{4–70}$$

where $\Delta E_{n',\nu'}^{n,\nu}(k_z) = E_{n',\nu'}(k_z) - E_{n,\nu}(k_z)$ is the transition energy. The function $f_{n,\nu}(k_z)$ in Eq. (4–70) is the probability that the state (n, ν, k_z), with energy $E_{n,\nu}(k_z)$, is occupied. It is given by the Fermi distribution

$$f_{n,\nu} = \frac{1}{1 + \exp[(E_{n,\nu}(k_z) - E_f)/kT]}. \tag{4–71}$$

The Fermi energy E_f in Eq. (4–71) depends on temperature and doping. If N_D is the donor concentration and N_A the acceptor concentration, then the net donor concentration $N_C = N_D - N_A$ can be either positive or negative depending on whether the sample is *n* or *p* type. For a fixed temperature and Fermi level, the net donor concentration is

$$N_C = \frac{1}{(2\pi)^2\lambda^2}\sum_{n,\nu}\int_{-\infty}^{\infty}dk_z[f_{n,\nu}(k_z) - \delta_{n,\nu}^v], \tag{4–72}$$

where $\delta_{n,\nu}^v = 1$ if the subband (n, ν) is a valence band and vanishes if (n, ν) is a conduction band. Given the net donor concentration and the temperature, the Fermi energy can be found from Eq. (4–72) using a root finding routine.

When doing the summation in Eq. (4–70), we separate the contributions into two cases according to the final states of the optical transitions

$$\epsilon_2(\hbar\omega) = \epsilon_{2\uparrow}(\hbar\omega) + \epsilon_{2\downarrow}(\hbar\omega) \qquad (4\text{–}73)$$

where both $\epsilon_{2\uparrow}(\hbar\omega)$ and $\epsilon_{2\downarrow}(\hbar\omega)$ are given by the same right hand side of Eq. (4–70) with the exception that $\epsilon_{2\uparrow}(\hbar\omega)$ includes those terms if the final state (n', ν', k_z) is spin-up and $\epsilon_{2\downarrow}(\hbar\omega)$ includes those terms if the final state (n', ν', k_z) is spin-down. We can do this separation because we know that, within each manifold, the energy eigenvalues can be put in order so that the highest energy eigenvalue always corresponds to the spin-down conduction electron $|CB \downarrow\rangle$ and the next highest energy eigenvalue corresponds to the spin-up conduction electron $|CB \uparrow\rangle$, noting that the effective g factor is negative. The only exceptions to this rule are $n = -1$ and $n = 0$ manifolds. For $n = -1$ manifold, there is no conduction band states at all, the only eigenstate in this manifold being a heavy hole state, and for $n = 0$ manifold, this is no conduction band spin-up state.

Accordingly, we can get the spin-resolved absorption coefficients $\alpha_\uparrow(\hbar\omega)$ and $\alpha_\downarrow(\hbar\omega)$ from Eq. (4–69) and the total absorption coefficient is just the sum of the spin-up and spin-down part of the absorption

$$\alpha(\hbar\omega) = \alpha_\uparrow(\hbar\omega) + \alpha_\downarrow(\hbar\omega). \qquad (4\text{–}74)$$

In the following we show our calculated spin-resolved absorption spectra at the magnetic field of 4.7T and 7.0T for both $\sigma+$ and $\sigma-$ polarizations. In Fig. 4-7 through Fig. 4-10 we separate the spin-up absorption $\alpha_\uparrow$ (red) from the spin-down absorption $\alpha_\downarrow$ (blue), and each transition is labeled with an arrow and two numbers. These are the same numbers used in Table 4-1 and Table 4-2 to label the energy eigenstate. For example in Fig. 4-7 the first major peak results from a transition from the ID= 1 state to the ID= 5 state in Table 4-1.

When we labeling these transitions with a pair of state ID numbers, note that each state is not a pure state but a mixture with components coming from the eight basis states given by Eq. (3–9). Each component does not contribute equally to the transition. To get a better understanding of the origin of the transition, i.e., to know whether the initial state of a particular transition is a heavy-hole state or light-hole state and the spin orientation of the final conduction electron, we need to identify the active components that contribute to each transition. This task is simplified according to the selection rule summarized in Table 4-3. From these selection rules one can immediately tell that, for $\sigma+$ polarization, the spin-up elections solely come from the light-hole component of the initial state and the spin-down elections solely come from the heavy-hole component. Things are exactly opposite for the $\sigma-$ polarization. Now we can label those transitions with the exact active components of the wave function instead of the numerical ID number, as shown in Fig. 4-11 through Fig. 4-14. Note that for every transition, the Landau level quantum number is conserved: $\Delta N = 0$, however, the Pidgeon-Brown manifold number n is not conserved. For $\sigma+$ polarization $\Delta n = +1$ and for $\sigma-$ polarization $\Delta n = -1$.

Our calculations are compared with experimental absorption spectra for a magnetic field of $B = 7.5T$ for both $\sigma+$ and $\sigma-$ polarization as shown in Fig. 4-15, where the experimental data are taken from [27]. We can see from this comparison that our theoretical model are well and sufficient to explain the major and minor features observed in the experiments. Note that the calculated curves are shifted as a whole to the left by 0.0025 eV to match the observed spectra.

4.6   Spin-Polarized Absorption and Optically Pumped NMR

In this section we compare our calculated spin-dependent absorption with the optically pumped NMR (OPNMR) experiments. OPNMR measurements involve two components: first optically pump the semiconductor system with circularly polarized photons then use the NMR detection of the nuclear spin. During the optically pumping,

the angular momentum of the photon can be transfered to the conduction band electrons and the resulting conduction band electrons will be spin polarized with a majority spin and a minority spin. These spin polarized electrons can interact with the nuclear spin so that the OPNMR spectra is very sensitive to the spin polarization of the conduction band electrons[28–32]. Note that the magneto-absorption experiment, which is a tradition tool to probe the electronic structures of a semiconductor system, measures the total excited electrons (the sum of the spin-up and spin-down electron populations) coming from valence bands to conduction bands, whereas the OPNMR measurement is only sensitive to the spin polarization (the difference between spin-up and spin-down electron populations) of the excited electrons. In this dissertation the oscillatory features in the OPNMR signal of GaAs are attributed to the Landau level transitions. We will show that the OPNMR signals are dominated by the weaker light-hole transitions whereas the magneto-absorptions are dominated by the stronger heavy-hole transitions. These properties of the OPNMR measurement make it a very useful tool to probe the spin-dependent electronic structures of a semiconductor system.

The experiment was performed by our collaborators, Dr. Sophia Hayes's group in St. Louis. The OPNMR spectra of ^{69}Ga spins in bulk semi-insulating GaAs polarized by a narrow-band laser were measured in two different external fields of 4.7T and 7.0T. We find that the OPNMR signal intensity oscillate as a function of the above-gap photon energy, as shown in Fig. 4-16 and Fig. 4-17. These oscillatory features of the OPNMR signal can be well explained using our electronic structure calculation[33]. Results of our calculated energy levels are shown in Fig. 4-18. In Fig. 4-19 we plot the theoretical calculations of the total magneto-absorption of σ^- light (upper black line), spin-up absorption $\alpha_\uparrow$ (blue dashed line), and spin-down absorption $\alpha_\downarrow$ (red dotted-dashed line) in a magnetic field of 4.7T. The theoretical calculations for all curves were shifted in energy by 6meV to account for the shift due to Coulomb interactions (i.e., the exciton binding energy) which we were not included in our calculations.

For σ^- excitation in Fig. 4-19, the total absorption (upper black line) is dominated by optical transitions from the heavy-hole spin-up Landau levels (solid black lines, Fig. 4-18) to conduction-band spin-up Landau levels. However there are also optical transitions from the light-hole spin-up Landau levels (solid red lines, Fig. 4-18) to the conduction-band spin-down Landau levels for σ^- excitation. These light-hole transitions are difficult to see in absorption spectra since the light-hole transitions are weaker (by a factor of 3) than the heavy-hole transitions and are separated by only a few meV from the dominant heavy-hole transitions.

In Fig. 4-20 we plot a combination of ^{69}Ga OPNMR experimental data (black symbols) for σ^- excitation. Superimposed onto the experimental OPNMR data are the calculated electron spin polarizations (red solid lines). A plot of the electron spin polarization shows whether peaks in the absorption came from transitions from heavy- or light-hole Landau levels. When we look at the conduction-band spin polarization for σ^- excitation, we see that the features which arise in the electron spin polarization are dominated by the transitions from the light-hole Landau levels. These light-hole spin-up to conduction-band spin-down transitions are very weak and barely visible in the plot of the total magneto-absorption for σ^- excitation; however these transitions are well resolved in the OPNMR data as a function of photon energy. We find that the conduction-band spin polarization is particularly sensitive to regions of photon energy where the total spin-polarized magneto-absorption ($\alpha_\uparrow + \alpha_\downarrow$) and the differential magneto-absorption ($\alpha_\uparrow - \alpha_\downarrow$) are different from one another, which occurs principally at the peaks of the light-hole transitions.

Table 4-1. Percentage probability of the zone center wave functions at 4.7T

ID	n	ν	$\lvert CB\uparrow\rangle$	$\lvert HH\uparrow\rangle$	$\lvert LH\downarrow\rangle$	$\lvert SO\downarrow\rangle$	$\lvert CB\downarrow\rangle$	$\lvert HH\downarrow\rangle$	$\lvert LH\uparrow\rangle$	$\lvert SO\uparrow\rangle$
1	-1	1	0	0	0	0	0	$100HH^0\downarrow$	0	0
2	0	1	0	0	0	$100SO^0\downarrow$	0	0	0	0
3	0	2	0	0	0	0	$0.3CB^0\downarrow$	$99.7HH^1\downarrow$	0	0
4	0	3	0	0	$100LH^0\downarrow$	0	0	0	0	0
5	0	4	0	0	0	0	$99.7CB^0\downarrow$	$0.3HH^1\downarrow$	0	0
6	1	1	$0.2CB^0\uparrow$	0	0	$99.8SO^1\downarrow$	0	0	0	0
7	1	2	0	0	0	0	$0.2CB^1\downarrow$	0	0	$99.8SO^0\uparrow$
8	1	3	0	0	0	0	$0.8CB^1\downarrow$	$90.3HH^2\downarrow$	$8.9LH^0\uparrow$	0
9	1	4	$0.1CB^0\uparrow$	0	$99.9LH^1\downarrow$	0	0	0	0	0
10	1	5	0	0	0	0	0	$9HH^2\downarrow$	$91LH^0\uparrow$	0
11	1	6	$99.7CB^0\uparrow$	0	$0.1LH^1\downarrow$	$0.1SO^1\downarrow$	0	0	0	0
12	1	7	0	0	0	0	$99.1CB^1\downarrow$	$0.7HH^2\downarrow$	$0.1LH^0\uparrow$	$0.1SO^0\uparrow$
13	2	1	$0.3CB^1\uparrow$	0	0	$99.7SO^2\downarrow$	0	0	0	0
14	2	2	0	0	0	0	$0.3CB^2\downarrow$	0	0	$99.6SO^1\uparrow$
15	2	3	0	0	0	0	$1.2CB^2\downarrow$	$84.7HH^3\downarrow$	$14.1LH^1\uparrow$	0
16	2	4	$0.5CB^1\uparrow$	$29.8HH^0\uparrow$	$69.6LH^2\downarrow$	0	0	0	0	0
17	2	5	0	0	0	0	0	$14.3HH^3\downarrow$	$85.7LH^1\uparrow$	0
18	2	6	0	$69.8HH^0\uparrow$	$30.1LH^2\downarrow$	0	0	0	0	0
19	2	7	$99.1CB^1\uparrow$	$0.3HH^0\uparrow$	$0.2LH^2\downarrow$	$0.3SO^2\downarrow$	0	0	0	0
20	2	8	0	0	0	0	$98.5CB^2\downarrow$	$1.0HH^3\downarrow$	$0.2LH^1\uparrow$	$0.3SO^1\uparrow$
21	3	1	$0.5CB^2\uparrow$	0	0	$99.5SO^3\downarrow$	0	0	0	0
22	3	2	0	0	0	0	$0.5CB^3\downarrow$	$0.1HH^4\downarrow$	0	$99.4SO^2\uparrow$
23	3	3	0	0	0	0	$1.6CB^3\downarrow$	$81.2HH^4\downarrow$	$17.1LH^2\uparrow$	$0.1SO^2\uparrow$
24	3	4	$0.9CB^2\uparrow$	$46.3HH^1\uparrow$	$52.7LH^3\downarrow$	$0.1SO^3\downarrow$	0	0	0	0
25	3	5	0	0	0	0	0	$17.4HH^4\downarrow$	$82.6LH^2\uparrow$	0
26	3	6	0	$53.0HH^1\uparrow$	$46.9LH^3\downarrow$	0	0	0	0	0
27	3	7	$98.6CB^2\uparrow$	$0.7HH^1\uparrow$	$0.3LH^3\downarrow$	$0.4SO^3\downarrow$	0	0	0	0
28	3	8	0	0	0	0	$98CB^3\downarrow$	$1.3HH^4\downarrow$	$0.3LH^2\uparrow$	$0.4SO^2\uparrow$

Table 4-1. Continued

ID	n	ν	$\lvert CB\uparrow\rangle$	$\lvert HH\uparrow\rangle$	$\lvert LH\downarrow\rangle$	$\lvert SO\downarrow\rangle$	$\lvert CB\downarrow\rangle$	$\lvert HH\downarrow\rangle$	$\lvert LH\uparrow\rangle$	$\lvert SO\uparrow\rangle$
29	4	1	$0.6CB^3\uparrow$	$0.1HH^2\uparrow$	0	$99.3SO^4\downarrow$	0	0	0	0
30	4	2	0	0	0	0	$0.7CB^4\downarrow$	$0.1HH^5\downarrow$	0	$99.2SO^3\uparrow$
31	4	3	0	0	0	0	$1.9CB^4\downarrow$	$78.8HH^5\downarrow$	$19.1LH^3\uparrow$	$0.2SO^3\uparrow$
32	4	4	$1.3CB^3\uparrow$	$53.4HH^2\uparrow$	$45.1LH^4\downarrow$	$0.1SO^4\downarrow$	0	0	0	0
33	4	5	0	0	0	0	0	$19.5HH^5\downarrow$	$80.5LH^3\uparrow$	0
34	4	6	0	$45.5HH^2\uparrow$	$54.4LH^4\downarrow$	0	0	0	0	0
35	4	7	$98CB^3\uparrow$	$1.0HH^2\uparrow$	$0.4LH^4\downarrow$	$0.6SO^4\downarrow$	0	0	0	0
36	4	8	0	0	0	0	$97.4CB^4\downarrow$	$1.6HH^5\downarrow$	$0.4LH^3\uparrow$	$0.6SO^3\uparrow$

Table 4-2. Percentage probability of the zone center wave functions at 7.0T

ID	n	ν	$|CB\uparrow\rangle$	$|HH\uparrow\rangle$	$|LH\downarrow\rangle$	$|SO\downarrow\rangle$	$|CB\downarrow\rangle$	$|HH\downarrow\rangle$	$|LH\uparrow\rangle$	$|SO\uparrow\rangle$
1	-1	1	0	0	0	0	0	$100HH^0\downarrow$	0	0
2	0	1	0	0	0	$100SO^0\downarrow$	0	0	0	0
3	0	2	0	0	0	0	$0.5CB^0\downarrow$	$99.5HH^1\downarrow$	0	0
4	0	3	0	0	$100LH^0\downarrow$	0	0	0	0	0
5	0	4	0	0	0	0	$99.5CB^0\downarrow$	$0.5HH^1\downarrow$	0	0
6	1	1	$0.2CB^0\uparrow$	0	0	$99.8SO^1\downarrow$	0	0	0	0
7	1	2	0	0	0	0	$0.2CB^1\downarrow$	0	0	$99.7SO^0\uparrow$
8	1	3	0	0	0	0	$1.1CB^1\downarrow$	$90.0HH^2\downarrow$	$8.8LH^0\uparrow$	0
9	1	4	$0.2CB^0\uparrow$	0	$99.8LH^1\downarrow$	0	0	0	0	0
10	1	5	0	0	0	0	0	$9HH^2\downarrow$	$91LH^0\uparrow$	0
11	1	6	$99.6CB^0\uparrow$	0	$0.2LH^1\downarrow$	$0.2SO^1\downarrow$	0	0	0	0
12	1	7	0	0	0	0	$98.6CB^1\downarrow$	$1.0HH^2\downarrow$	$0.2LH^0\uparrow$	$0.2SO^0\uparrow$
13	2	1	$0.5CB^1\uparrow$	0	0	$99.5SO^2\downarrow$	0	0	0	0
14	2	2	0	0	0	0	$0.5CB^2\downarrow$	$0.1HH^3\downarrow$	0	$99.4SO^1\uparrow$
15	2	3	0	0	0	0	$1.7CB^2\downarrow$	$84.2HH^3\downarrow$	$13.9LH^1\uparrow$	$0.2SO^1\uparrow$
16	2	4	$0.7CB^1\uparrow$	$29.5HH^0\uparrow$	$69.7LH^2\downarrow$	0	0	0	0	0
17	2	5	0	0	0	0	0	$14.3HH^3\downarrow$	$85.7LH^1\uparrow$	0
18	2	6	$0.1CB^1\uparrow$	$70.0HH^0\uparrow$	$29.9LH^2\downarrow$	0	0	0	0	0
19	2	7	$98.7CB^1\uparrow$	$0.5HH^0\uparrow$	$0.3LH^2\downarrow$	$0.4SO^2\downarrow$	0	0	0	0
20	2	8	0	0	0	0	$97.8CB^2\downarrow$	$1.4HH^3\downarrow$	$0.3LH^1\uparrow$	$0.4SO^1\uparrow$
21	3	1	$0.7CB^2\uparrow$	$0.1HH^1\uparrow$	0	$99.2SO^3\downarrow$	0	0	0	0
22	3	2	0	0	0	0	$0.8CB^3\downarrow$	$0.2HH^4\downarrow$	0	$99.1SO^2\uparrow$
23	3	3	0	0	0	0	$2.2CB^3\downarrow$	$80.5HH^4\downarrow$	$17.0LH^2\uparrow$	$0.3SO^2\uparrow$
24	3	4	$1.3CB^2\uparrow$	$45.7HH^1\uparrow$	$52.9LH^3\downarrow$	$0.1SO^3\downarrow$	0	0	0	0
25	3	5	0	0	0	0	0	$17.5HH^4\downarrow$	$82.5LH^2\uparrow$	0
e 26	3	6	$0.1CB^2\uparrow$	$53.3HH^1\uparrow$	$46.6LH^3\downarrow$	0	0	0	0	0
27	3	7	$97.9CB^2\uparrow$	$1.0HH^1\uparrow$	$0.5LH^3\downarrow$	$0.6SO^3\downarrow$	0	0	0	0
28	3	8	0	0	0	0	$97.0CB^3\downarrow$	$1.9HH^4\downarrow$	$0.5LH^2\uparrow$	$0.6SO^2\uparrow$

Table 4-2. Continued

ID	n	ν	$|CB\uparrow\rangle$	$|HH\uparrow\rangle$	$|LH\downarrow\rangle$	$|SO\downarrow\rangle$	$|CB\downarrow\rangle$	$|HH\downarrow\rangle$	$|LH\uparrow\rangle$	$|SO\uparrow\rangle$
29	4	1	$1.0CB^3\uparrow$	$0.1HH^2\uparrow$	0	$98.8SO^4\downarrow$	0	0	0	0
30	4	2	0	0	0	0	$1.0CB^4\downarrow$	$0.3HH^5\downarrow$	0	$98.6SO^3\uparrow$
31	4	3	0	0	0	0	$2.7CB^4\downarrow$	$77.9HH^5\downarrow$	$18.9LH^3\uparrow$	$0.5SO^3\uparrow$
32	4	4	$1.9CB^3\uparrow$	$52.6HH^2\uparrow$	$45.3LH^4\downarrow$	$0.3SO^4\downarrow$	0	0	0	0
33	4	5	0	0	0	0	0	$19.6HH^5\downarrow$	$80.4LH^3\uparrow$	0
34	4	6	0	$45.9HH^2\uparrow$	$54.1LH^4\downarrow$	0	0	0	0	0
35	4	7	$97.1CB^3\uparrow$	$1.4HH^2\uparrow$	$0.6LH^4\downarrow$	$0.8SO^4\downarrow$	0	0	0	0
36	4	8	0	0	0	0	$96.3CB^4\downarrow$	$2.3HH^5\downarrow$	$0.6LH^3\uparrow$	$0.8SO^3\uparrow$

Table 4-3. Selection rules

$\sigma+$ polarization	$\lvert HH \downarrow \rangle \Rightarrow \lvert S \downarrow \rangle$
Left circular polarization	$\lvert LH \downarrow \rangle \Rightarrow \lvert S \uparrow \rangle$
$\sigma-$ polarization	$\lvert HH \uparrow \rangle \Rightarrow \lvert S \uparrow \rangle$
Right circular polarization	$\lvert LH \uparrow \rangle \Rightarrow \lvert S \downarrow \rangle$
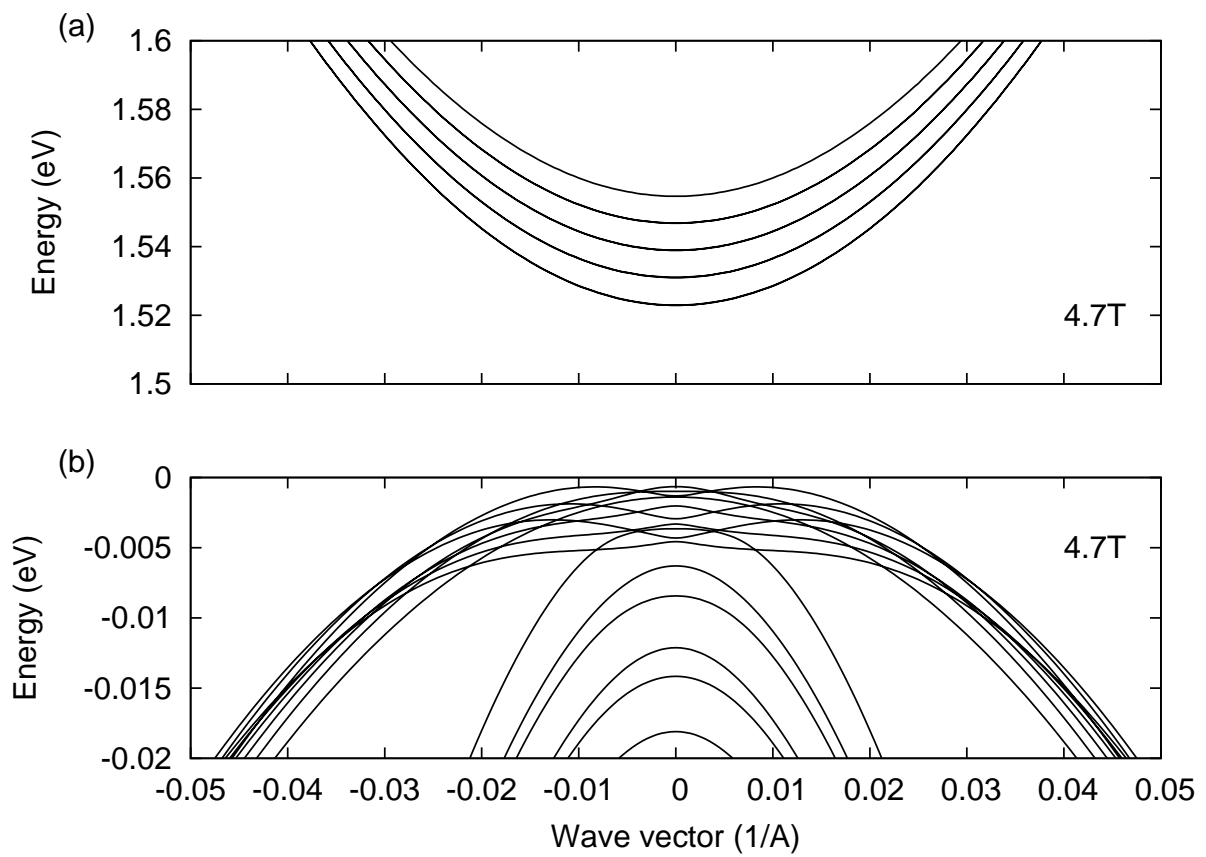
Figure 4-1. Energy band structure for GaAs at $B = 4.7\text{T}$
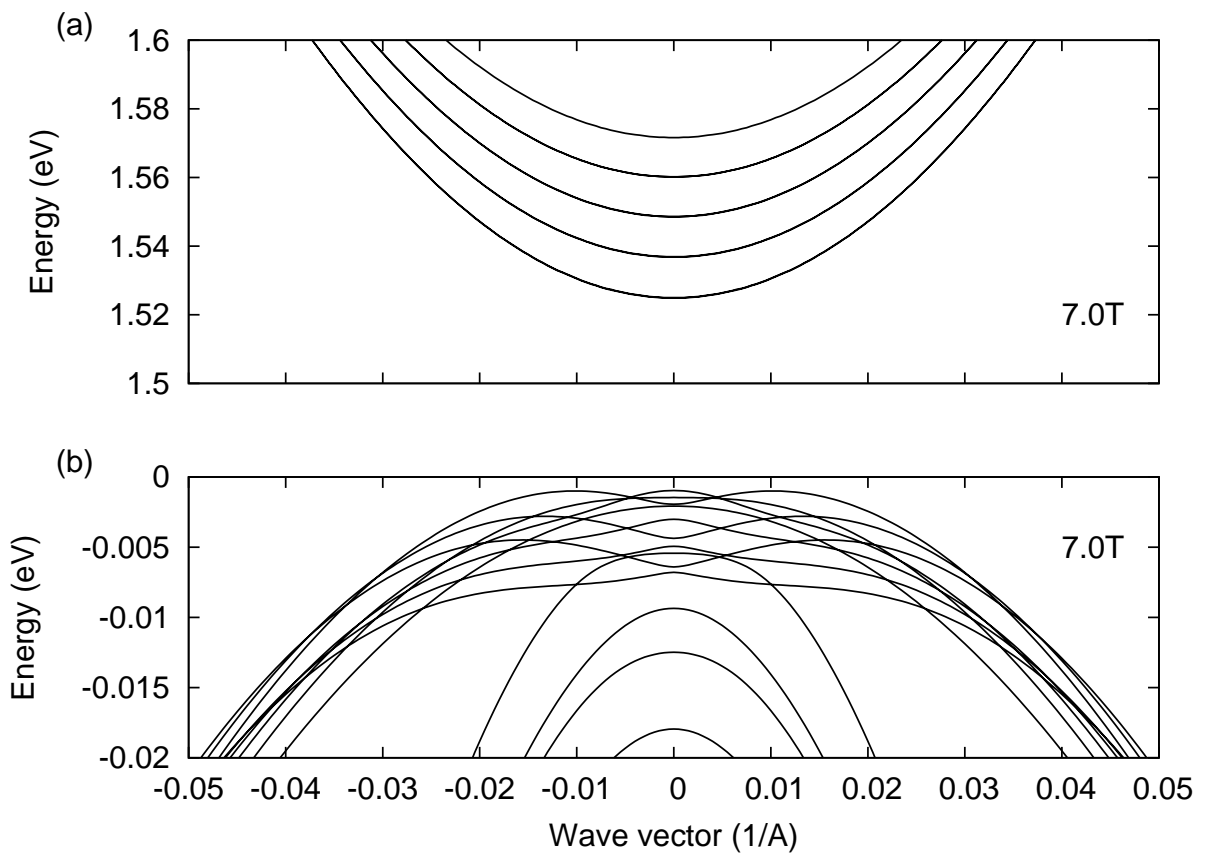
Figure 4-2. Energy band structure for GaAs at $B = 7.0T$
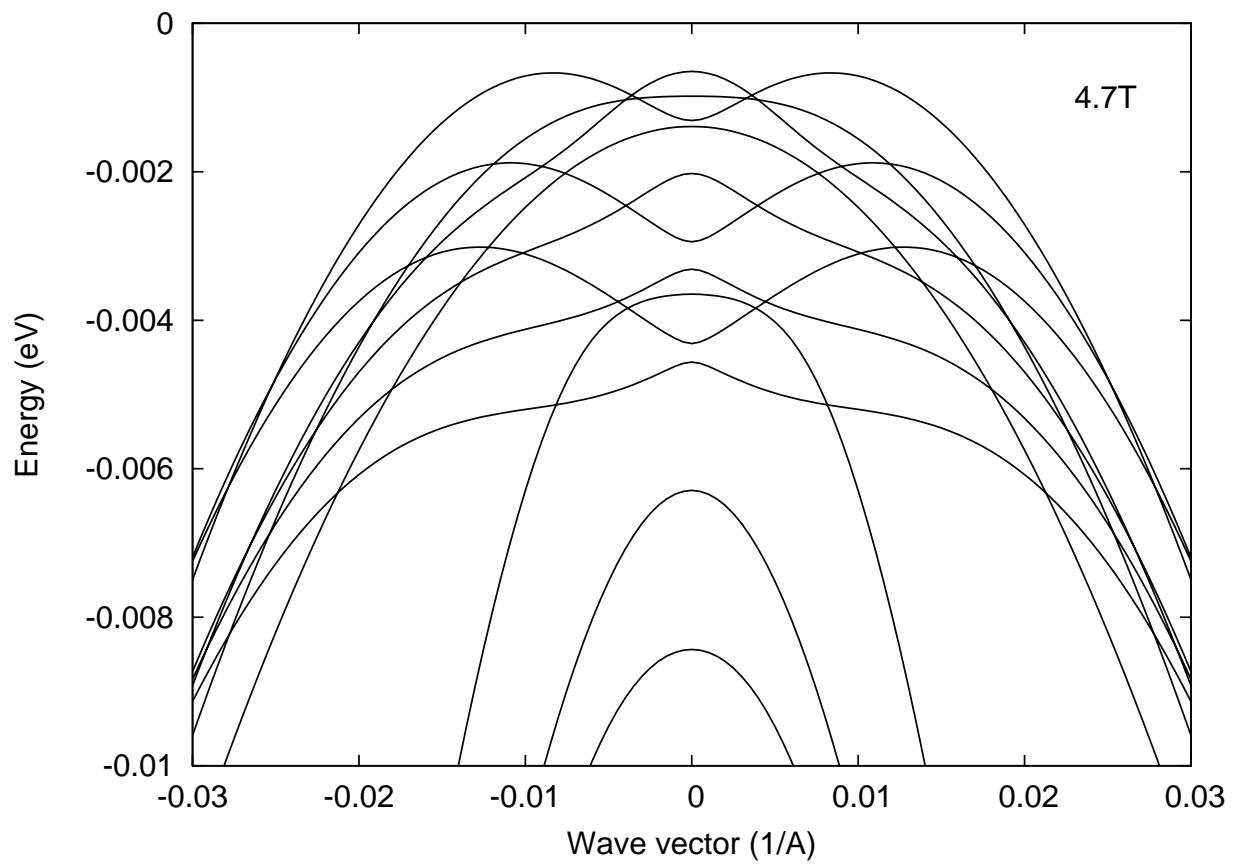
Figure 4-3. Valence band structure for 4.7T
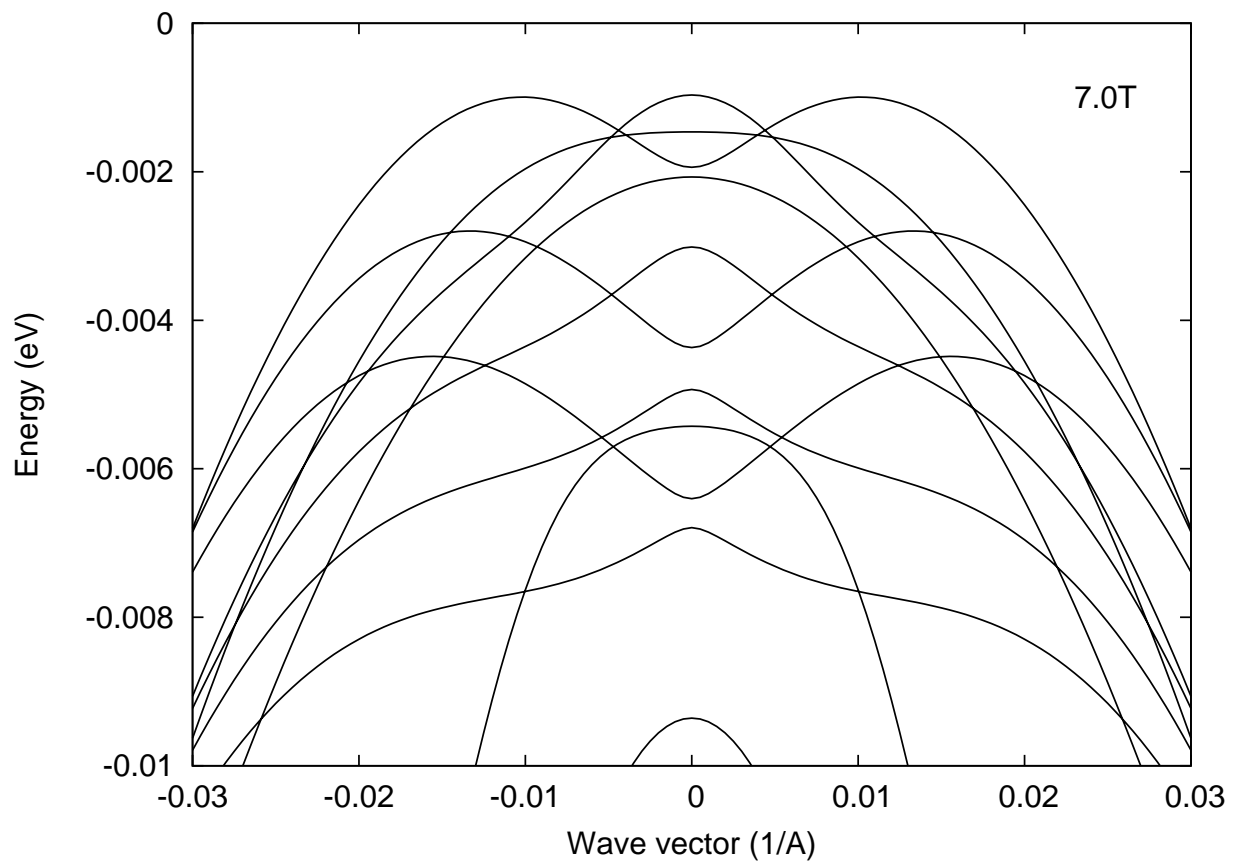
Figure 4-4. Valence band structure for 7.0T
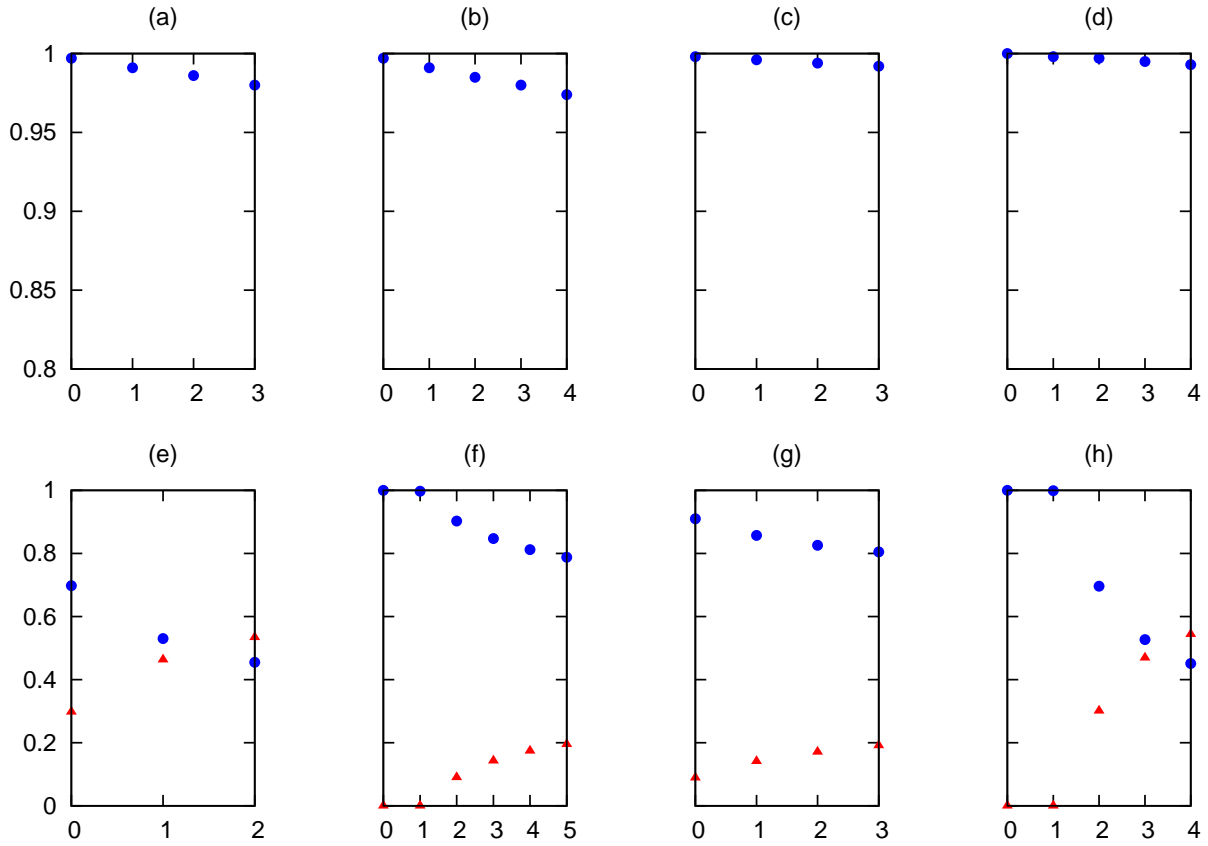
Figure 4-5. Wave function components vs Landau level quantum number at $B = 4.7$T. The subfigures (a) through (h) correspond the eight components in the order of $|CB\uparrow\rangle$, $|CB\downarrow\rangle$, $|SO\uparrow\rangle$, $|SO\downarrow\rangle$, $|HH\uparrow\rangle$, $|HH\downarrow\rangle$, $|LH\uparrow\rangle$, $|LH\downarrow\rangle$. The horizontal axis labels Landau level quantum number and the vertical axis gives the percentage of that particular components. Note that vertical axis of the subfigure (a) through (d) have different scales from those from the subfigure (e) through (h).
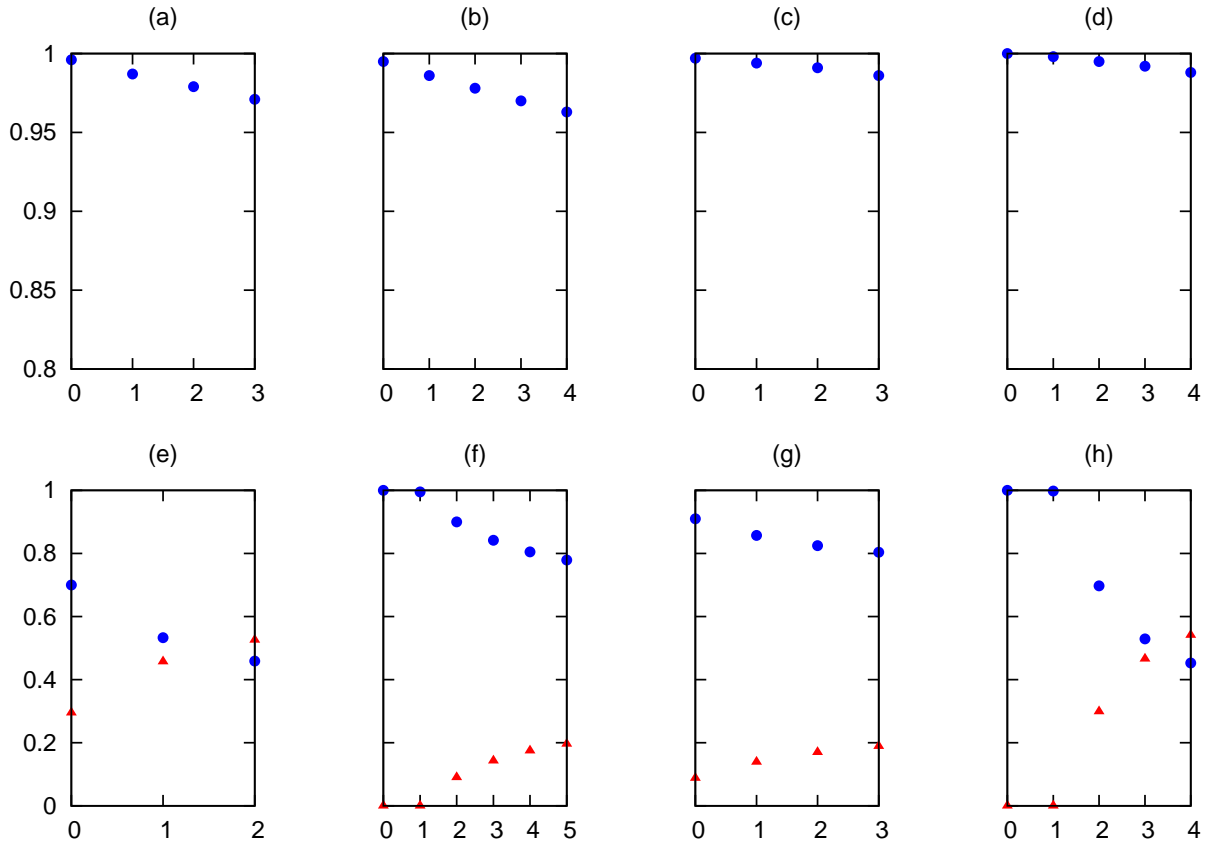
Figure 4-6. Wave function components vs Landau level quantum number at $B = 7.0T$. The subfigures (a) through (h) correspond the eight components in the order of $|CB\uparrow\rangle$, $|CB\downarrow\rangle$, $|SO\uparrow\rangle$, $|SO\downarrow\rangle$, $|HH\uparrow\rangle$, $|HH\downarrow\rangle$, $|LH\uparrow\rangle$, $|LH\downarrow\rangle$. The horizontal axis labels Landau level quantum number and the vertical axis gives the percentage of that particular components. Note that vertical axis of the subfigure (a) through (d) have different scales from those from the subfigure (e) through (h).
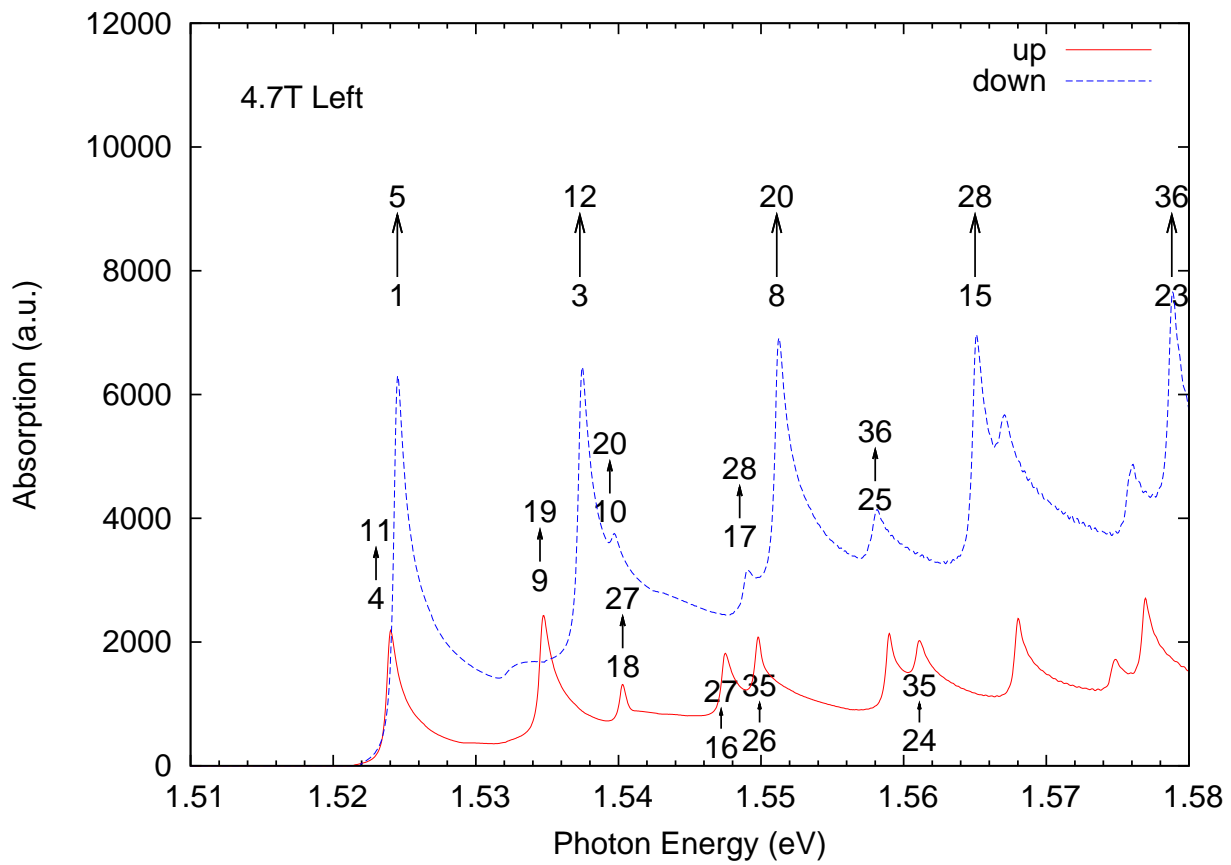
Figure 4-7. Spin dependent absorption for B=4.7T (σ^+ polarization)
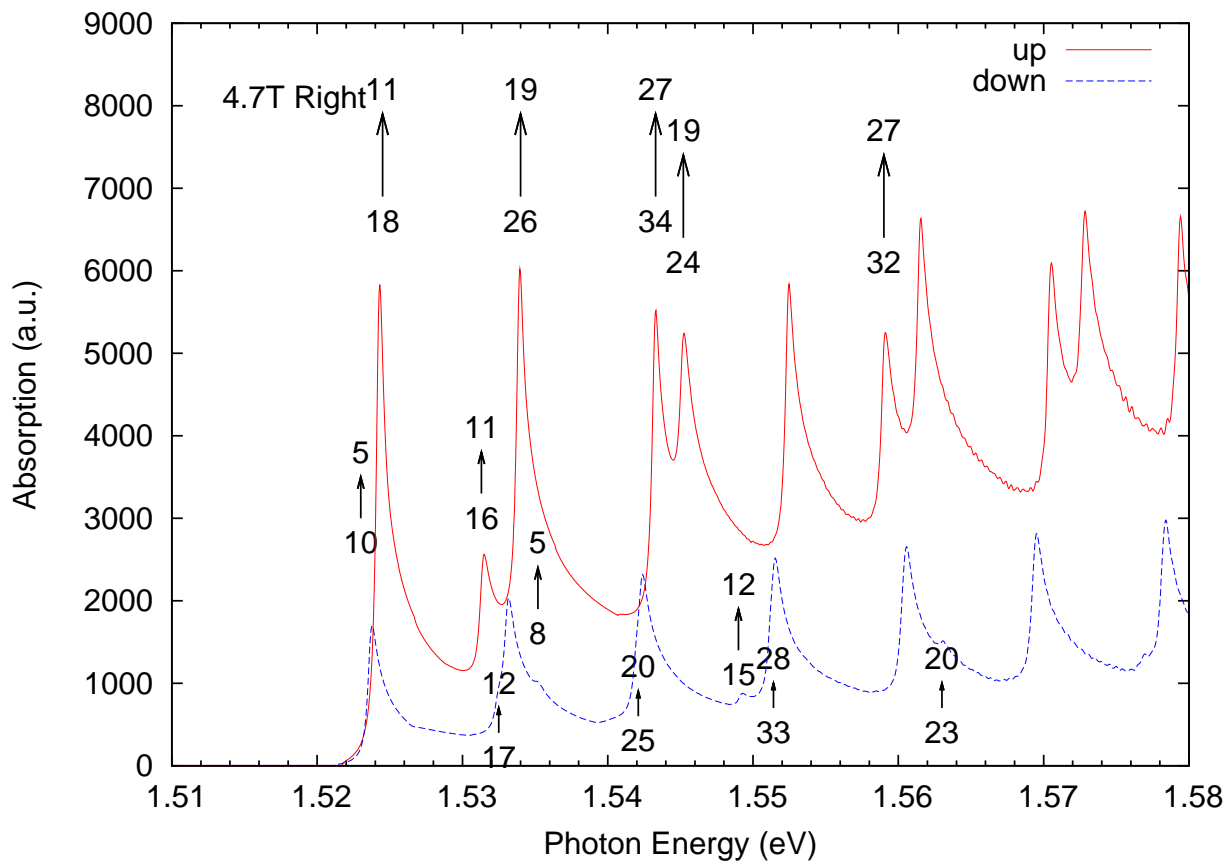
Figure 4-8. Spin dependent absorption for B=4.7T (σ^- polarization)
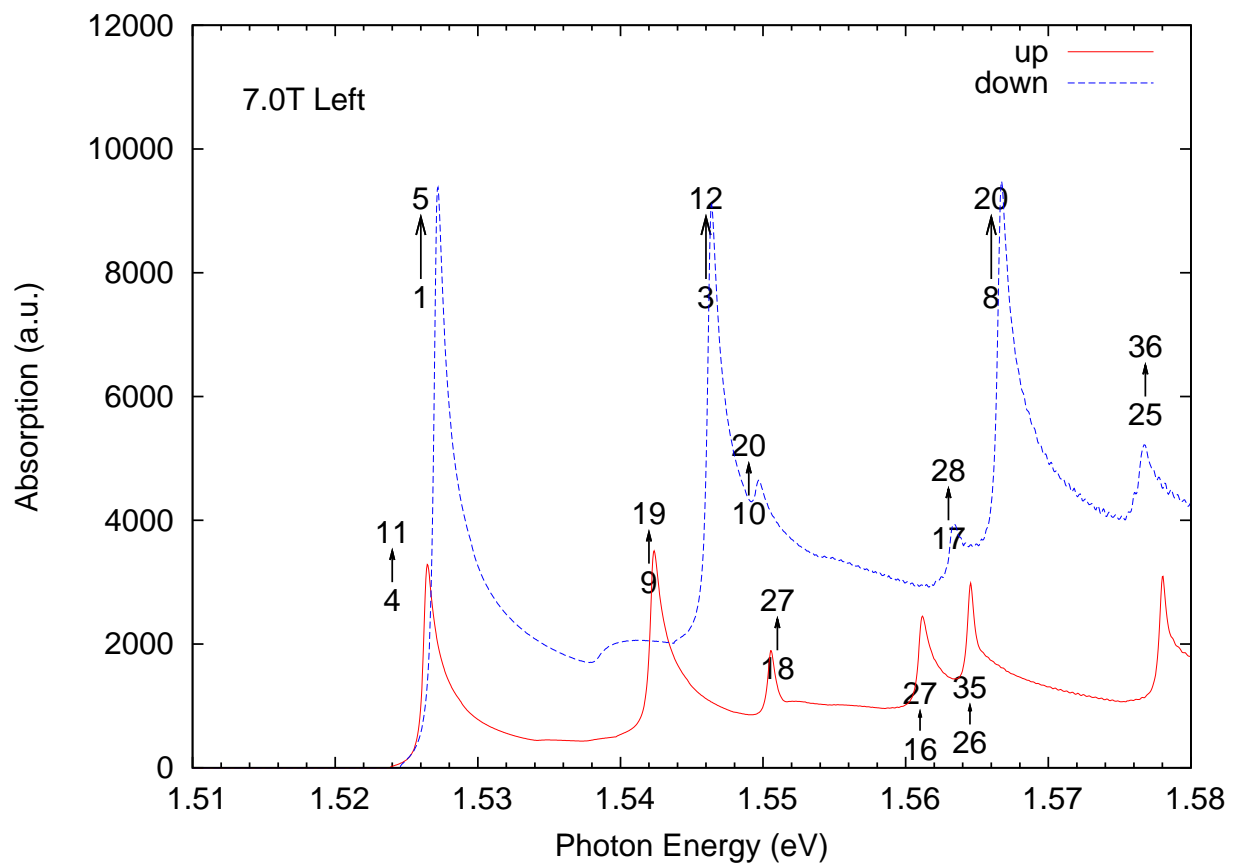
Figure 4-9. Spin dependent absorption for B=7.0T (σ^+ polarization)
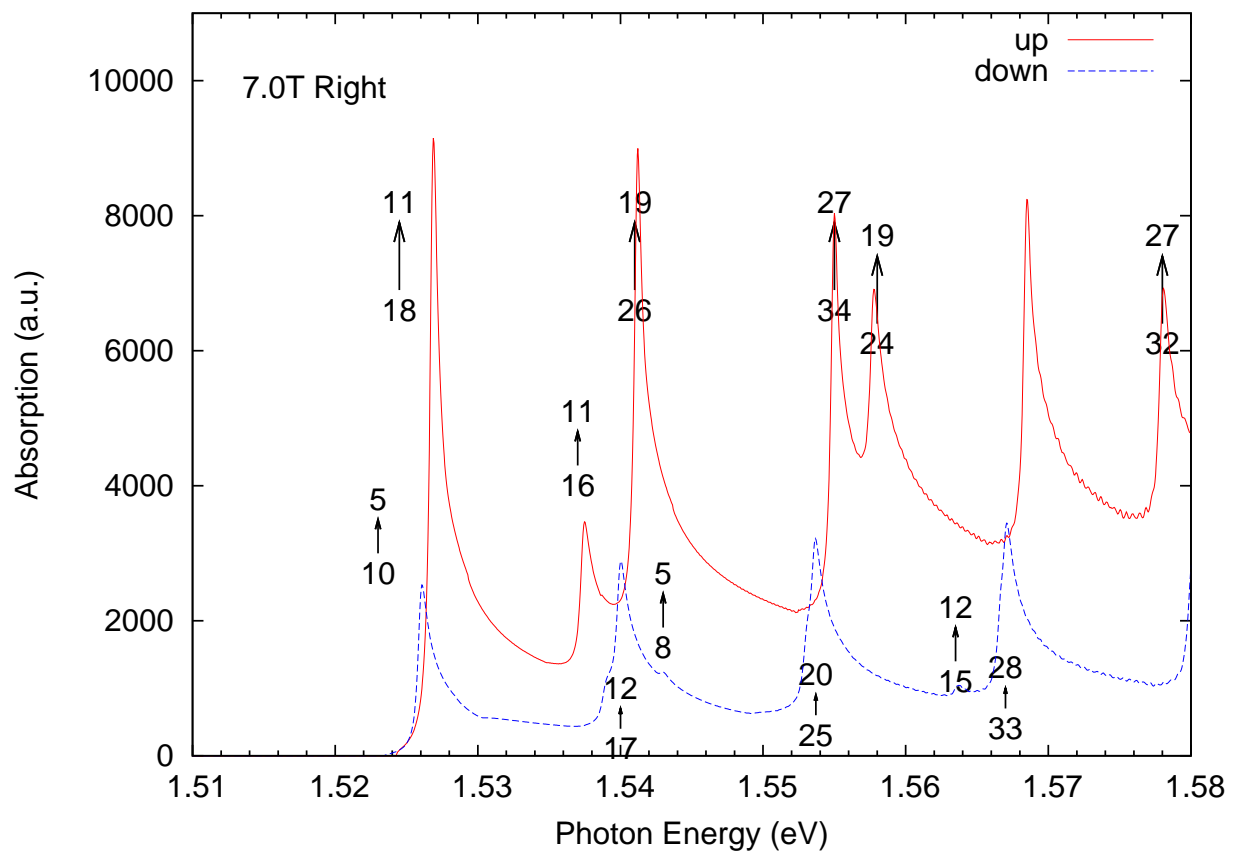
Figure 4-10. Spin dependent absorption for B=7.0T (σ^- polarization)
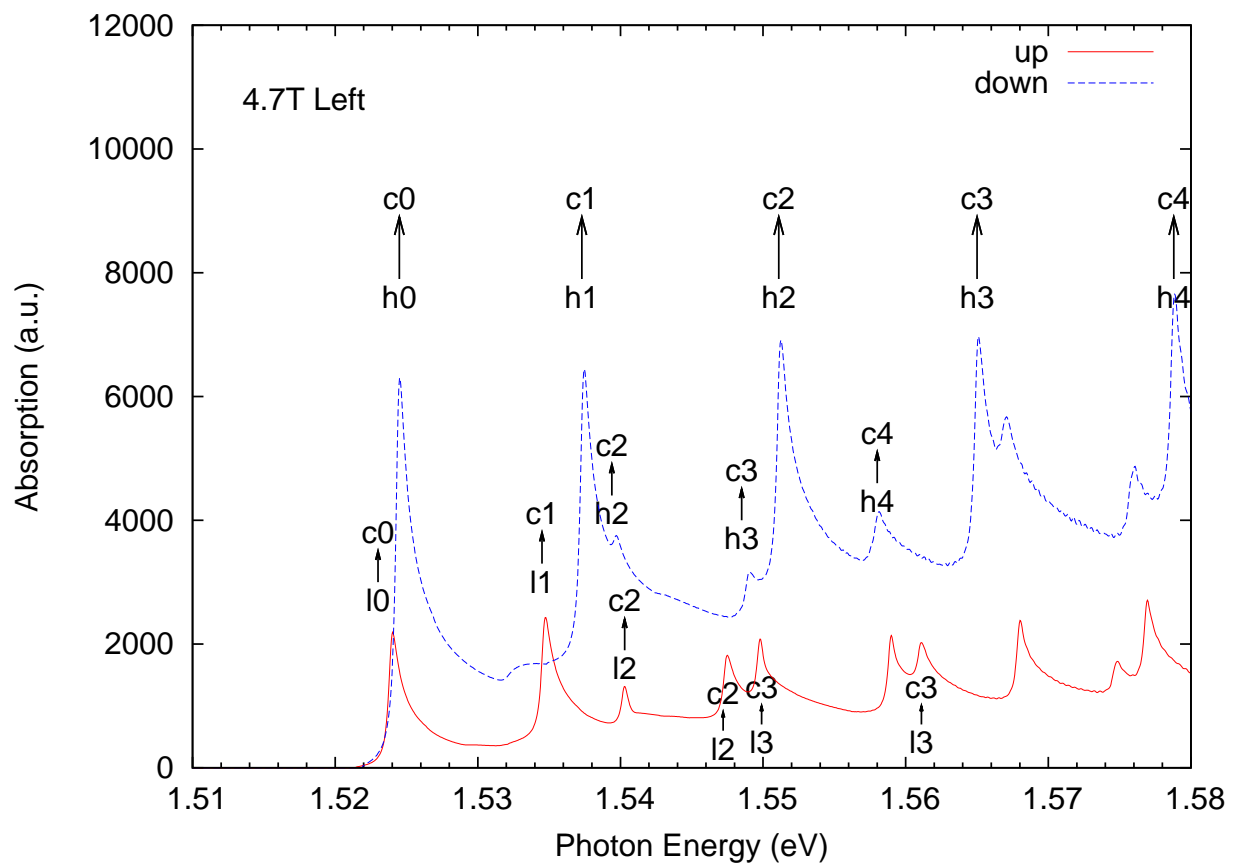
Figure 4-11. Active components for absorption at B=4.7T (σ^+ polarization)
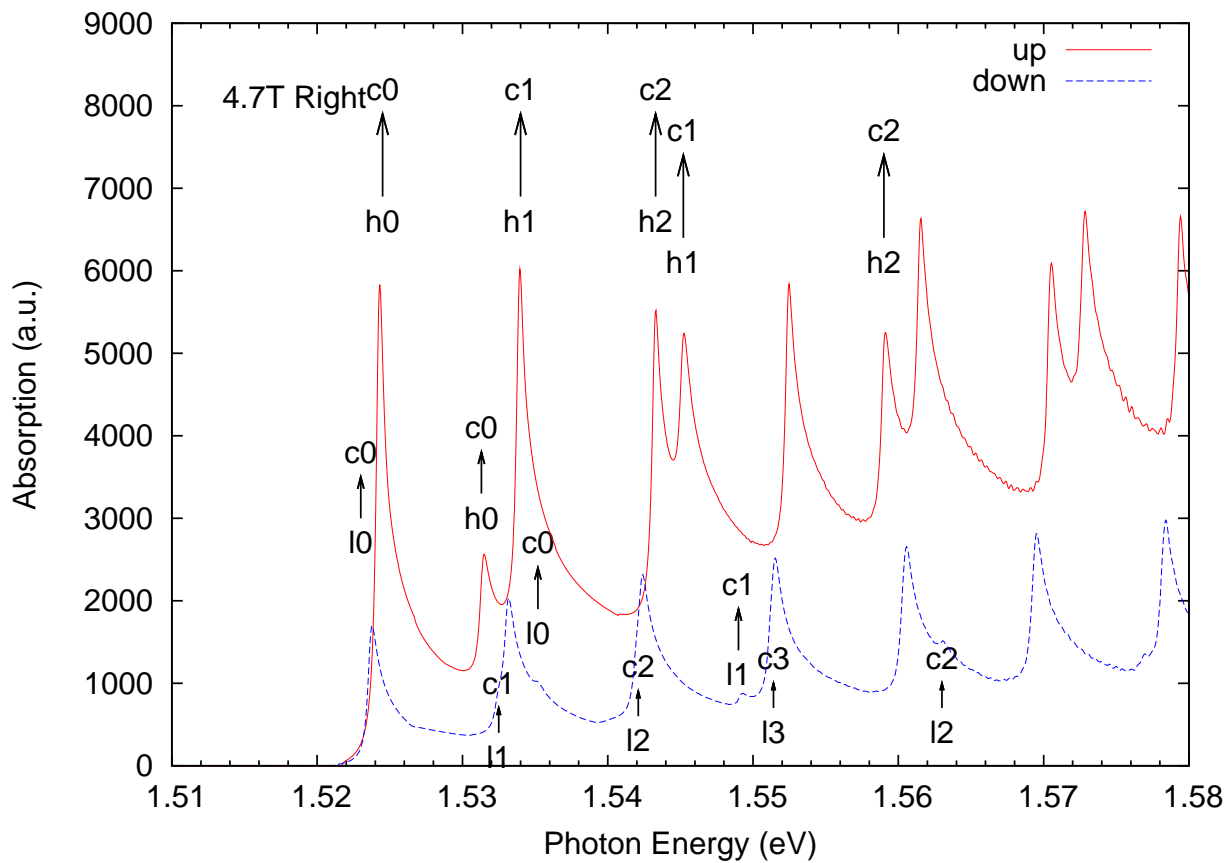
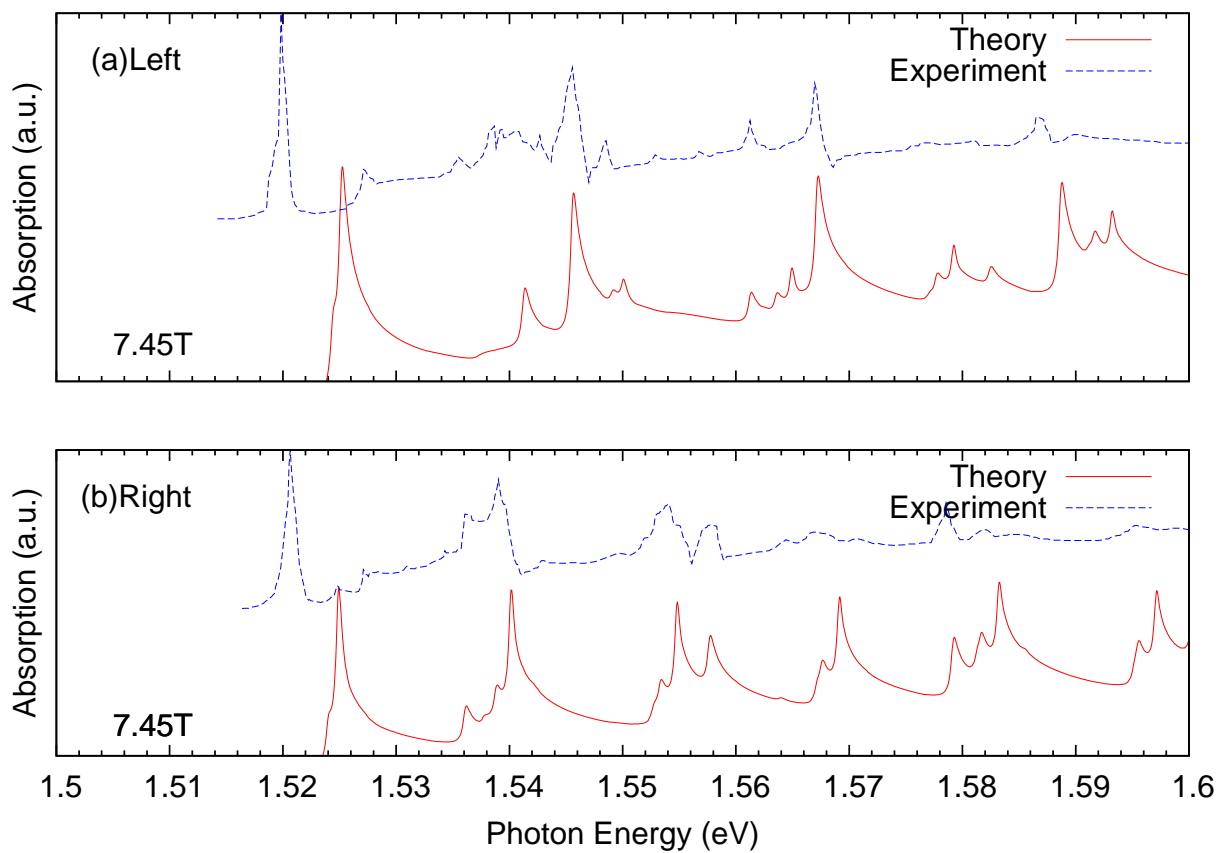Figure 4-12. Active components for absorption at B=4.7T (σ^- polarization)
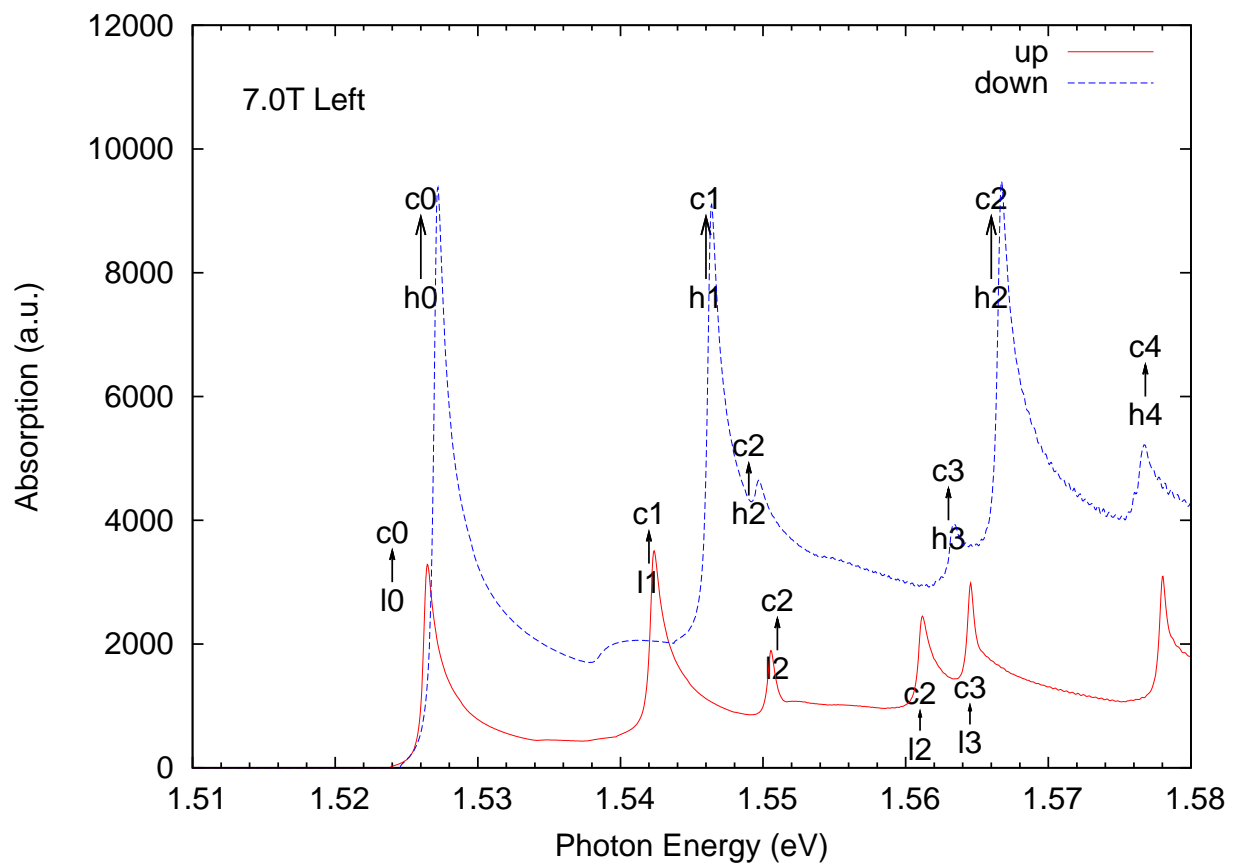
Figure 4-13. Active components for absorption at B=7.0T (σ^+ polarization)
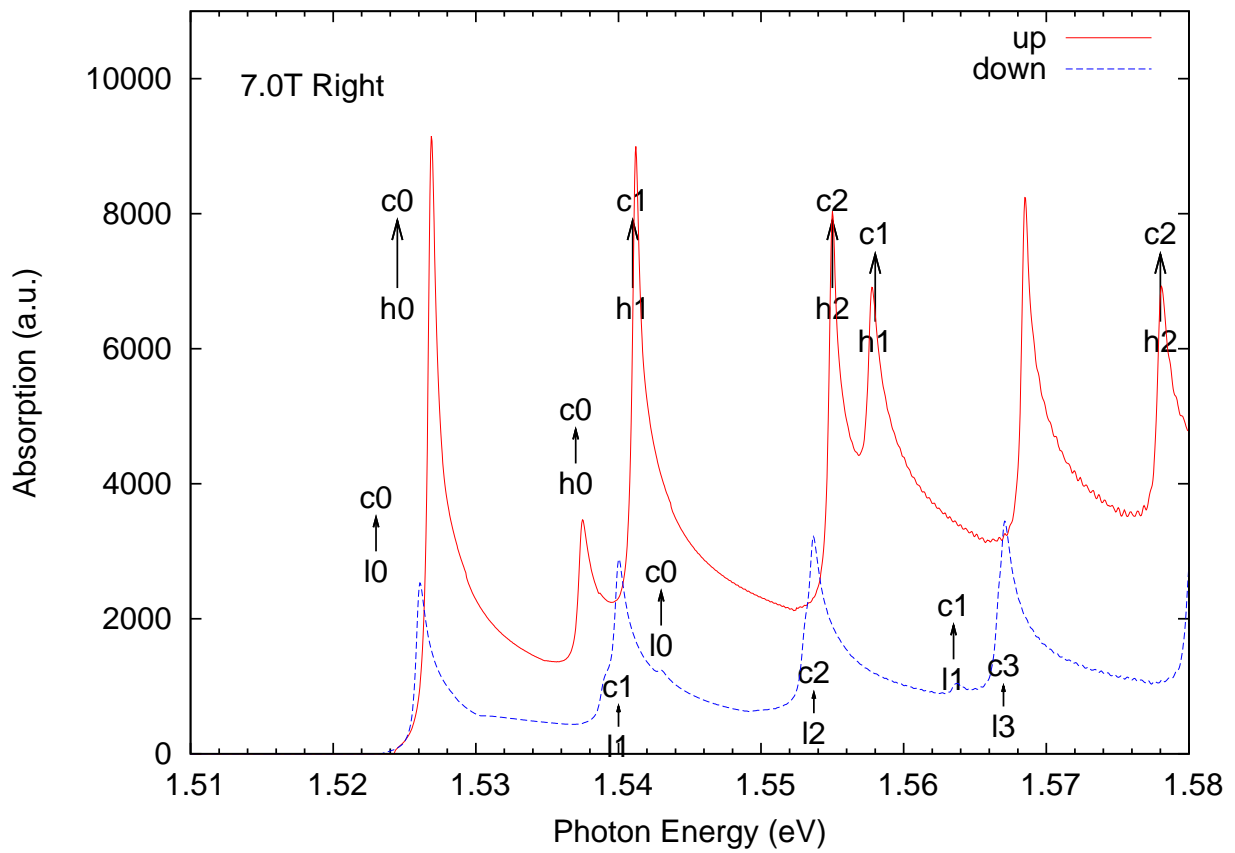
Figure 4-14. Active components for absorption at B=7.0T (σ^- polarization)

Figure 4-15. Calculated absorption compared with experiments
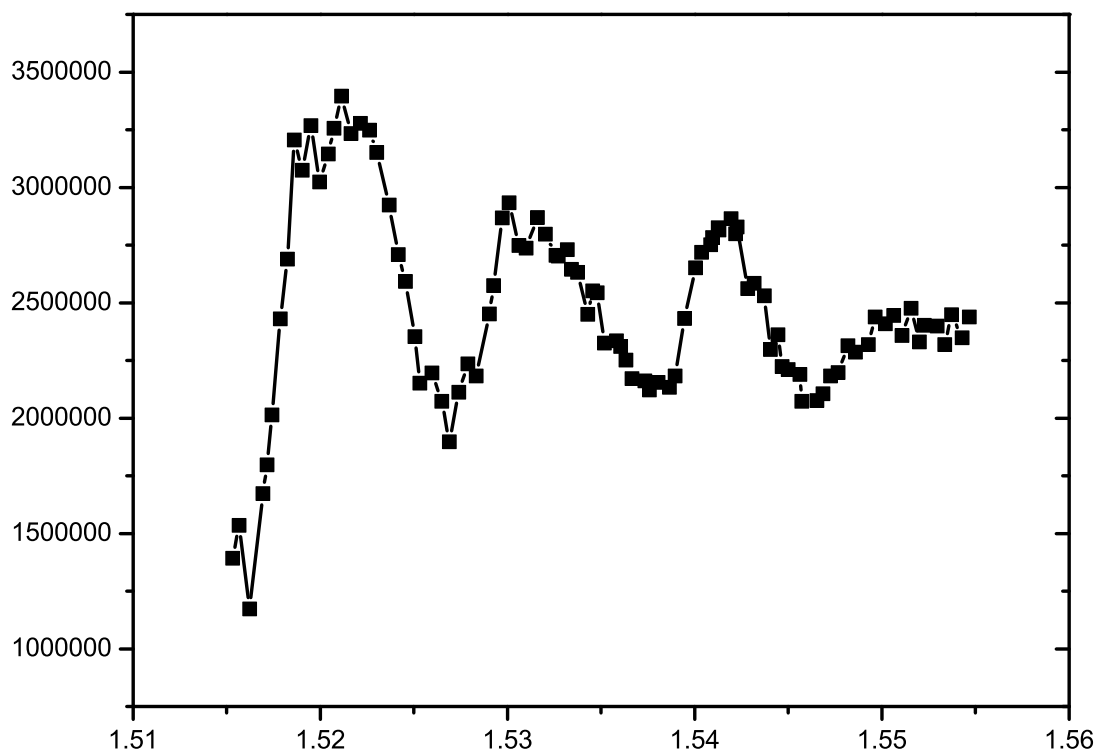
Figure 4-16. OPNMR signal intensity as a function of photon energy for σ^- excitation
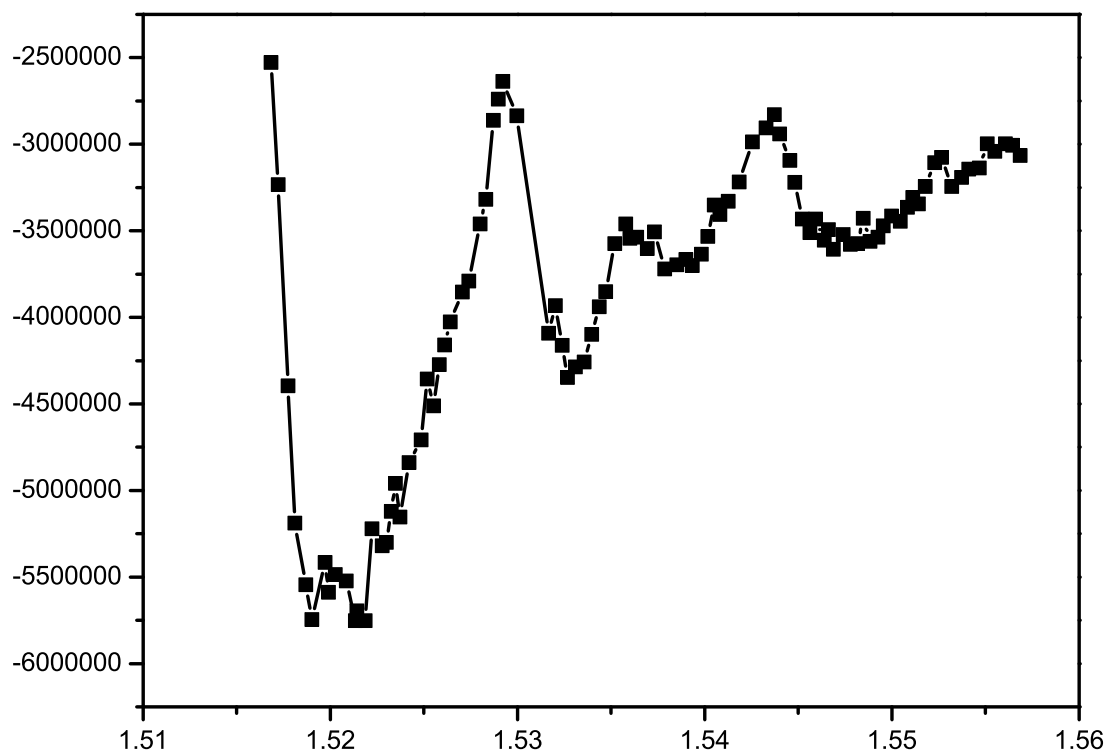
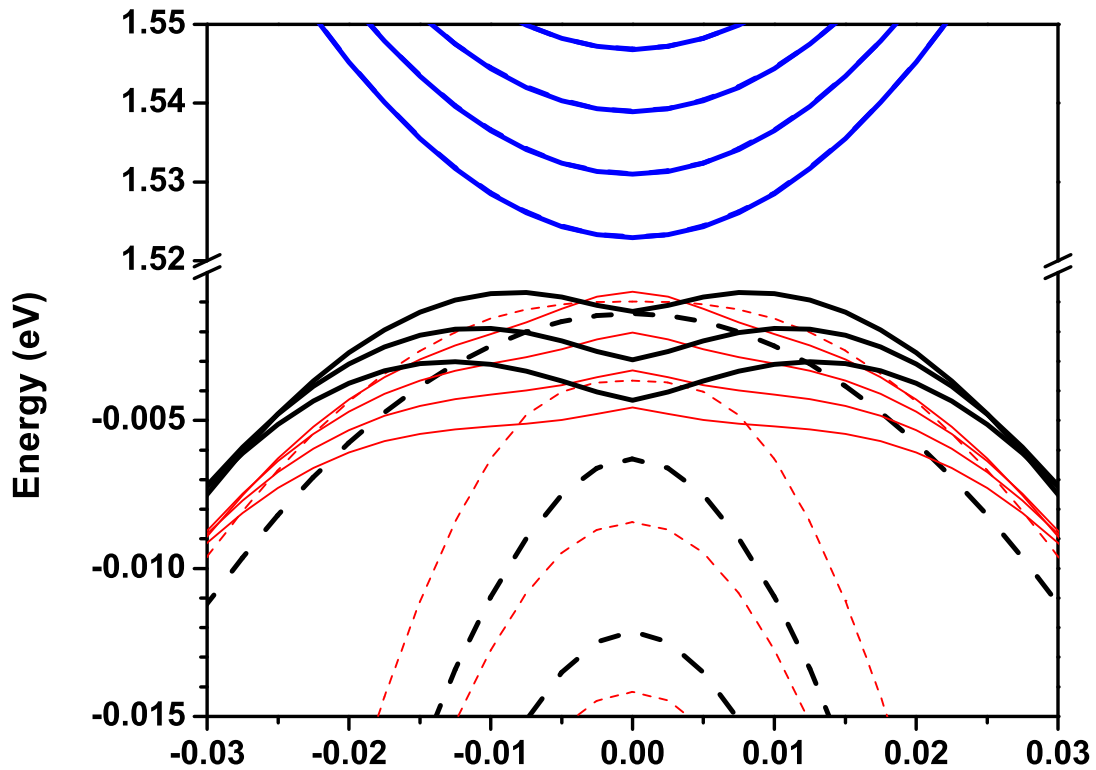Figure 4-17. OPNMR signal intensity as a function of photon energy for σ^+ excitation

Figure 4-18. Calculated spin-split valence-band and conduction-band Landau levels in GaAs at 4.7T. Black (thick) lines correspond to heavy holes, red (thin) lines to light holes, and blue lines to conduction band levels. Solid lines are for spin-up and dashed lines are for spin-down states. These assignments are only approximate due to band mixing. Only the lowest few Landau levels of each type are shown. Spin-up and spin-down states for the conduction band are nearly degenerate and are not resolved in this figure.
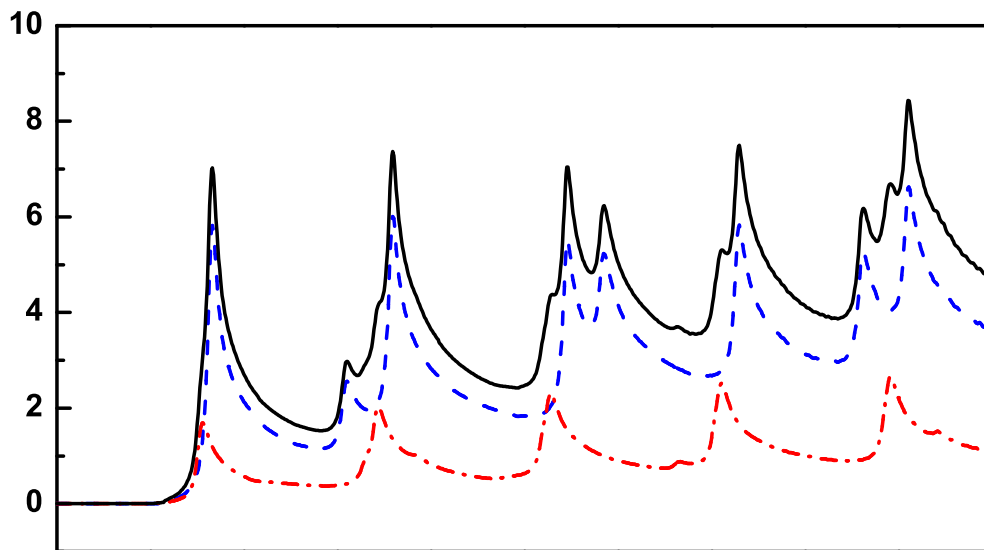
Figure 4-19. Theoretical calculations of absorption of σ^- light by bulk GaAs at 4.7T. Blue dashed line shows the absorption that produces spin-up electrons ($\alpha_\uparrow$, primarily from heavy-hole transitions). Red dotted-dash line shows the absorption that produces spin-down electrons ($\alpha_\downarrow$, primarily from light-hole transitions). Black solid lines shows total absorption, $\alpha_\uparrow + \alpha_\downarrow$.
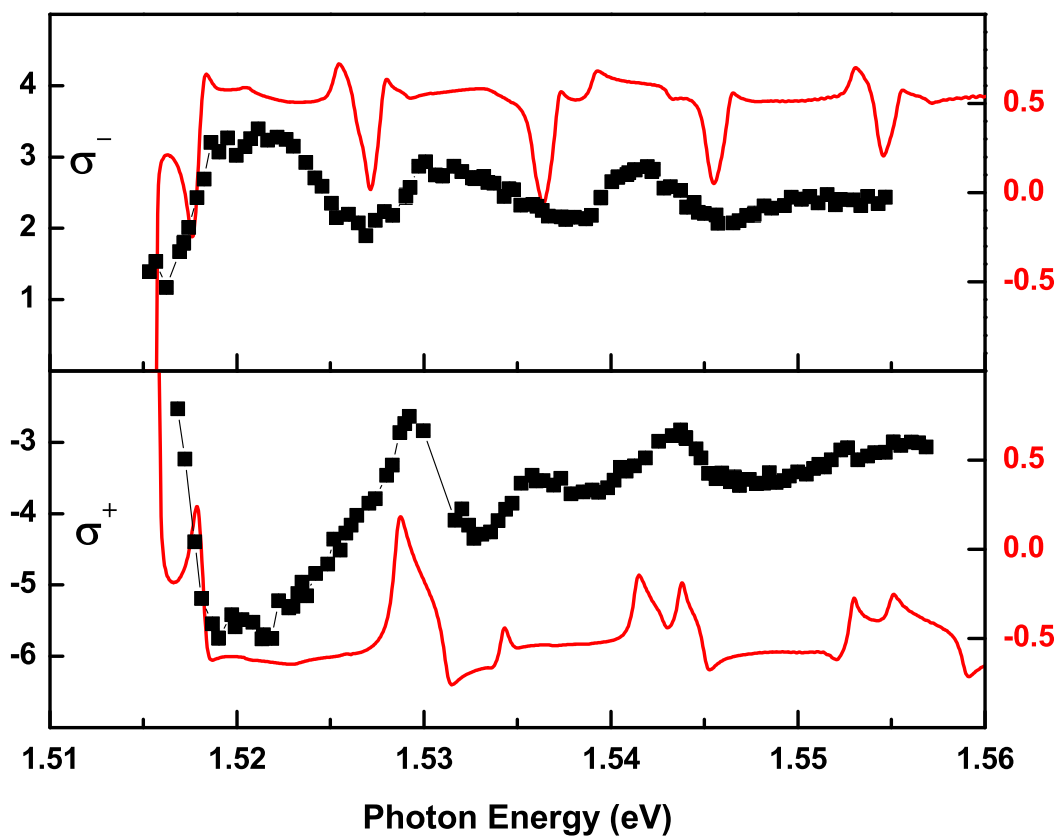
Figure 4-20. Depiction of the [69]Ga OPNMR signal intensity as a function of photon energy for σ^- and σ^+ polarized light at 4.7T. The experimental data (black symbols) are compared with the calculated electron polarization (solid red line), $(\alpha_\uparrow - \alpha_\downarrow)/(\alpha_\uparrow + \alpha_\downarrow)$.

CHAPTER 5
MAGNETO-PROPERTIES OF INDIUM ANTIMONIDE QUANTUME WELLS

5.1   Experimental Details

Experiment was carried out by Santos and co-workers at the University of Oklahoma. The InSb/AlInSb heterostructure as shown in Fig. 5-1 was grown by molecular beam epitaxy on an [001] GaAs substrates. The structure contains 40 InSb wells that are 15nm thick and separated by $In_{0.9}Al_{0.1}Sb$ barrier layers that are 50nm thick. A 0.5μm-thick InAlSb buffer layer with a graded Al composition was deposited between the multiple-quantum-well (MQW) layers and the substrate in order to reduce the density of dislocations that result from the $\sim$ 14% lattice mismatch between the substrate and the MQW layers. A 3μm $In_{0.9}Al_{0.1}Sb$ layer, which is almost completely relaxed, was grown just prior to the MQW layers. The InSb wells are compressively strained to the lattice constant of the 3μm $In_{0.9}Al_{0.1}Sb$ layer. A Fourier Transform Infrared spectrometer was used to nomitor the transmission through the MQW structure as a function of photon frequency, which is also shown in Fig. 5-1. The structure was wedged at 4° to reduce unwanted Fabry-Perot interference. In their previous exciton studies without a magnetic field, they deduced the band offsets for InSb/AlInSb[34] and the strain parameters for InSb[35]. In the current study, a perpendicular magnetic field of $0 \leq B \leq 7.5$T was applied in far infrared transmission measurements at a temperature of 4.2K. We observed rich spectra of transitions between Landau levels of hole and electron subbands.

5.2   Extension of the Theoretical Model

We want to look at the magneto-optical properties of InSb quantum wells. The InSb quantum wells system have three major differences form the bulk GaAs system which we already studied in detail in the previous chapter. These three differences between the two physical system make it much more complicated to deal with the InSb quantum well than bulk GaAs. In this section I will outline these three differences and extend

our current theoretical model to a form that can be used to calculate the electronic and optical properties of the InSB quantum wells.

5.2.1 Narrow Energy Gap

The first thing we want to notice is that, unlike GaAs, the InSb is a narrow-gap material. Simple Kane model tells us that narrow band gap will lead to strong coupling between the conduction bands and the valence bands so that the electronic wave function will have components mixed from the conduction band and valence bands. In our previous treatment of GaAs system, the conduction band wave functions are nearly 100%, for example, see Table 4-1 and Table 4-2, and we can take the approximation that the valence bands are only mixed with the six-dimensional subspace. However this will not be true for InSb since it has strong coupling between the conduction bands and the valence bands. The good news for us is that even we can take the approximation to treat conduction bands and valence bands seperatelly for GaAs, we did not do that and we still keep all eight bands in our theoretical model introduced in previous chapters. In this concern we were treating GaAs as a narrow gap material just like InSb, so when we do need to treat InSb we do not need to modify our previous theorectical model.

5.2.2 Strain Effect

In our MQW structure, the InSb layers are compressively strained to the lattice constant of the 3μm In$_{0.9}$Al$_{0.1}$Sb layer. This will give us one more term in our EFA Hamiltonian, so that instead of using equation (4–34), we have now

$$H^{EFA} = H^L + H^Z + H^S. \tag{5–1}$$

The strain contribution to the envelope function approximation is

$$H^S = \begin{bmatrix} S_a & S_c \\ S_c^\dagger & S_b \end{bmatrix} \tag{5–2}$$

where the submatrices S_a, S_b and S_c are given by

$$
S_a = \begin{bmatrix}
A_\varepsilon & 0 & 0 & 0 \\
0 & -P_\varepsilon - Q_\varepsilon & -M_\varepsilon & i\sqrt{2}M_\varepsilon \\
0 & -M_\varepsilon^* & -P_\varepsilon + Q_\varepsilon & i\sqrt{2}Q_\varepsilon \\
0 & -i\sqrt{2}M_\varepsilon^* & -i\sqrt{2}Q_\varepsilon & -P_\varepsilon
\end{bmatrix},
\tag{5–3a}
$$

$$
S_b = \begin{bmatrix}
A_\varepsilon & 0 & 0 & 0 \\
0 & -P_\varepsilon - Q_\varepsilon & -M_\varepsilon^* & i\sqrt{2}M_\varepsilon^* \\
0 & -M_\varepsilon & -P_\varepsilon + Q_\varepsilon & i\sqrt{2}Q_\varepsilon \\
0 & -i\sqrt{2}M_\varepsilon & -i\sqrt{2}Q_\varepsilon & -P_\varepsilon
\end{bmatrix},
\tag{5–3b}
$$

$$
S_c = \begin{bmatrix}
0 & 0 & 0 & 0 \\
0 & 0 & -L_\varepsilon & -i\sqrt{\tfrac{1}{2}}L_\varepsilon \\
0 & L_\varepsilon & 0 & i\sqrt{\tfrac{3}{2}}L_\varepsilon^* \\
0 & -i\sqrt{\tfrac{1}{2}}L_\varepsilon & i\sqrt{\tfrac{3}{2}}L_\varepsilon^* & 0
\end{bmatrix}.
\tag{5–3c}
$$

In terms of the strain tensor components ε_{ij}, the quantities A_ε, P_ε, Q_ε, L_ε and M_ε in equation (5–3) are given by

$$
A_\varepsilon = a_c(\varepsilon_{xx} + \varepsilon_{yy} + \varepsilon_{zz}),
\tag{5–4a}
$$

$$
P_\varepsilon = -a_v(\varepsilon_{xx} + \varepsilon_{yy} + \varepsilon_{zz}),
\tag{5–4b}
$$

$$
Q_\varepsilon = -\frac{b}{2}(\varepsilon_{xx} + \varepsilon_{yy} - 2\varepsilon_{zz}),
\tag{5–4c}
$$

$$
L_\varepsilon = id(\varepsilon_{xz} - i\varepsilon_{yz}),
\tag{5–4d}
$$

$$
M_\varepsilon = -\frac{\sqrt{3}}{2}b(\varepsilon_{xx} - \varepsilon_{yy}) + i\frac{2\sqrt{3}}{3}d\varepsilon_{xy}.
\tag{5–4e}
$$

In equation (5–4), a_c, a_v, b and d are deformation potentials. Values of the deformation potentials for a wide range of III-V semiconductor alloys are tabulated in Ref. [4].

We assume that strain in the AlInSb/InSb MQW is pseudomorphic which means that the lattice constant in the InSb and AlInSb layers are equal to the lattice constant in

the $In_{0.9}Al_{0.1}Sb$ substrate. In our pseudomorphic strain approximation, the non-vanishing strain tensor components in the InSb layer are given by

$$\varepsilon_{xx} = \varepsilon_{yy} = \frac{a_0(\text{AlInSb}) - a_0(\text{InSb})}{a_0(\text{InSb})} \tag{5–5a}$$

$$\varepsilon_{zz} = -2\frac{c_{12}}{c_{11}}\varepsilon_{xx}, \tag{5–5b}$$

where $a_0(\text{InSb})$ is the unstrained lattice constant in bulk InSb, $a_0(\text{AlInSb})$ is the lattice constant of the AlInSb substrate, and c_{11} and c_{12} are elastic stiffness constants tabulated in Ref. [4]. Similar expressions hold for the AlInSb layers. From equation (5–5) we see that L_ε and M_ε in equation (5–4) vanish in the pseudomorphic strain approximation. This implies $S_c = 0$ and $S_a = S_b$ in the strain Hamiltonian, H_S. Thus H_S is block diagonal.

5.2.3 Quantum Confinement Effect

We consider an InSb/InAlSb multiple quantum well (MQW) grown on a thick (strain-relaxed) $In_{0.9}Al_{0.1}Sb$ buffer layer on a GaAs (001) substrate. The band diagram for the MQW is shown schematically in Fig. 5-2. Note the band gap of InSb lies within the band gap of AlInSb. The band gap mismatch between InSb and AlInSb is $\Delta E_g = E_g(\text{AlInSb}) - E_g(\text{InSb}) = 0.446\text{eV} - 0.240\text{eV} = 0.206\text{eV}$, using the band gap values for InSb and AlInSb from experimental data from Dr. Santos group at the University of Oklahoma. The conduction band offset, Q_c, which is defined as the ratio of the depth of the conduction-band square well to the band gap difference of the well(InSb) and the barrier(AlInSb), is assumed to be 0.62 [34] and the valence band offset Q_v is assumed to be 0.38. Thus the conduction band barrier height is $\Delta E_c = Q_c\Delta E_g = 0.128\text{eV}$ and the valence band barrier height is $\Delta E_v = Q_v\Delta E_g = 0.078\text{eV}$. With these band offsets both the electrons and the holes are confined in the InSb layers.

To take into account the quantum confined structures we treat the MQW sample as infinite superlattices with wide barrier regions. Stay in the same Landau gauge given by

equation (4–18), the envelope function of the EFA Hamiltonian can be written as

$$\mathcal{F}_{n,\nu} = \frac{e^{i(k_x x + k_z z)}}{\sqrt{\mathcal{A}}} \begin{bmatrix} U_{n,1,k_z,\nu}(z)\phi_{n-1} \\ U_{n,2,k_z,\nu}(z)\phi_{n-2} \\ U_{n,3,k_z,\nu}(z)\phi_n \\ U_{n,4,k_z,\nu}(z)\phi_n \\ U_{n,5,k_z,\nu}(z)\phi_n \\ U_{n,6,k_z,\nu}(z)\phi_{n+1} \\ U_{n,7,k_z,\nu}(z)\phi_{n-1} \\ U_{n,8,k_z,\nu}(z)\phi_{n-1} \end{bmatrix}. \tag{5–6}$$

In equation (5–6), n is the manifold quantum number associated with the Hamiltonian matrix, ν labels the eigenvectors, $\mathcal{A} = L_x L_y$ is the cross sectional area of the sample in the xy plane, $\phi_n(\xi)$ are harmonic oscillator eigenfunctions evaluated at $\xi = y - \lambda^2 k_x$, and $U_{n,m,k_z,\nu}(z)$ are eight complex envelope functions ($m = 1 \dots 8$) for the ν-th eigenstate. From Bloch's theorem, the envelope functions, $U_{n,m,k_z,\nu}(z)$ have the periodicity of the superlattice and the wave vector k_z, is defined within the minizone, $-\pi/L \leq k_z \leq \pi/L$, where L is the superlattice period. The envelope functions are normalized over the superlattice unit cell, i.e.

$$\sum_m \int_{-L/2}^{L/2} \frac{dz}{L} U^*_{n,m,k_z,\nu}(z) U_{n,m,k_z,\nu}(z) = 1. \tag{5–7}$$

Note that the wave functions themselves will be given by the envelope functions in equation (5–6) with each component multiplied by the corresponding $k_z = 0$ Bloch basis states given in equation (3–9).

We use a finite difference scheme to obtain the energies and wave functions in the superlattice. We divide the superlattice unit cell into an evenly spaced grid of points, z_i, where $i = 1 \dots N$. Substituting $\mathcal{F}_{n,\nu}$ from equation (5–6) into the EFA equation with

Hamiltonian given by equation (5–1), we obtain a matrix eigenvalue equation

$$H_n F_{n,\nu} = E_{n,\nu}(k_z) F_{n,\mu},$$ (5–8)

that can be solved for each allowed value of the manifold quantum number n and wave vector k_z to obtain eigenvalues and eigenvectors. Since the harmonic oscillator functions $\phi_{n'}(\xi)$, are only defined for $n' \geq 0$, it is necessary to delete rows and columns of H_n for which $n' < 0$. It follows from equation (5–6) that $F_{n,\nu}$ is defined for $n \geq -1$. The resulting eigenvalues are the Landau levels, denoted $E_{n,\nu}(k_z)$, where n labels the manifold quantum number and ν labels the eigenenergies belonging to the same manifold in ascending order. The corresponding eigenvectors, $F_{n,\nu}$, are the cell periodic functions, $U_{n,m,k_z,\nu}(z_i)$, evaluated at the grid points, z_i. In finite differencing the EFA Schrödinger equation, we allow all the material parameters to vary with position. To ensure that H_n is Hermitian, we make the operator replacements

$$B(z)\frac{\partial^2}{\partial z^2} \rightarrow \frac{\partial}{\partial z}B(z)\frac{\partial}{\partial z}$$ (5–9a)

$$B(z)\frac{\partial}{\partial z} \rightarrow \frac{1}{2}\left[B(z)\frac{\partial}{\partial z} + \frac{\partial}{\partial z}B(z)\right]$$ (5–9b)

when differencing derivatives with respect to z. The cell periodic boundary conditions on $U_{n,m,k_z,\nu}(z_i)$ are satisfied by letting $U_{n,m,k_z,\nu}(z_{N+i}) = U_{n,m,k_z,\nu}(z_i)$ in the difference formulas for the derivatives.

5.3 Magneto-Optical Absorption

We can still use equation (4–70) to calculate the optical properties for our InSb/AlInSb MQW structure. Since the envelope functions and vector potentials are slowly varying over a unit cell, the dominant contributions to the optical matrix elements are given by

$$\mathbf{P}_{n,\nu}^{n',\nu'}(k_z) = \sum_{m,m'} \int \frac{dz}{L} U_{n,m,k_z,\nu}^*(z) U_{n',m',k_z,\nu'}(z)\langle\phi_{N(n,m)}|\phi_{N(n',m')}\rangle\langle m|\mathbf{P}|m'\rangle$$ (5–10)

where $\phi_{N(n,m)}$ are orthonormalized harmonic oscillator wave functions. Their quantum numbers $N(n, m)$ depend explicitly on n and m as defined in equation (5–6). In equation (5–10) we have neglected a term that depends on the momentum matrix element, $\langle \phi_{N(n,m)}|\mathbf{P}|\phi_{N(n',m')}\rangle$ between the oscillator states. Owing to strong band mixing in the narrow gap materials, this term is much smaller than the momentum matrix elements between the Bloch basis functions, even for intraband optical absorption such as for cyclotron resonance, hence we neglect it.

The momentum matrix elements $\langle m|P_x|m'\rangle$, $\langle m|P_y|m'\rangle$ and $\langle m|P_z|m'\rangle$ are the momentum matrix elements between the Bloch basis functions $|m\rangle$ defined in equation (3–9). For P_x we have the explicit representation

$$P_x = \begin{bmatrix} P_x^a & 0 \\ 0 & P_x^b \end{bmatrix} \tag{5–11a}$$

$$P_x^a = \frac{m_0}{\hbar} \begin{bmatrix} 0 & iV\sqrt{\frac{1}{2}} & iV\sqrt{\frac{1}{6}} & V\sqrt{\frac{1}{3}} \\ -iV\sqrt{\frac{1}{2}} & 0 & 0 & 0 \\ -iV\sqrt{\frac{1}{6}} & 0 & 0 & 0 \\ V\sqrt{\frac{1}{3}} & 0 & 0 & 0 \end{bmatrix} \tag{5–11b}$$

$$P_x^b = \frac{m_0}{\hbar} \begin{bmatrix} 0 & -V\sqrt{\frac{1}{2}} & -V\sqrt{\frac{1}{6}} & iV\sqrt{\frac{1}{3}} \\ -V\sqrt{\frac{1}{2}} & 0 & 0 & 0 \\ -V\sqrt{\frac{1}{6}} & 0 & 0 & 0 \\ -iV\sqrt{\frac{1}{3}} & 0 & 0 & 0 \end{bmatrix} . \tag{5–11c}$$

Likewise, for P_y we have

$$P_y = \begin{bmatrix} P_y^a & 0 \\ 0 & P_y^b \end{bmatrix} \tag{5–12a}$$

$$P_y^a = \frac{m_0}{\hbar} \begin{bmatrix} 0 & -V\sqrt{\tfrac{1}{2}} & V\sqrt{\tfrac{1}{6}} & -iV\sqrt{\tfrac{1}{3}} \\ -V\sqrt{\tfrac{1}{2}} & 0 & 0 & 0 \\ V\sqrt{\tfrac{1}{6}} & 0 & 0 & 0 \\ iV\sqrt{\tfrac{1}{3}} & 0 & 0 & 0 \end{bmatrix} \qquad (5\text{–}12b)$$

$$P_y^b = \frac{m_0}{\hbar} \begin{bmatrix} 0 & iV\sqrt{\tfrac{1}{2}} & -iV\sqrt{\tfrac{1}{6}} & -V\sqrt{\tfrac{1}{3}} \\ -iV\sqrt{\tfrac{1}{2}} & 0 & 0 & 0 \\ iV\sqrt{\tfrac{1}{6}} & 0 & 0 & 0 \\ -V\sqrt{\tfrac{1}{3}} & 0 & 0 & 0 \end{bmatrix}. \qquad (5\text{–}12c)$$

and for P_z we have

$$P_z = \begin{bmatrix} 0 & P_z^c \\ iP_z^c & 0 \end{bmatrix} \qquad (5\text{–}13a)$$

$$P_z^c = \frac{m_0}{\hbar} \begin{bmatrix} 0 & 0 & V\sqrt{\tfrac{2}{3}} & iV\sqrt{\tfrac{1}{3}} \\ 0 & 0 & 0 & 0 \\ -iV\sqrt{\tfrac{2}{3}} & 0 & 0 & 0 \\ -V\sqrt{\tfrac{1}{3}} & 0 & 0 & 0 \end{bmatrix}. \qquad (5\text{–}13b)$$

In performing the integral in equation (4–70) the Dirac delta function $\delta(x)$ in Fermi's golden rule is replaced by the Lorentzian line shape function $\Delta_\gamma(x)$ with full width at half maximum (FWHM) of γ.

5.4   Results and Discussion

In this section we discuss our results for our calculation of the electronic structure and magneto optical properties of InSb/AlInSb MQW, and compare with experimental studies.

In Fig. 5-3, we show the full evolution of the absorption spectra up to 8T in a waterfall display. Fig. 5-3(a) shows the experimental data. The spectra are dominated by the absorption peaks that, with increasing field, evolve from the zero-field H_1-C_1 transition (at 0.295 eV) and to a lesser degree by those from the H_2-C_2 transition (at

0.385 eV). Although the L_1-C_1 transition is clearly seen at zero field at 0.350 eV, no clearly associated evolving magnetic-level structure is obvious in the figure. Because the conduction-band mass is much less than the heavy-hole mass, the change of the transition energies with B is dominated by the Landau-level structure of the conduction band where the Landau level spacing is much larger than the spacing in the valence band. Thus to extract the details of the hole band-structure will require a detailed comparison to theory.

Fig. 5-3(b) shows the theoretical calculation of the absorption spectrum of the InSb/AlInSb MQW structure. The figure includes the effects of strain at the pseudomorphic interface. In Fig. 5-3(c), we plot the theoretical calculation of the absorption spectrum without including the effects of strain. As can be seen by comparing Fig. 5-3(b) and Fig. 5-3(c) to Fig. 5-3(a), the inclusion of strain has a dramatic effect on the magneto-absorption spectra. We see that strain is essential to calculate the correct spectrum. This can be seen again in Fig. 5-4, where we plot the experimental spectrum (a) at 6 T and compare it to the theoretical calculation with strain (b) and without strain (c). Clearly the calculations with strain more accurately reproduce the experimental data.

From Fig. 5-3 it is clear that the main absorption features due to the H_1-C_1 and H_2-C_2 transitions are dominant in both theory and experiment. In addition, one can see that the 1st and 2nd H_1-C_1 Landau level transitions have been spin-split but the 0th Landau level transition does not show spin-splitting. Another clear difference is the anti-crossing-like structure at 0.35 eV near 6T in the experimental plot that is not reproduced in the theory plot.

Next we want to examine our results in details in terms of the relation between electronic structure and the magneto spectra. Fig. 5-5, shows the magnetic field dependence of some of the conduction and valence bands for the square well. Fig. 5-5(a) shows the lowest Landau levels for the first and second conduction subbands

and Fig. 5-5(b) shows the lowest Landau levels for the first three heavy hole subbands and the first light hole subband. The bands in Fig. 5-5 are color coded to indicate the Pidgeon-Brown manifold index ($N = -1, 0, 1, ...$) with $N = -1$ black; $N = 0$ red; $N = 1$ green; $N = 2$ blue; $N = 3$ magenta; and $N = 4$ yellow. The numbers labeling the bands in Fig. 5-5 are the band numbers given in Fig. 5-6 and allow the components of the Landau levels and dominant contributions to the wave functions at 6 T to be determined. The bands are labeled in Fig. 5-6 according to the dominant wave function component, i.e. band number 10 is 85.3% heavy hole up and labeled (1st heavy hole subband, 0th Landau level, spin up (m_j = +3/2)). Solid lines in Fig. 5-5 indicate (primarily) spin-up bands while dotted lines indicate (primarily) spin-down bands.

The band diagram in Fig. 5-5 aids us in identifying the major optical transitions. We calculate the absorption spectra for both σ^+ and σ^- circularly polarized light as well as for linearly polarized light. The optical dipole selection rules are as follows. In the axial approximation the Pidgeon-Brown Manifold index changes by +1 for transitions involving σ^+ polarized light and -1 for transitions with σ^- polarized light. Note that the Pidgeon-Brown Manifold index takes on values $-1, 0, 1, 2, ...$ and is not the same as the Landau Level index (which takes on the value $0, 1, 2, ...$). Each Pidgeon Brown manifold has up to eight Bloch states and the Landau Level index depends on the Bloch state. i.e. for the $N = -1$ Pidgeon-Brown manifold, only the Heavy Hole spin down Bloch state is in that manifold and the Landau level index n is related to the Pidgeon Brown Manifold number by $n = N + 1$. Within a given Pidgeon Brown manifold, m_j (for the Bloch state) plus n (the Landau level) is a constant.

The band diagram in Fig. 5-5 together with Fig. 5-6 and the selection rules aid us in identifying transition peaks in the magneto-absorption spectra. Some of the dominant transition peaks are shown in Fig. 5-7. For σ^+ polarization, (Fig. 5-7(b)) the dominant transitions are between the first heavy hole down and first conduction band down subbands. We see transitions from the 0th, 1st, 2nd and 3rd Landau levels. We also see

weaker transitions between the first light hole down and first conduction band spin up subbands (0th, 1st and 2nd Landau levels). These transitions are much weaker since their oscillator strength is down by a factor of 3 compared to the heavy hole transitions and they are in close proximity to the heavy hole transitions.

For σ^- polarization (Fig. 5-7(c)) , we also see the dominant transitions between the first heavy hole up to the first conduction band up subbands (for the 0th, 1st , 2nd and 3rd Landau levels) together with the dominant transitions between the second heavy hole up subband (0th Landau level) to the second conduction band up subband. In addition, we also see weaker transitions from the first light hole up to the first conduction band down subbands (0th, 1st and 2nd Landau levels), but now they are further separated from the heavy hole transitions.

The σ^+ and σ^- polarization spectra in Fig. 5-7(b) and (c) can be added up to give the linearly polarized spectrum in Fig. 5-7(a) which can be compared to experiment. Looking at the spectrum (and also Fig. 5-3 and Fig. 5-4), we see that the 1st and 2nd Landau levels are spin split, but the 0th Landau level is not. This is somewhat surprising since if we look at the splitting of the Landau levels in the conduction bands in Fig. 5-5(a), we see that the 0th Landau level in the first subband has the largest splitting. The reason for this can be seen by examining the valence band Landau levels in Fig. 5-5(b). The 0th heavy hole Landau levels for the 1st hole subband (bands 9, 10) spin-split in exactly the same manner and direction as the 0th Landau levels for the conduction band. While the 1st (bands 11, 12) and 2nd (bands 13, 14) heavy hole Landau levels initially split in the same direction as the conduction bands, they cross at fields of about 4.5 T for the 1st level and about 3 T for the 2nd level. This is precisely where we see the 1st and 2nd Landau level spin-split in both the experimental and theoretical data (see Fig. 5-3(a) and Fig. 5-3(b)). While the 0th heavy hole Landau levels do not cross, their splitting is smaller than the conduction band 0th Landau level splitting.

Our calculations predict that the splitting of the 0th Landau level should be observable for magnetic fields greater than 10 T.

If we carefully examine the splitting of the 1st Landau level in the experimental spectrum (Fig. 5-3(a)), it appears that three levels anticross near the point where the splitting occurs (5 T and 0.34 eV). This is not reproduced in the theoretical calculations (Fig. 5-3(b)). If we look at the calculated valence band levels in Fig. 5-5(b). The splitting occurs when the two spin-split heavy hole subbands (band 11, 12) of the 1st Landau level cross. When they cross, they also cross with the 0th Landau levels of the second subband (bands 17, 18). In the theoretical calculations, we make the axial approximation and assume that the valence bands are cylindrically symmetric about the direction of the magnetic field (or more technically that the Luttinger parameters γ_2, γ_3 are equal) and as a result, these levels do not mix. In the axial approximation, only levels which belong to the same Pidgeon-Brown manifold can mix, but if we go beyond the axial approximation, then levels in different Pidgeon-Brown manifolds can mix (and the calculations become much more difficult). This shows that the experimental measurements are sensitive enough to show deviations from the axial approximation.

In the calculated spectra shown in Fig. 5-7 (and also in the experimental spectrum) we can also see minor transitions. Some of these are labeled in Fig. 5-7(b,c) and the assignment of some of these minor transitions might seem strange. For instance, there is a transition labeled $H_2^1 \downarrow \rightarrow C_1^0 \uparrow$ in Fig. 5-7(b) just to the right edge of the dominant $H_1^0 \downarrow \rightarrow C_1^0 \downarrow$ transition that is also seen in the experimental data in Fig. 5-3(a). From Fig. 5-6, we see that although band number 19 is 85.4% heavy hole down (and hence labeled $H_2^1 \downarrow$), it is the mixing in of the light hole down state that is responsible for the observed minor transition.
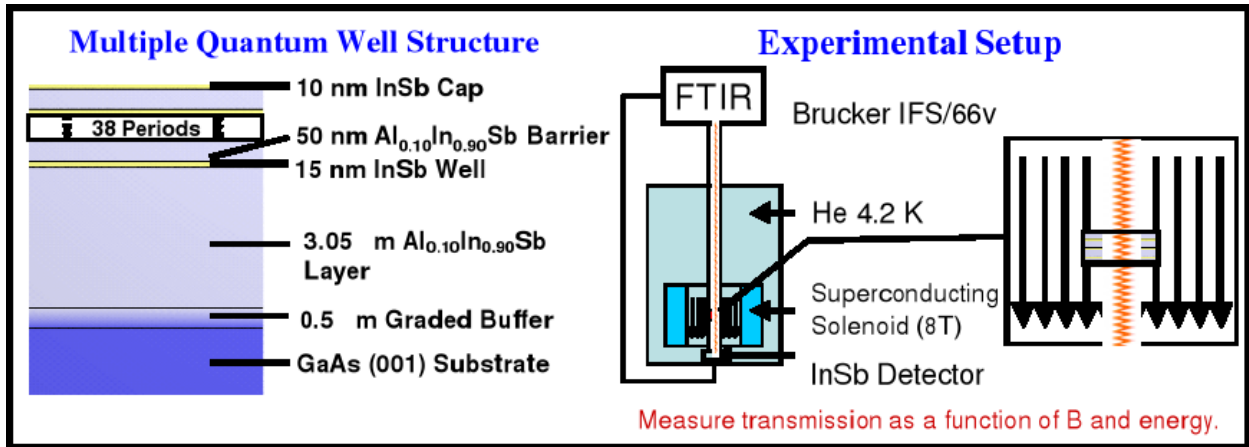
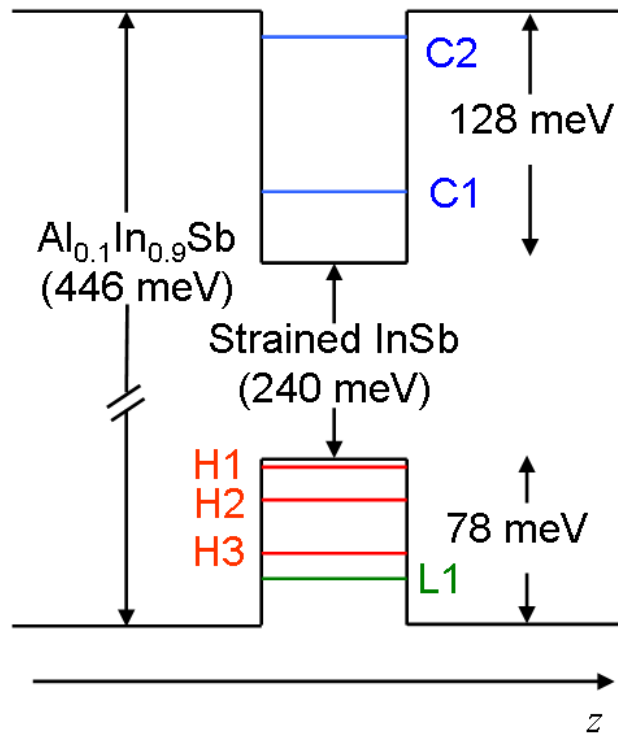Figure 5-1. Sample structure and experimental setup

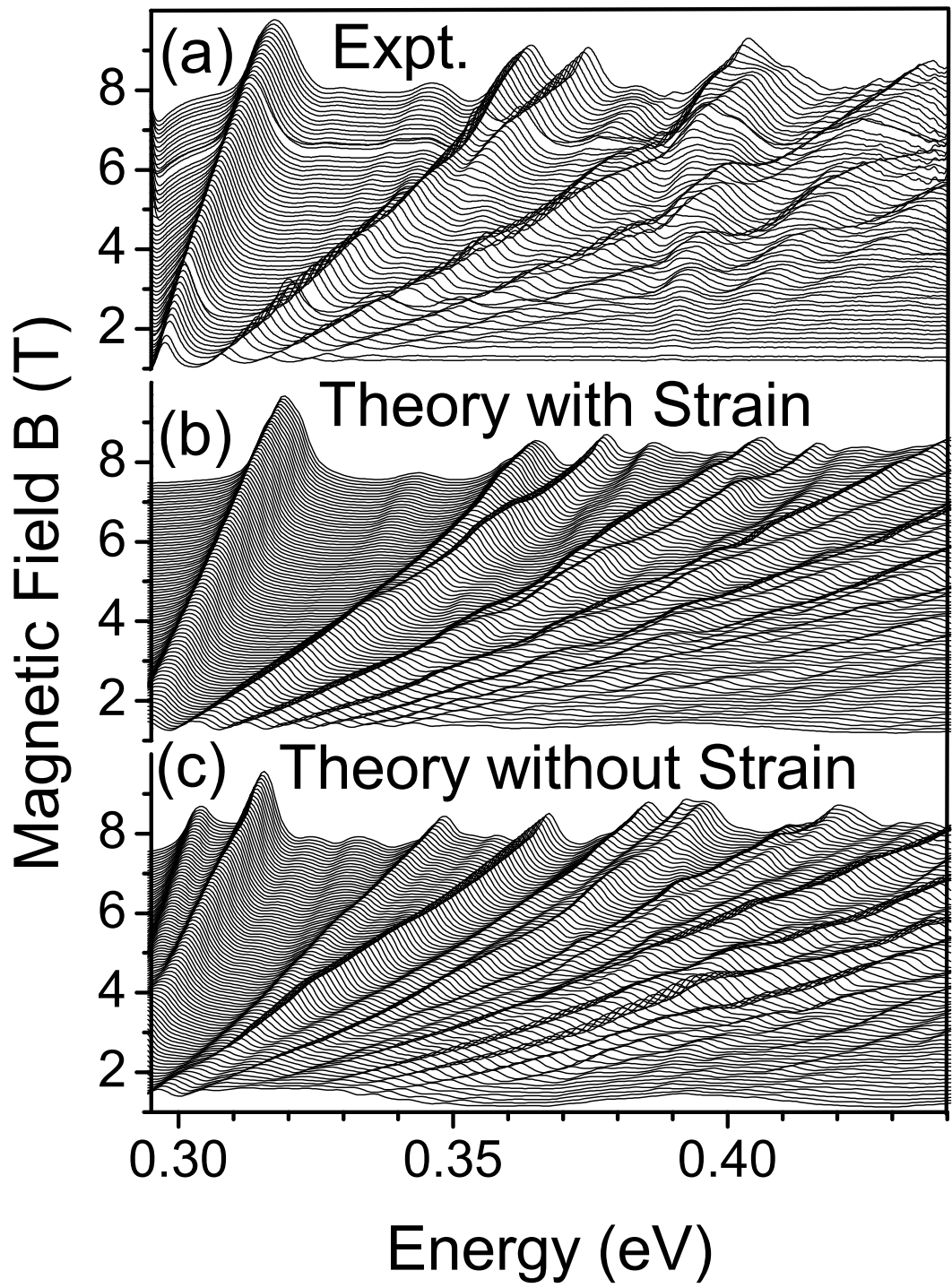Figure 5-2. Band diagram for an InSb/AlInSb multiple quantum well

98

Figure 5-3. Absorption spectra waterfall plot for (a) experiment and (b) theory for a strained interface and (c) theory for an unstrained interface.
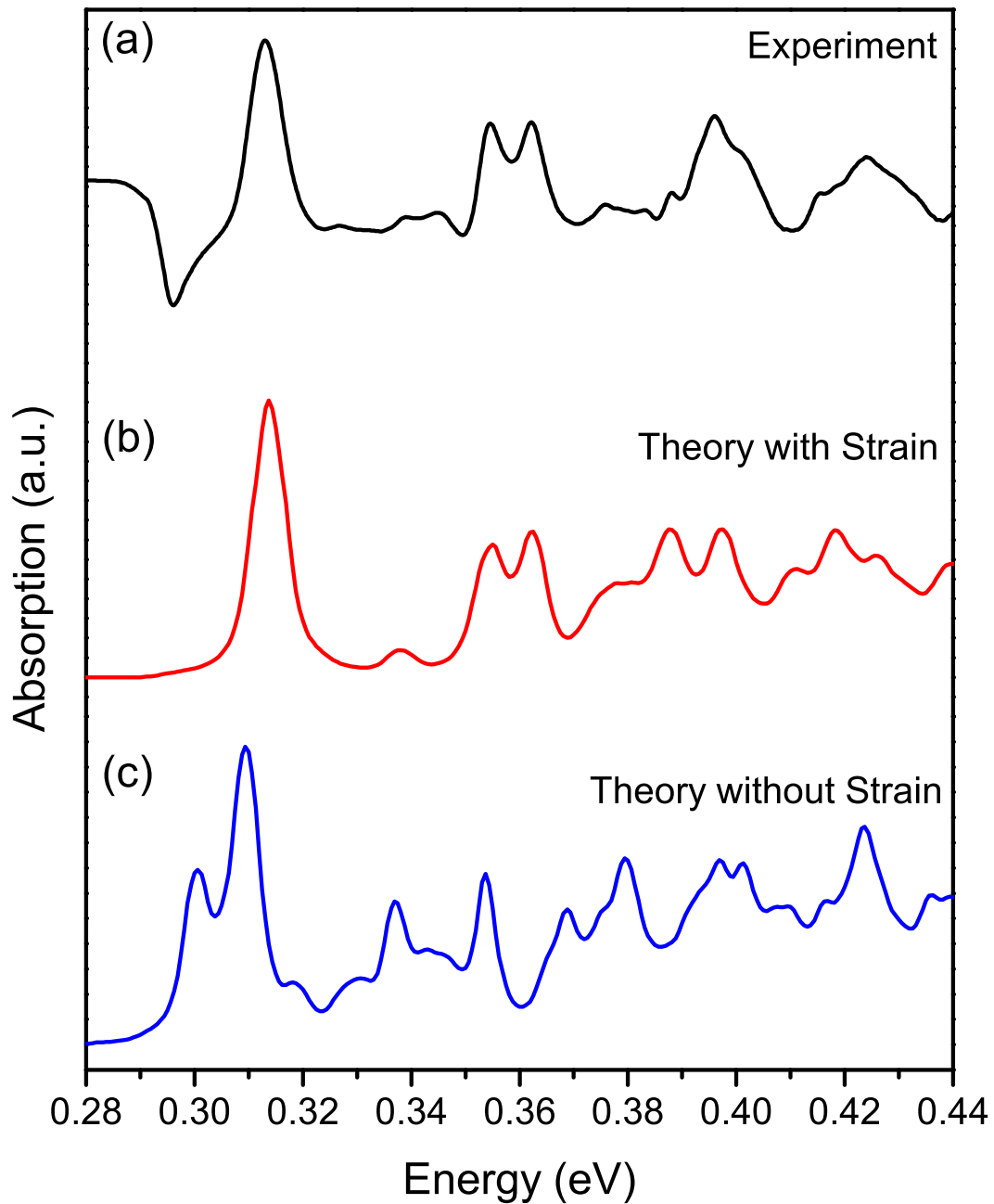
Figure 5-4. Experimental and calculated absorption spectra for the MQW for B=6T. (a) The experimental measured absorption. (b) Theoretically calculated absorption including the effects of strain. (c) Theoretically calculated spectrum not including the effects of strain at the interface.
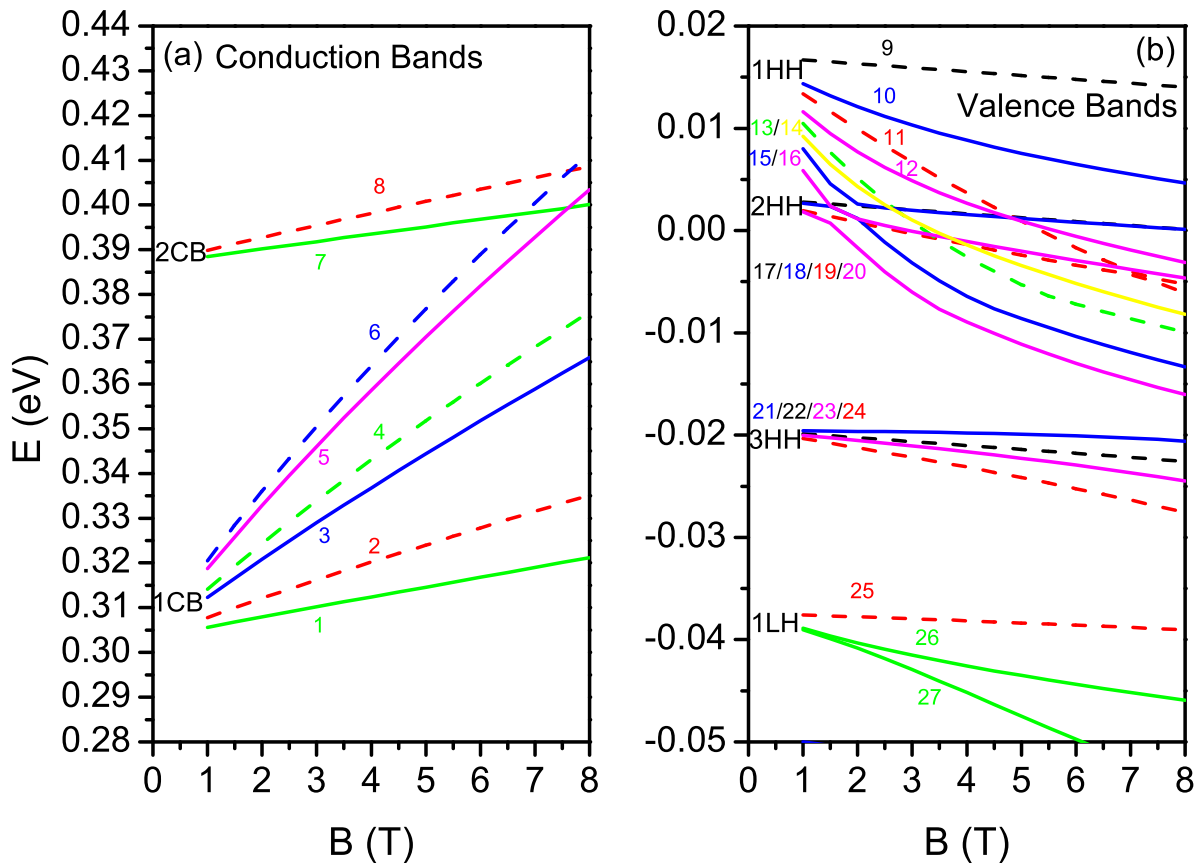
Figure 5-5. Calculated conduction band (a) and valence band (b) Landau levels for the MQW structure. The colors of the bands indicate the Pidgeion-Brown manifold index ($N = -1, 0, 1, ...$) with $N = -1$ black; $N = 0$ red; $N = 1$ green; $N = 2$ blue; $N = 3$ magenta; and $N = 4$ yellow. The numbers refer to the band number given in Fig. 5-6 and allow one to determine the components of the Landau levels and dominant contributions at 6T.

Band Number	Pidgeon-Brown Manifold	|CB↑>	|HH↑>	|LH↓>	|CB↓>	|HH↓>	|LH↑>		Label
8	0			0.117	0.839	0.038			$C_2^0\downarrow$
7	1	0.853		0.011			0.125		$C_2^0\uparrow$
6	2	0.001		0.017	0.817	0.132	0.025		$C_1^2\downarrow$
5	3	0.834	0.096	0.04			0.018	Conduction Bands	$C_1^2\uparrow$
4	1			0.02	0.852	0.107	0.015		$C_1^1\downarrow$
3	2	0.877	0.06	0.033			0.021		$C_1^1\uparrow$
2	0			0.024	0.906	0.069			$C_1^0\downarrow$
1	1	0.945		0.022			0.027		$C_1^0\uparrow$
9	-1					1			$H_1^0\downarrow$
10	2	0.017	0.853	0.077		0.005	0.047		$H_1^0\uparrow$
11	0			0.094	0.03	0.875			$H_1^1\downarrow$
12	3	0.015	0.733	0.165		0.015	0.072		$H_1^1\uparrow$
13	1			0.197	0.005	0.769	0.028		$H_1^2\downarrow$
14	4	0.012	0.651	0.231		0.022	0.084	Valence Bands	$H_1^2\uparrow$
15	2	0.002	0.867	0.004		0.012	0.114		$H_2^0\uparrow$
16	3	0.003	0.765	0.01		0.026	0.197		$H_2^1\uparrow$
17	-1					1			$H_2^0\downarrow$
18	2	0.001	0.039	0.209	0.003	0.694	0.054		$H_1^3\downarrow$
19	0			0.144	0.002	0.854			$H_2^1\downarrow$
20	3	0.001	0.094	0.19	0.003	0.608	0.104		$H_1^4\downarrow$
21	2	0.004	0.902	0.025		0.033	0.035		$H_3^0\uparrow$
22	-1					1			$H_3^0\downarrow$
23	3	0.006	0.796	0.067	0.001	0.078	0.052		$H_3^1\uparrow$
24	0			0.045	0.011	0.944			$H_3^1\downarrow$
25	0			0.796	0.014	0.189			$L_1^0\downarrow$
26	1	0.01		0.547	0.006	0.425	0.01		$L_1^1\downarrow$
27	1	0.015		0.072	0.025	0.196	0.69		$L_1^0\uparrow$

Figure 5-6. Eigenfunctions of the lowest lying bands for the MQW for B=6T. The numbers give the fraction of a given component in that band. (The spin-split hole contributions were negligible.) Bands are color coded according to the Pidgeon-Brown manifold index ($N = -1, 0, 1, ...$) with $N = -1$ black; $N = 0$ red; $N = 1$ green; $N = 2$ blue; $N = 3$ magenta; and $N = 4$ yellow. The band number corresponds to the number shown in Fig. 5-5. The bands are labeled according to the dominant component, i.e., band number 10 is 85.3% heavy hole up and labeled $H_1^0 \uparrow$ (1st heavy hole subband, 0th Landau level, spin up $m_j = +3/2$).
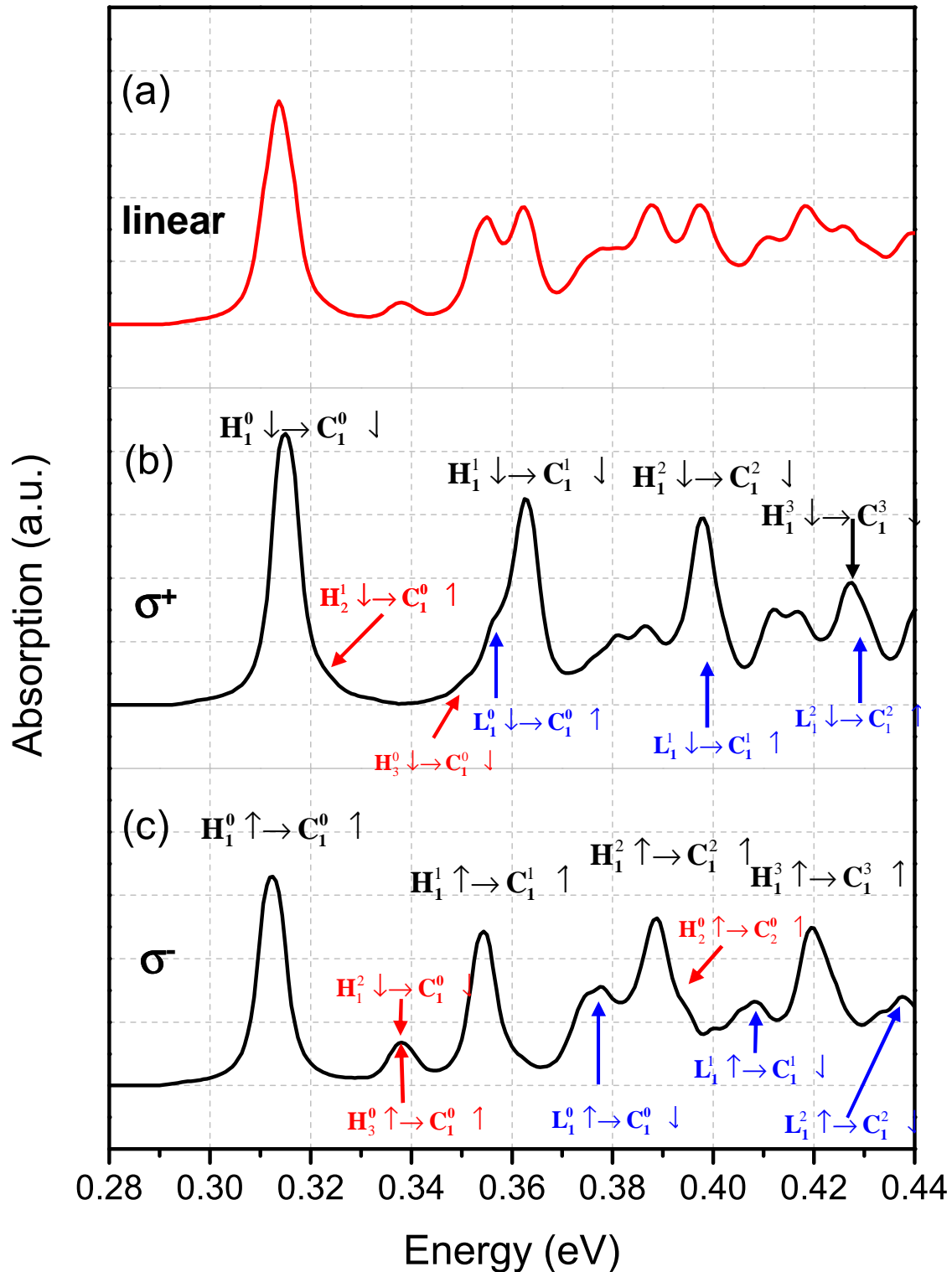
Figure 5-7. Calculated magneto-absorption spectra for (a)linear polarized light, (b)σ^+ circularly polarized light and (c)σ^- circularly polarized light. Peaks are labeled by the dominant transitions. For σ^+ light, within the axial approximation, transitions occur only between states whose Pidgeon-Brown manifold index change by +1. For σ^- light, the Pidgeon-Brown manifold index changes by -1 for a transition.

CHAPTER 6
CONCLUSIONS AND FUTURE DIRECTIONS

6.1   Conclusions

In this section we summarize the whole dissertation and emphasize the key steps in our development of the theoretical model, and the important results from our calculations. We want to study the InSb material because it has the narrowest gap of the III-V compound semiconductors. This leads to a very small conduction band effective mass and a large effective g-factor which can lead to important applications in digital nano-electronics and spintronics as well as possible uses in infra-red detectors. The conduction bands of InSb are relatively simple to understand but the details of the valence band structures are needed in order to make use of this material, for example, in the application of p-channel field effect transistors (FET).

We have measured the experimental magneto-absorption in a InSb/InAlSb multiple quantum well structures and compared them to detailed calculations. Our theoretical model starts from the 8-band $k \cdot p$ method with spin-orbit interaction considered explicitly. We use the quasi-degenerate perturbation theory (Löwdin's partitioning) to treat the effects of coupling with remote bands. The external magnetic field is built into our model on the basis of Pidgeon-Brown model, and generalized to include the wave vector dependence.

Because this is an 8-band model (not Luttinger's 6-band model), which treat the coupling of conduction bands and valence bands explicitly, it is suited for both wide-gap and narrow-gap semiconductors. Before applying this model in the narrow-gap InSb/AlInSb multiple quantum well structures, we use this model to calculate the spin-dependent electronic structures of bulk GaAs system in the external magnetic field. The optical properties then can be obtained from the electronic structures by using Fermi's Golden rule. We found that for bulk GaAs system, the conduction bands are almost degenerate at the field of 7T, but the valence bands are spin-splitting. Our

calculated optical absorptions predict the dominant transitions (coming from the heavy hole), secondary transitions (coming from the light hole) and also very weak transitions which are due to band mixing. We propose two experimental tools to probe the details of the valence band structures: i) magneto-optical absorption, which is sensitive to heavy-hole transitions; ii)optically pumped NMR (OPNMR) measurement, which is sensitive to the light-hole transitions. By using magneto-absorption and OPNMR together we can probe the valence band splitting easily.

Next we extend our theoretical model so that it can be applied to the InSb/AlInSb multiple quantum well system. We treat the quantum confinement effects via a finite difference method. Because the lattice constant of InSb is bigger that that of AlInSb, there will be a compressive strain in the InSb layers. We incorporate the pseudomorphic strain in our model and it turns our the this strain effect will deeply affect the electronic structures. We found that within the axial approximation the infinite dimensional eigenvalue problems decouples into different Pidgeon-Brown manifolds. The optical properties can be still calculated by using Fermi's golden rule.

Just like the case of bulk GaAs, our detailed calculation help us to identify the dominant (bright) transitions, secondary transitions, and very weak (dark) transitions due to band mixing, in the magneto-absorption spectrum. Because of InSb's large g-factor, spin splitting of the Landau levels can be seen in the spectrum at a relatively low magnetic field. However, the 0th Landau level splitting is not seen for fields up to 8 T since 0th heavy hole Landau levels split in same direction as conduction band. We predict that spin-splitting of the 0th level in the square well can be seen for fields above 10 T. We have also identified several minor (dark) transitions. These transitions occur because of band-mixing which mixes in small components of the 8-Bloch functions into levels dominated by a Bloch function which would not normally lead to an optical transition. Furthermore, we have seen that the experimental data is detailed enough

that it leads to mixing of states between Pidgeon-Brown manifolds which arises from non-axial symmetric terms in the potential.

In summarize, we have very accurately model the spin-dependent electronic structures of both bulk and quantum confined semiconductor systems. Our model can be applied not only to wide-band material but also narrow-gap material which has strong coupling between conduction bands and valence bands. We expect that detailed understanding of the InSb valence band structures can help us to make device applications such as optical detectors and CMOS, as well as application in spintronics.

6.2   Future Directions

Although our current theoretical model can be successfully applied to predict semiconductor electronic structures, it can still be improved from several aspects. In this section I propose some improvements on the model we can possibly make beyond its current form.

6.2.1   Exciton Absorption

In our previous calculation of optical properties we have completely neglect the Coulomb interaction between the excited electron in the conduction band and the hole left behind at the valence band. This approximation may be good enough for those transition with photon energy much bigger than the fundamental band gap, because in this case the electron and the hole have sufficient kinetic energy. However when the excitation energy is close to the band gap, we need to consider the attractions between the electron and hole pair. This attraction can lead to a set of discrete hydrogen-like levels which can be observed experimentally. For InSb, due to the small effective mass, the exciton binding energy is 0.6 meV. For GaAs the exciton binding energy is 4 meV. We expect that the exciton absorption effect is more important for GaAs system, especially near the band gap. In fact we saw the discrepancy between the calculated absorption and the observed absorption near the band gap. We expect that by considering exciton effect in the future work this discrepancy can be removed.

6.2.2 Beyond the Axial Approximation

In order to convert the infinite dimensional eigenvalue problem into a tractable form, we take the Luttinger parameters $\gamma_2 = \gamma_3$ and neglect the term proportional to $a^{\dagger 2}$ in the definition of the M operator in equation (4–47), and this is called the axial approximation. Different Pidgeon-Brown manifolds can only be separated (block-diagonalized) within this approximation. Decoupled manifolds means that only states within the same manifolds can mix with each other, i.e. the interaction between states in the same manifold will make them anti-cross each other when the energy levels meet at a certain magnetic field.

We successfully observed levels anti-crossings in both the magneto-optical absorption measurement and cyclotron resonance measurements. Part of these anti-crossings can be understand within current model, in terms of the mixing states belonging to the same manifold, however we also found anti-crossings that cannot be explained within current model, since those mixing states belong to different manifolds. In order to have interactions between different manifolds we have to abandon the axial approximation and deal with the much more complicated problem. One possible way of doing it is still starting with the axial approximation and only afterward we treat the coupling between manifolds as a perturbation. One can hope that numerical results can be obtained in this way. Another possibility is starting from the general principles of group theory[20, 36, 37] and separate the Hamiltonian into terms according to the symmetry hierarchy, i.e., the full Hamiltonian can be separated into axial term, cubic term and tetrahedral term. This way can help us physically understand when two levels cross each other and when they anti-cross, but it is difficult to get any numerical results.

6.2.3 Carrier Dynamics

We have successfully calculated the electronic structures in the magnetic field and the next step we can go is to model the carrier dynamics [38–40]. The generation and relaxation of carriers, and the time dependent carrier distribution function can

be modeled and compared with experiments so that information about scattering

mechanisms and coupling constants can be obtained.

REFERENCES

[1] T. Ashley, A. B. Dean, C. T. Elliott, G. J. Pryce, A. D. Johnson, and H. Willis, Applied Physics Letters, **66**, 481 (1995).

[2] S. A. Solin, D. R. Hines, A. C. H. Rowe, J. S. Tsai, Y. A. Pashkin, S. J. Chung, N. Goel, and M. B. Santos, Applied Physics Letters, **80**, 4012 (2002).

[3] A. M. Gilbertson, M. Fearn, J. H. Jefferson, B. N. Murdin, P. D. Buckle, and L. F. Cohen, Phys. Rev. B, **77**, 165335 (2008).

[4] I. Vurgaftman, J. R. Meyer, and L. R. Ram-Mohan, J. Appl. Phys., **89**, 5815 (2001).

[5] M. Razeghi, Opto-Electron. Rev., **6**, 155 (1998).

[6] R. Chau, S. Datta, and A. Majumdar, 2005 IEEE CSICS Technical Digest, **17** (2005).

[7] E. O. Kane, J. Phys. Chem. Solids, **1**, 249 (1957).

[8] G. D. Sanders, Y. Sun, F. V. Kyrychenko, C. J. Stanton, G. A. Khodaparast, M. A. Zudov, J. Kono, Y. H. Matsuda, N. Miura, and H. Munekata, Phys. Rev. B, **68**, 165205 (2003).

[9] C. R. Pidgeon, D. L. Mitchell, and R. N. Brown, Phys. Rev., **154**, 737 (1967).

[10] W. Gempel, X. Pan, T. Kasturiarachchi, G. D. Sanders, M. Edirisooriya, T. D. Mishima, R. E. Doezema, C. J. Stanton, and M. B. Santos, Springer Proceedings in Physics, **119**, 213 (2008).

[11] N. W. Ashcroft and N. D. Mermin, *Solid State Physics* (Holt, Rinehart and Winston, 1976).

[12] R. Shankar, *Principles of Quantum Mechanics* (Plenum Press, New York, 1994).

[13] R. J. Elliott, Phys. Rev., **96**, 266 (1954).

[14] G. Dresselhaus, A. F. Kip, and C. Kittel, Phys. Rev., **98**, 368 (1955).

[15] G. Dresselhaus, Phys. Rev., **100**, 580 (1955).

[16] R. H. Parmenter, Phys. Rev., **100**, 573 (1955).

[17] J. M. Luttinger and W. Kohn, Phys. Rev., **97**, 869 (1955).

[18] J. M. Luttinger, Phys. Rev., **102**, 1030 (1956).

[19] P.-L. Löwdin, J. Chem. Phys, **19**, 1396 (1951).

[20] R. Winkler, *Spin-Orbit Coupling Effects in Two-Dimensional Electrons and Hole Systems* (Springer-Verlag, 2003).

[21] G. F. Koster, *Space Groups and Their Applications* (Academic Press, New York, 1957).

[22] G. F. Koster, J. O. Dimmock, R. G. Wheeler, and H. Statz, *Properties of the Thirty-Two Point Groups* (MIT Press, Cambridge, 1964).

[23] E. O. Kane, *The $k \cdot p$ Method* (Academic Press, New York, 1966).

[24] G. Bastard, *Wave Mechanics Applied to Semiconductor Heterostructures* (Les Editions de Physique, les Ulis, 1988).

[25] C. K. Pidgeon and R. N. Brown, Phys. Rev., **146**, 575 (1966).

[26] F. Bassani and G. P. Parravicini, *Electronic States and Optical Transitions in Solids* (Pergamon, New York, 1975).

[27] D. V. Vasilenko, N. V. Luk'yanova, and R. P. Seisyan, Semiconductors, **33**, 15 (1999).

[28] D. Paget, G. Lampel, B. Sapoval, and V. I. Safarov, Phys. Rev. B, **15**, 5780 (1977).

[29] S. E. Barrett, R. Tycko, L. N. Pfeiffer, and K. W. West, Phys. Rev. Lett., **72**, 1368 (1994).

[30] R. Tycko, S. E. Barrett, G. Dabbagh, L. N. Pfeiffer, and K. W. West, science, **268**, 1460 (1995).

[31] C. R. Bowers, Solid State Nuclear Magnetic Resonance, **11**, 11 (1998), ISSN 0926-2040.

[32] S. E. Hayes, S. Mui, and K. Ramaswamy, The Journal of Chemical Physics, **128**, 052203 (2008).

[33] K. Ramaswamy, S. Mui, S. A. Crooker, X. Pan, G. D. Sanders, C. J. Stanton, and S. E. Hayes, Phys. Rev. B, **82**, 085209 (2010).

[34] N. Dai, G. A. Khodaparast, F. Brown, R. E. Doezema, S. J. Chung, and M. B. Santos, Applied Physics Letters, **76**, 3905 (2000).

[35] T. Kasturiarachchi, F. Brown, N. Dai, G. A. Khodaparast, R. E. Doezema, S. J. Chung, and M. B. Santos, Applied Physics Letters, **88**, 171901 (2006).

[36] K. Suzuki and J. C. Hensel, Phys. Rev. B, **9**, 4184 (1974).

[37] H. R. Trebin, U. Rössler, and R. Ranvaud, Phys. Rev. B, **20**, 686 (1979).

[38] G. Khodaparast, M. Bhowmick, M. Frazier, R. Kini, K. Nontapot, T. Mishima, M. Santos, and B. Wessels, Proc. of SPIE, **7608**, 760800 (2010).

[39] A. V. Kuznetsov, C. S. Kim, and C. J. Stanton, Journal of Applied Physics, **80**, 5899 (1996).

[40] G. A. Khodaparast, D. C. Larrabee, J. Kono, D. S. King, J. Kato, T. Slupinski, A. Oiwa, H. Munekata, G. D. Sanders, and C. J. Stanton, Journal of Applied Physics, **93**, 8286 (2003)

BIOGRAPHICAL SKETCH

Xingyuan Pan was born in 1981 in Qinhuangdao, Hebei province, China. He spent 18 years there until 1999 when he finished his high school study in No.1 Middle School in Qinhuangdao and went to the University of Science and Technology of China (USTC) at Hefei, Anhui province, China. His major is physics and he got an Bachelor of Science degree in July 2004. He then went to graduate school in August 2004, in the Department of Physics at the University of Florida. His graduate work was on theoretical condensed matter physics, or more specifically, the spin dependent phenomena in semiconductor physics, under the supervision of Dr. Christopher Stanton. Xingyuan Pan was married to Shuyang Gu, who is Xingyuan's high school classmate on the Christmas day of the year 2007.